AN ABSTRACT OF THE DISSERTATION OF

Weekit Sirisaksoontorn for the degree of Doctor of Philosophy in Chemistry presented on January 16, 2014.

Title: Graphite Intercalation Compounds Containing Tetra-n-alkylammonium Cations.

Abstract approved:

Michael M. Lerner

Novel donor-type graphite intercalation compounds (GICs) containing tetra-n-alkylammonium (TAA) cations have been synthesized by using both ion-exchange and electrochemical methods. Structural and compositional data of the resulting TAA-GICs are investigated by using powder X-ray diffraction (PXRD), one-dimensional electron density calculations, thermogravimetric and elemental analyses, and capillary zone electrophoresis (CZE).

A new GIC with composition of $[(C_4H_9)_4N]C_{44}$ is prepared by intercalation of tetra-n-butylammonium cation, $(C_4H_9)_4N^+$, via ion exchange from a $[Na(en)_{1.0}]C_{15}$ GIC (en = ethylenediamine). The synthesis reaction proceeds at 60°C for 90 min in a *N*,*N*-dimethylformamide (DMF) solvent. A dull-black stage-1 $[(C_4H_9)_4N]C_{44}$ provides the

gallery height of d_i = 0.802 nm, indicating a presence of flattened cation conformation. CZE data reveal that the $Na(en)^+$ cationic complex is quantitatively displaced by $(C_4H_9)_4N^+$ cations.

A homologous series of TAA-GICs; i.e. TAA = symmetric $(C_nH_{2n+1})_4N^+$ (n = 3-8) and asymmetric $(CH_3)_3(C_{12}H_{25})N^+$, $(CH_3)_3(C_{18}H_{37})N^+$ and $(CH_3)_2(C_{18}H_{37})_2N^+$, are prepared using the similar ion-exchange procedure, albeit with shorter reaction time (10 min), in dimethylsulfoxide (DMSO). The obtained TAA-GICs contain either monolayer or bilayer arrangement of flattened TAA intercalates with significant co-intercalation of DMSO molecules in a bilayer arrangement. PXRD data suggest that the monolayer is also observed with small TAA intercalates such as $(C_3H_7)_4N^+$ and $(C_4H_9)_4N^+$ with d_i ~ 0.80 nm. On the other hand, larger symmetric TAA cations, $(C_nH_{2n+1})_4N^+$ (n = 5-8), and asymmetric TAA cations all form only the bilayer arrangement with d_i ~ 1.10 nm. Thermogravimetric analyses combined with mass spectrometry and elemental analyses show a presence of ~1-2 DMSO co-intercalates per bilayer cation. The generated electron density map is sufficient to confirm the existence of bilayer structures, including DMSO co-intercalates. These GICs have very low charge density on graphene sheets for stage-1 GICs, namely C_{63}^- for $[(C_7H_{15})_4N]C_{63}$·1.4DMSO, as confirmed by Raman peak shifts.

In addition, TAA-GICs are also synthesized using the electrochemical reduction on a graphite electrode in TAABr/DMSO-based electrolytes. Similar to GIC products obtained from a chemical ion-exchange method, large TAA cations, $(C_nH_{2n+1})_4N^+$ (n = 5-8), form the bilayer arrangement with 0.7-1.2 DMSO co-intercalates per TAA cation and

d_i ~ 0.11 nm. A mixed phase product, including a stable $(C_4H_9)_4N^+$ monolayer arrangement (d_i = 0.815 nm), is observed in $(C_4H_9)_4N^+$ intercalation with a little amount of DMSO. No stable and isolable GIC products are obtained in case of TAA cations smaller than $(C_4H_9)_4N^+$ even though cyclic voltammograms show the characteristic features of reversible intercalation/de-intercalation for these cations. Therefore, a surface passivation model is proposed to describe the relative stabilities of GICs containing large TAA intercalates.

The effect of surface passivation is further studied on the preparation of $(C_2H_5)_4N$-GIC. Large TAA cation such as $(C_6H_{13})_4N^+$, $(C_7H_{15})_4N^+$ or $(C_8H_{17})_4N^+$, is used to passivate the graphite surface of $[Na(en)_{1.0}]C_{15}$, followed by ion exchange with $(C_2H_5)_4N^+$ to obtain a $(C_2H_5)_4N$-GIC product. PXRD data suggest the formation of a stage-1 compound with d_i ~ 0.81 nm, indicating monolayer arrangement of intercalate. The GIC composition is found to be $[(C_2H_5)_4N]C_{57}\cdot 0.5$DMSO. Additionally, the hydrophobic nature of passivated GIC surfaces enhances the chemical stabilities in aqueous media and other protic solvents.

Graphite Intercalation Compounds Containing Tetra-n-alkylammonium Cations

by

Weekit Sirisaksoontorn

A DISSERTATION

submitted to

Oregon State University

in partial fulfillment of
the requirements for the
degree of

Doctor of Philosophy

Presented January 16, 2014

Commencement June 2014

Doctor of Philosophy dissertation of Weekit Sirisaksoontorn presented on January 16, 2014.

APPROVED:

Major Professor, representing Chemistry

Chair of the Department of Chemistry

Dean of the Graduate School

I understand that my dissertation will become part of the permanent collection of Oregon State University libraries. My signature below authorizes release of my dissertation to any reader upon request.

Weekit Sirisaksoontorn, Author

ACKNOWLEDGEMENTS

I would like to thank my thesis advisor Prof. Michael M. Lerner for his valuable guidance, patience and encouragement throughout my study and research at Oregon State University. He is an excellent mentor who always provides me with useful suggestions and a thorough understanding of chemistry. I gratefully acknowledge Prof. Mas Subramanian, Prof. Douglas Keszler, Prof. David Cann and Prof. David Ji for the time and interest of being my thesis committee.

I also wish to thank Prof. Vincent T. Remcho and Dr. Adeniyi A. Adenuga for assistance with CZE, Prof. Chin-Hung Chang and Changqing Pan for assistance with Raman measurements, Teresa Sawyer for helping me in SEM sample preparation, Dr. Christine Pastorek for TGA assistance, and the past and present members of the Lerner group; Dr. Bahar Özmen-Monkul, Dr. Tosapol Maluangnont, Amila Liyanage, Hanyang Zhang and Xiaochao Liu, for their help and discussion.

I am specially appreciated the following awards given to me during my time here; OSU Teaching award (2012), Milton Harris graduate fellowship (2013) and Oregon Lottery graduate scholarship (2013). I myself would like to thank my family members for supporting me and boosting my morale throughout my Ph.D. study. Lastly, I want to express my cordial thanks to my colleagues and Thai friends for devoting their valuable time to helping me and sharing good experiences during my stay in the U.S.

CONTRIBUTION OF AUTHORS

Prof. Michael M. Lerner has contributed to the design and writing of each manuscript. Prof. Vincent T. Remcho and Dr. Adeniyi A. Adenuga assisted in capillary zone electrophoresis experiments in Chapter 2.

TABLE OF CONTENTS

TABLE OF CONTENTS (Continued)

TABLE OF CONTENTS (Continued)

TABLE OF CONTENTS (Continued)

LIST OF FIGURES

LIST OF FIGURES (Continued)

LIST OF FIGURES (Continued)

LIST OF FIGURES (Continued)

Figure Page

LIST OF TABLES

CHAPTER 1

INTRODUCTION

1.1 INTERCALATION CHEMISTRY

The chemical process in which a guest ion and/or molecule is inserted into a host lattice to form a new compound with kinetic stability is termed 'intercalation'. The general reaction involves a mobile guest species (G) and either a solid host lattice (H) that contains accessible unoccupied lattice sites (□) or exchangeable mobile guest (G´) in the interconnected framework as represented by equations (1.1) and (1.2).

$$xG + \square_x[H] \rightleftharpoons G_x[H] \qquad (1.1)$$

$$xG + G'_x[H] \rightleftharpoons G_x[H] + xG' \qquad (1.2)$$

Unlike conventional solid state processes, intercalation reactions do not require major rearrangement and bond breaking of a host lattice and therefore often occur at moderate temperatures. The host lattice may exhibit anisotropy in chemical bonding with directional dependence that allows a guest species to diffuse through vacant sites or displace a mobile species.[1–4]

The difference in structural dimensionality (0D to 3D) of the host lattice can result in selective intercalation behavior. A host lattice with 3D frameworks presents rigid pores that constrain guest access.[5] For example, zeolite 3A that has a pore diameter of 0.3 nm can adsorb water (with an effective molecular diameter of 0.28 nm) but not adsorb larger molecules such as alkanes; i.e. CH_4 (0.39 nm diameter).[6] For lower dimensional host

(1D chains or 2D layers), the structure cohesive interactions within the host include either van der Waals forces for neutral units and electrostatic forces for charged units. These chain- or layer-type hosts are expandable and can therefore often accommodate guest species with different sizes.[7,8] Three major driving forces for intercalation processes are ion/molecular exchange, acid-base and redox reactions.

Zeolites, a three dimensional framework structure with rigid pores, are typical insulating hosts. Their general composition is $M_{x/n}^{n+}[Al_xSi_{1-x}O_2]\cdot nH_2O$ where M^{n+} is a charge-compensating cation for the AlO_4 and SiO_4 tetrahedral frameworks. Both M^{n+} and water molecules can be selectively displaced by other cationic or neutral guests via an ion/molecular exchange reaction. As with zeolites most clay minerals are aluminosilicates.[9] Clays have layered structures and most exhibit negative host charges, except for the neutral clays such as kaolinite ($Al_2Si_2O_5(OH)_4$) and pyrophyllite ($Al_2(Si_4O_{10})(OH)_2$). The net negative charge derives from chemical substitution in the host and is balanced by interlayer cations such as Na^+ or K^+, leading to a large range of clay compositions, as indicated in Table 1.1. A wide variety of new intercalation compounds can be obtained via ion-exchange of these interlayer cations with new inorganic/organic cations, and the solvation chemistry of these ions. This is in part facilitated by the adjustable interlayer separation for the uptake of variable guest species to accommodate guests with different dimensions.[6,10]

On the other hand, layered double hydroxides (LDHs) have a positive charge on their metal hydroxide layers and show anion exchange behavior. The general composition

of LDH is given as $M_{1-x}M'_x(OH)_2 \cdot A_{x/n} \cdot mH_2O$ (M = divalent cation, M′ = trivalent cation, A = exchangeable anion).[11]

Intercalation chemistry with acid-base reactions is clearly observed in $M^{IV}(HPO_4)_2 \cdot nH_2O$ where acidic protons are found in P-OH groups that are oriented perpendicularly to the metal phosphate layers and point toward the interlayer region. These protic groups readily react with bases to form new intercalation compounds with the expansion of the host lattice. In addition, these protons can be partially or completely exchanged by other atomic/molecular cations depending on synthetic conditions.[12,13]

Host lattices with electronically conducting structures (*see* Table 1.2) can undergo redox reactions by electron/ion transfer to form new intercalation compounds. The host contains reducible or oxidizable species, and ionic intercalating species compensate the charge change resulting from the redox reaction. Electrochemical methods are often employed to study redox reactions because they can provide quantitative information about the extent of charge transfer and phase equilibrium with the variation of cell potential. Intercalation via redox chemistry can often be accomplished by use of either electrochemistry or with chemical reducing or oxidizing reagents.

Metal dichalcogenides, MX_2 (M = transition metals group 14, 15 and 16, X = S, Se), are an extensively studied host lattices; these have layered structures where metals occupy either octahedral or trigonal prismatic sites between two chalcogen layers. The interaction between two adjacent MX_2 layers is via weak van der Waals forces. Intercalation reactions occur when the host lattice is reduced by electron transfer, and a

cationic guest diffuses into the interlayer space to form AMX_2 compounds (A = mobile guest). With subsequent reactions, these mobile guests can undergo ion exchange by another atomic/molecular cation, yielding products that cannot be obtained by direct insertion chemistry.[14]

Table 1.1 Non redox-active host lattices for intercalation.[6]

Three-dimensional structures
Zeolites $M_{x/n}^{n+}(Al_xSi_{1-x}O_2)\cdot nH_2O$
$AlPO_4$-n, SAPO-n
Zeotypes: phosphates and silicates containing transition metal ions
Pyrochlores: $Ca_2Nb_2O_7$, $KNbWO_6$, W_2O_6
$KSbO_3$ related phase, $LiNbO_3$
β-Alumina
Two-dimeinsional structures
Clays and layered silicates
Kaolinite $Al_2Si_2O_5(OH)_4$
Hectorite $Na_x(Mg_{3-x}Li_x)Si_4O_{10}(OH)_2\cdot mH_2O$
Montmorillonite $Na_x(Al_{2-x}Mg_x)Si_4O_{10}(OH)_2\cdot mH_2O$
Vermiculite $(Na,Ca)Mg_3(Al_xSi_{4-x}O_{10})(OH)_2\cdot mH_2O$
Niobates, tantalates, titanates and molybdates
$K[Ca_2Na_{n-3}Nb_nO_{3n+1}]$, $3 \leq n \leq 7$; $K_2Ti_4O_9$, $KTiNbO_5$
Acid phosphates $M(HPO_4)_2\cdot H_2O$; M = Ti, Zr, Hf, Ce, Sn
Hydrous oxides $A_xUO_2XO_4\cdot mH_2O$
Layered double hydroxides
$[Mg_2Al(OH)_6]NO_3\cdot 1.2H_2O$, $[Zn_2Cr(OH)_6]Cl\cdot 2H_2O$
$Ni(CN)_2$

Table 1.2 Redox-active host lattices for intercalation.[6]

Three-dimensional structures
Intersecting channels
Chevrel phases $M_xMo_6X_8$ (X = S, Se)
Perovskite related oxides WO_3, ReO_3, V_6O_{13}
Tunnel structures
Nb_3X_4 (X = S, Se); Ti_3S_4, $Tl_xV_6S_8$
Rutile oxides MO_2 (M = Ti, Mn, Cr, Mo, W, Ru, Os, Ir)
h-WO_3
Two-dimeinsional structures
Graphite
Dichacogenides
MX_2 (M = Ti, Zr, Hf, V, Nb, Ta, Mo, W; X = S, Se, Te)
Metal phosphorous trichalcogenides
MPX_3 (M = Mg, V, Mn, Fe, Co, Ni, Zn, Cd, In; X = S, Se)
Metal oxyhalides MOX (M = Ti, V, Cr, Fe; X = Cl, Br)
Metal nitride halides MNX (M = Zr, Hf; X = Cl, Br, I)
Ternary chalcogenides
AMX_2 (A = group 1; M = Ti, V, Cr, Mn, Fe, Co, Ni; X = O, S)
$MOXO_4$ (M = Ti, Zr, Hf, Nb, Ta; X = S, Se)
MoO_3; V_2O_5
One-dimensional structures
Carbon nanotubes
MX_3 (M = Ti, Zr, Hf, Nb, Ta; X = S, Se)
$AFeS_2$ (A = Na, K, Rb, Cs)
AMo_3X_3 (A = group 1; X = S, Se)

1.2 GRAPHITE STRUCTURE

Graphite, an allotrope of carbon, is a two dimensional layered structure. In each layer, sp^2-carbon atoms are bonded together with a regular hexagonal network, this unit is called a graphene sheet. The C-C bond length in a planar sheet is 0.142 nm (vs 0.135 nm in benzene) because each p_z orbital interacts with three rather than two neighbors. Graphene sheets are 0.335 nm thick and are the layers stack with van der Waals interactions to form graphite.[15] Two known stacking sequences known in graphite are AB (hexagonal) and ABC (rhombohedral) arrangements. The latter is a metastable phase and transforms into the hexagonal (more stable) structure at high temperature. The graphite structure is shown in Figure 1.1.

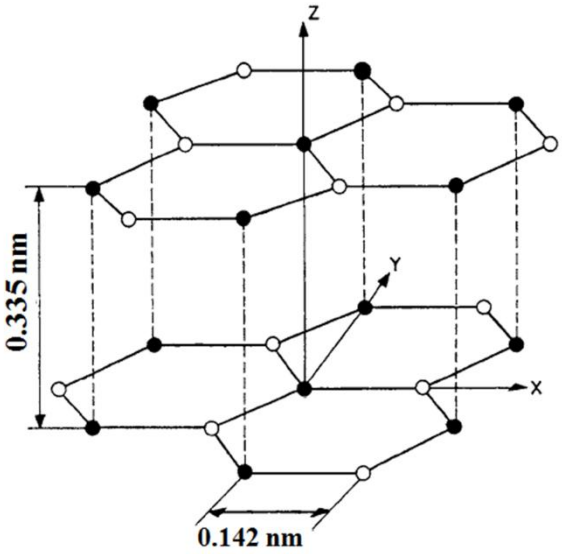

Figure 1.1 The layered structure of graphite formed by AB stacking of graphene.[15]

1.3 GRAPHITE INTERCALATION COMPOUNDS (GICs)

Graphite has a near-zero band gap where the top of a filled valence band (VB, π-bonding) is very close to the bottom of an empty conduction band (CB, π*-antibonding), resulting from the overlapping of p_z orbitals perpendicular to graphene sheets. This electronic structure enables graphite to undergo intercalation by either a reduction or an oxidation reaction. For reduction, the electron transfers from a donor species to the empty CB. On the other hand, the electron is partially removed from the VB when graphite is oxidized by an acceptor species.[16] Two examples of intercalation reactions via redox chemistry are indicated in equations (1.3) and (1.4). For the first reaction, nitric acid (HNO_3) oxidizes graphite and then both ionized and neutral forms of HNO_3 are intercalated into the graphite gallery. Under a reductive environment, graphite is readily reduced by potassium metal at a high temperature to form an intercalation product.

$$xC\ (s) + 5HNO_3\ (aq) \longrightarrow C_x^{+}NO_3^{-}\cdot 3HNO_3\ (s) + NO_2\ (g) + H_2O\ (g) \qquad (1.3)$$

$$xC\ (s) + K\ (m) \longrightarrow K^{+}C_x^{-}\ (s) \qquad (1.4)$$

Graphite also exhibits a unique staging phenomenon in intercalation. Staging refers to an ordered sequence of graphene sheets sandwiching intercalate galleries. For example, stage-1 means a single layer of graphene alternates regularly with a single layer of intercalate. Stage-2 means two graphene layers remain adjacent, and etc.[17] Stage transition can be more accurately described using the Daumas-Hérold (DH) model where an intercalate forms an island within the graphitic lattice, as shown in Figure 1.2. An intercalate island can migrate through the graphite gallery to convert the product from

one stage to another. Importantly, the propagation of intercalate islands requires deformable boundaries of graphene sheets, which is not observed and probably too energetically demanding with more rigid hosts.[18] This model has been directly supported by high-resolution transmission electron microscopic studies on $FeCl_3$-GIC.[19]

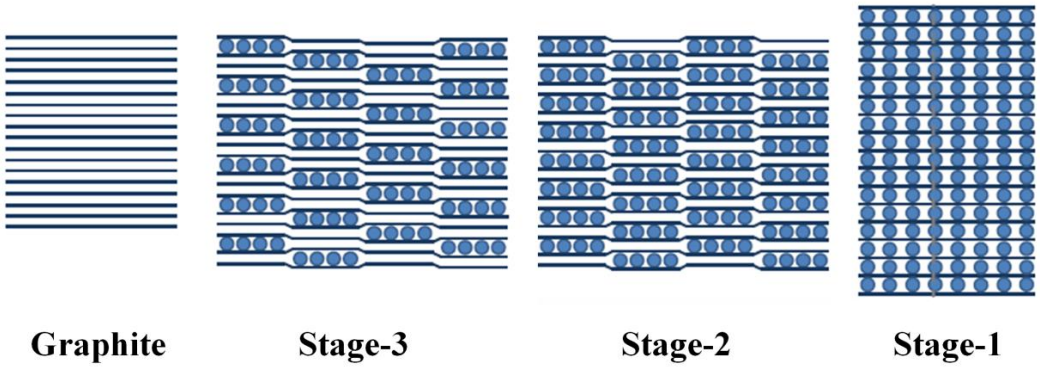

Figure 1.2 Schematic representations of staging in GICs with DH domains. The continuous lines and circle balls represent graphene layers and intercalate species, respectively.

When an intercalation compound is formed, graphene layers facing an intercalate layer may be staggered (as in graphite), eclipsed, or randomly displaced but graphene layers that remain adjacent are stacked in a similar fashion to pristine graphite.[20] Additionally, the relationship of the gallery height (d_i), repeated distance along *c*-axis (I_c), and stage number (n) is given as follows:

$$I_c = d_i - 0.355 \text{ nm } (n\text{-}1) \qquad (1.5)$$

and $$I_c = l^* d_{obs} \quad (1.6)$$

where 0.335 nm is the thickness of single graphene sheet,

l is index of ($00l$) planes that are oriented in the c-direction,

d_{obs} is the observed value of the spacing between two adjacent planes.

Both l and d_{obs} can be obtained directly from X-ray diffraction data. In addition, a gallery expansion (Δd) is calculated by subtracting the GIC gallery height (d_i) from single graphene sheet thickness (0.335 nm); $\Delta d = d_i - 0.335$nm. The Δd value is related to the lattice enthalpy for GICs. In general, the lattice enthalpy is more favorable with a smaller expansion, with implications on the orientation and arrangement of intercalate species inside the graphite gallery (to be discussed in subsequent chapters). The relationships described above are schematically depicted in Figure 1.3.

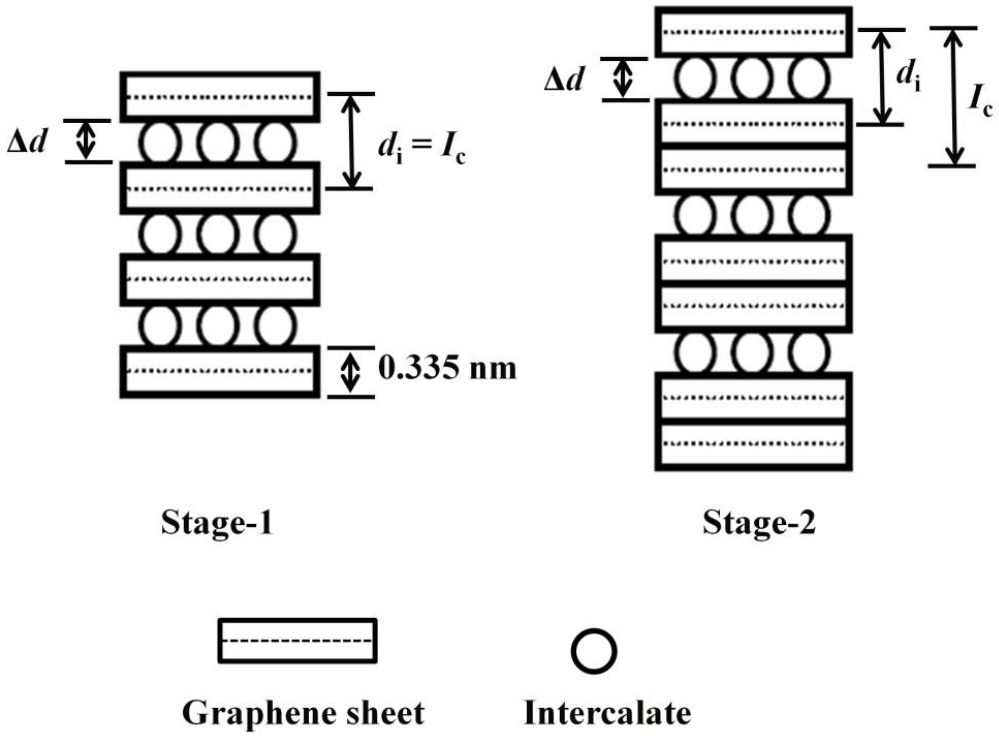

Figure 1.3 Schematic representations of the gallery height (d_i), repeat distance along c-axis (I_c), stage number (n), gallery expansion (Δd) and single graphene sheet thickness.

1.4 TYPES OF GICs

1.4.1 Acceptor-type GICs

Many different guest species, including conjugate base anions of strong acids, halogens and halides, and oxides, can be intercalated into graphite to form GICs via the oxidation of the graphite host. Graphite sulfate is a typical acid GIC first reported by Schauffaütl in 1841. Due to a non-oxidizing nature of sulfuric acid (H_2SO_4), the intercalation occurs only with the assistance of an oxidizing agent such as HNO_3, HIO_4, $(NH_4)_2S_2O_8$, MnO_2, CrO_3 or $KMnO_4$, or under anodic oxidation. A stage-1 H_2SO_4-GIC has d_i of 0.8 nm and a composition close to $C_{24}HSO_4{\cdot}2H_2SO_4$. This composition indicates that both HSO_4^- ions and additional molecular H_2SO_4 coexist in the graphite galleries.[21,22] Unlike H_2SO_4, nitric acid (HNO_3) itself can act as an oxidant to form stage-1 $C_{24}NO_3{\cdot}3HNO_3$ (d_i = 0.78 nm) where the N atoms form a tetrahedral coordination. After evacuation to remove intercalated HNO_3, this GIC converts to a phase with d_i of 0.66 nm where the intercalate planar nitrate anions must be oriented parallel to graphene sheets.[23,24] Many examples of other stage-1 GICs containing small anions, such as ClO_4^-, $CF_3SO_3^-$ or CF_3COO^-, all with $d_i \sim 0.8$ nm, have been reported.[22,25,26]

When exposed to a bromine vapor at a low temperature, graphite undergoes the oxidation reaction to form $C_xBr_3{\cdot}\delta Br_2$ with d_i of 0.70 nm.[27] For fluorine gas, intercalation at ambient temperature has been shown in the presence of liquid anhydrous HF to produce $C_xHF_2{\cdot}\delta HF$ (d_i = 0.60 nm). At higher temperatures (300-600°C), the reaction

with elemental fluorine can destroy delocalized-π system by forming covalent C-F bonds, resulting in the formation of fluorinated carbon compounds: $(CF)_n$ and $(C_2F)_n$.[28,29]

With the oxidizing class of metal/non-metal halides, graphite can react directly via the disproportionation of metal halides (e.g. $SbCl_5$, SbF_5 and AsF_5) as shown below.

$$3/2MX_5\ (g) + xC\ (s) \longrightarrow C_xMX_6\ (s) + 1/2MX_3\ (s) \qquad (1.7)$$

For a $C_xAsF_6 \cdot \delta AsF_5$ GIC, neutral species (AsF_5) will cointercalate but can be removed by pumping under vacuum, which eventually yields a C_xAsF_6 compound.[30] The gallery dimension is associated with the size of the MX_6^- octahedral intercalate, e.g. 0.95 nm for C_xSbCl_6, 0.85 nm for C_xSbF_6 and 0.76 nm for C_xAsF_6.[31–35] Additionally, the intercalation of non-oxidizing metal halides can be accomplished by adding an oxidant as illustrated in equation (1.8):

$$xC\ (s) + MCl_n\ (g) + 1/2Cl_2\ (g) \longrightarrow C_xMCl_{n+1}\ (s) \qquad (1.8)$$

where MCl_n is a non-oxidizing metal chloride (e.g. $AlCl_3$, $BiCl_3$ or $NiCl_2$).[36–38] Similar reactions can also proceed with transition-metal fluorides (e.g. VF_5, TaF_5 and NbF_5), or main-group fluorides (e.g. BF_3 and PF_5) with a presence of oxidant gas (Cl_2 or F_2) to produce C_xMF_{n+1}.[39–42] Some oxidizing metal fluorides (e.g. OsF_6, PtF_6 and IrF_6) directly react with graphite to form C_xMF_6 GICs (*see* equation 1.9).[43]

$$xC\ (s) + MF_6\ (g) \longrightarrow C_xMF_6\ (s) \qquad (1.9)$$

The gallery height of these latter GICs is about 0.8 nm, and the 'x' value varies depending on the stage number and the nature of the intercalate guest.

Another example is an acceptor-type GIC containing CrO_3. Refluxing the mixtures of graphite, CrO_3 and glacial acetic yielded a stage-3 $C_{13.6}CrO_3$ GIC (d_i = 0.79 nm).[44]

1.4.2 Donor-type GICs

In a reducing environment, donor-type intercalation compounds can be produced with several types of guests, including alkali metals, alkali earth metals, rare earth metals, and organic species. Both chemical and electrochemical methods have been employed in these syntheses.

1.4.2.1 Binary M-GICs

Alkali metal GICs have been widely studied since many are readily prepared by a vapor-phase reaction of alkali metal and graphite in a sealed tube at moderate temperatures (200-400°C). This direct method can give GIC products with well-defined single stage phases. The general formula of K-, Rb- and Cs-GICs is MC_8 for stage-1 and MC_{12n} for a higher stage when n is the stage number.[45,46] These gallery heights range from 0.535 to 0.594 nm depending upon the ionic diameter of intercalate cations (K^+ = 0.304 nm, Rb^+ = 0.332 nm, Cs^+ = 0.362 nm).[47] Lithium forms LiC_{6n} ($n \geq 1$) with d_i of 0.371 nm.[48] It is interesting that a low-stage Na-GIC has not been synthesized, but only high-stage phases are known with the composition NaC_{8n} (n = 4-8).[49] As described by Asher et al., a stage-8 NaC_{64} GIC was prepared by heating graphite powder with purified sodium at 400°C for 10 hours in a stainless steel crucible. The as-prepared

product showed a d_i value of 0.455 nm with a monolayer of Na intercalates.[50] At very low temperature (150°C) and long reaction time, Metrot et al. obtained a stage-4 compound mixed with unreacted graphite due to a low vapor pressure of metal. Pure binary phases of stage-6 and 7 NaC_{8n} were also observed at temperatures of 175°C and 235°C, respectively.[49] When compared with the other alkali metals, sodium intercalation into the graphite has proven elusive.

There are several previous papers discussing the relative stabilities of MC_x compounds. Boersma reported the relationship between the ionization energy of alkali metals and the molar free energy of formation of MC_x (M = K, Rb, Cs).[51] A linear correlation was observed for these with KC_x, RbC_x and CsC_x (stage 1-3, 5), all of which are energetically stable. Using the known ionization energies of Na and Li, they could predict molar free energies of NaC_x and LiC_x that indicated the instability of these compounds (stage 1-3). This conclusion may be valid for NaC_x, but in the case of LiC_x both LiC_6 (stage-1) and LiC_{12} (stage-2) are well known. A separate calculation on LiC_6 stability was reported by Kganyago et al. using a local-density functional theory (LDA-DFT) method.[52] The enthalpy of formation was determined to be -14.0 kJ/mol of Li, as compared with the experimental value of $\Delta H_{rxn,455\ K}$ -13.9±1.2 kJ/mol of Li, indicating a good agreement and confirming that the formation of LiC_6 is energetically favorable. Recently, Nobuhara et al. performed theoretical calculations on the stability of MC_x compounds (M = Li, Na, K; x = 6, 8, 12, 16, 36) using a first-principles method.[53] The formation energy (ΔE) was then used to estimate stabilities using:

$$\Delta E = E_{MC_x} - [E_{graphite} + E_M] \quad (1.10)$$

where E_{MC_x}, $E_{graphite}$ and E_M are total energies of the MC_x, graphite and alkali metal, respectively. The calculated results indicated that KC_x and LiC_x GICs are energetically stable for a whole range of 'x' while NaC_x is only stable at low Na content (x = 36). NaC_x with high concentrations of Na, specifically NaC_8 and NaC_6, were found to be unstable, in good agreement with experimental observations.

Under high pressure conditions, new phases of MC_x compounds, including NaC_x, are observed with a highly-dense alkali metal layer incorporated between graphene sheets. The limiting compositions of such superdense phases are MC_2 (M = Li, Na) and MC_4 (M = K, Rb, Cs). Several MC_x compounds were reported to form monolayer intercalates in the graphite galleries under high pressure. When the pressure decreases, these compounds are not stable and decompose by evolving an excess amount of alkali metal without significantly changing the gallery dimension, except for sodium which forms a bilayer structure.[54–56]

Additionally, alkali earth (Ca, Sr, Ba) and rare earth (Eu, Sm, Yb) elements can undergo a similar solid-vapor phase reaction, but at higher temperatures (400-500°C). Stage-1 compounds of these elements have compositions of MC_6 and the gallery dimensions are proportional to their ionic sizes (CaC_6; d_i = 0.460 nm, SrC_6; d_i = 0.494 nm, BaC_6; d_i = 0.525 nm, EuC_6; d_i = 0.486 nm, SmC_6; d_i = 0.503 nm and YbC_6; d_i = 0.457 nm).[57–59] Metal carbides, as well as unreacted graphite and metal, are always observed as impurities. Recently, a new flux-method was reported that avoids the

formation of carbide byproducts. Herold et al. reported the synthesis of pure and bulk MC_6 GICs (M = Ca, Ba, Eu) in molten Li-M based alloys with an appropriate atomic ratio of Li/M.[60–63] Reaction temperatures in a range of 350-450°C do not produce metal carbides. Two-step mechanisms are involved. Lithium intercalates first to pre-open the galleries, then the alloyed metal (M) progressively exchanges for lithium in a slow process, leading to a pure binary MC_6 compound. This mechanism is illustrated in Figure 1.4.

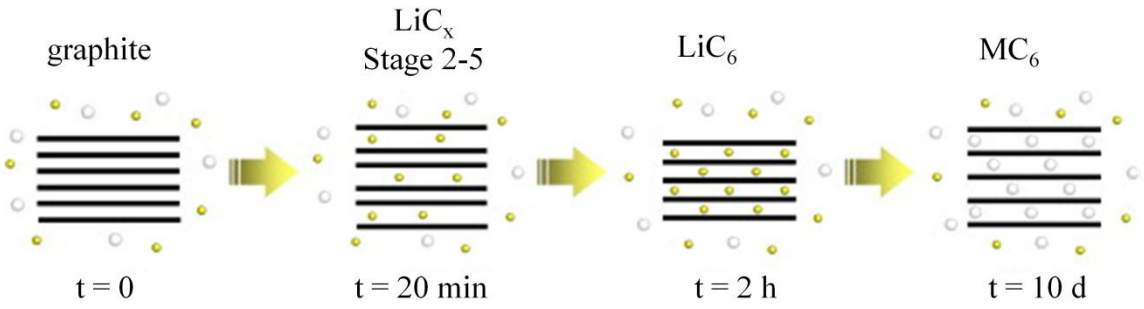

Figure 1.4 Two-step mechanism for the formation of MC_6 by a Li-M alloy reaction. This figure shows different phases during an intercalation process where graphite is placed in liquid Li-M alloys. The continuous lines and yellow and white balls represent graphene layers, lithium and alloyed metals, respectively.[61]

1.4.2.2 Ternary MM´-GICs or MY-GICs

Ternary GICs containing two metals can also be prepared. For example, $Na_2BaC_{7.5}$ was prepared by the reaction of a molten Na-Ba alloy and graphite. The observed d_i ~ 0.74 nm (Δd = 0.40 nm) is interpreted in terms of triple metallic intercalate

layers with two sodium planes encasing a barium plane.[64] Other ternary GICs with similar complex intercalate galleries, including more electronegative heteroatoms such as H, Cl, O, S, Se, Te, Hg, Bi and As, have been prepared in the presence of alkali metals (e.g. Na, K, Rb and Cs).[16,65,66] The structures are stabilized by heteroatom layers inserted between two positively charged alkali metal layers. In general, these structures show the layer stacking C - alkali metal - Y - alkali metal - C where Y is the heteroatom layer. For example, stage-1 $KH_{0.8}C_4$ was synthesized by reaction of H_2 gas with stage-1 KC_8. The structure contained K-H-K triple layers between graphene sheets with d_i of 0.85 nm as shown in Figure 1.5.[67]

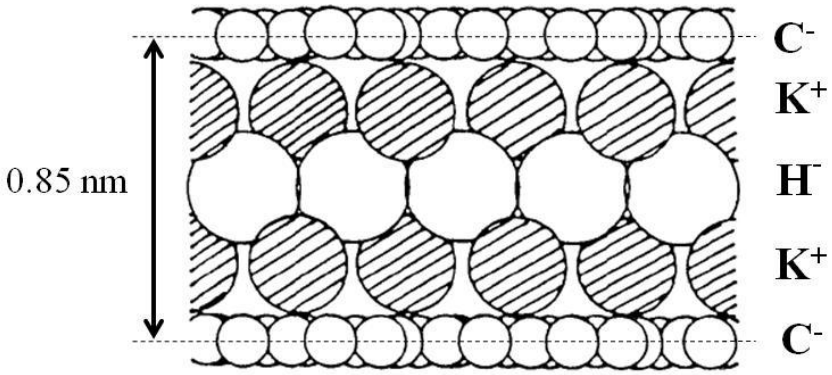

Figure 1.5 The multilayer structure of $KH_{0.8}C_4$.

1.4.2.3 Ternary solvated-M-GICs

Donor-type GICs with solvated cations have been well investigated and can be prepared via either chemical or electrochemical methods. GIC products may contain a

range of cations (e.g. alkali metals, alkali earth metals and rare earth metals) and solvating molecules as a co-intercalate species (e.g. amines, ethers, hydrocarbons and others). A wide variety of ternary $M(NH_3)_yC_x$ GICs have been prepared by interaction of graphite with metals dissolved in liquid ammonia:[68]

$$M\,(s) + yNH_3\,(l) + xC\,(s) \longrightarrow M(NH_3)_yC_x\,(s) \qquad (1.11)$$

Interestingly, the observed gallery dimensions (d_i ~ 0.66 nm) are relatively independent of the radius of M cations. This suggests that gallery dimension is mainly related to the size of NH_3, with the three-fold axis of NH_3 is slightly tilted from the graphene sheet to the stacking direction. These GICs are blue for stage-1 and grayish-blue for stage-2. Alternately, $M(NH_3)_yC_x$ GICs with well-defined stages can be electrochemically synthesized in a liquid ammonia solution of the corresponding metal.[69,70]

Besides NH_3, alkylamines have also been used to prepare solvated-cation ternary GICs. As recently reported by our group, a series of alkylamines with alkali metals can form ternary GICs by the one-pot solution method.[71–74] Different gallery arrangements and intercalate orientations were observed, including amine orientations parallel or perpendicular to graphene sheets, and monolayer or bilayers of intercalates. Similarly to NH_3, the alkylamines mainly determine the gallery dimensions. Monolayers of alkylamines show d_i of ~0.7 nm for parallel and 0.8-0.9 nm for perpendicular orientation. For bilayer intercalates, only a parallel orientation was observed with d_i about 1.1-1.3 nm. Results for selected M-alkylamine-GICs are summarized in Table 1.3 and their structural arrangements are illustrated in Figure 1.6.

Table 1.3 Summary of selected stage-1 ternay M-alkylamine-GICs

Intercalate arrangement	GICs	d_i (nm)
Parallel monolayer	$Li(n\text{-}C_3H_7NH_2)_{0.8}C_{16}$	0.70
	$Li(i\text{-}C_3H_7NH_2)_{0.4}C_{18}$	0.76
	$Na(n\text{-}C_4H_9NH_2)_yC_x$	0.70
	$Li(en)_{0.8}C_{15}$	0.68
	$Na(en)_{1.0}C_{15}$	0.69
Perpendicular monolayer	$Li(DAP)_{0.95}C_{14}$	0.81
	$Li(DMEDA)_yC_x$	0.91
Parallel bilayer	$Na(n\text{-}C_6H_{13}NH_2)_yC_x$	1.09
	$Na(n\text{-}C_8H_{17}NH_2)_{1.6}C_{40}$	1.09
	$Na(s\text{-}C_4H_9NH_2)_{1.6}C_{18}$	1.34
	$Na(i\text{-}C_4H_9NH_2)_{2.0}C_{28}$	1.28

en = ethylenediamine; DMEDA = *N*,*N*-dimethylethylenediamine; DAP = 1,2-diaminopropane

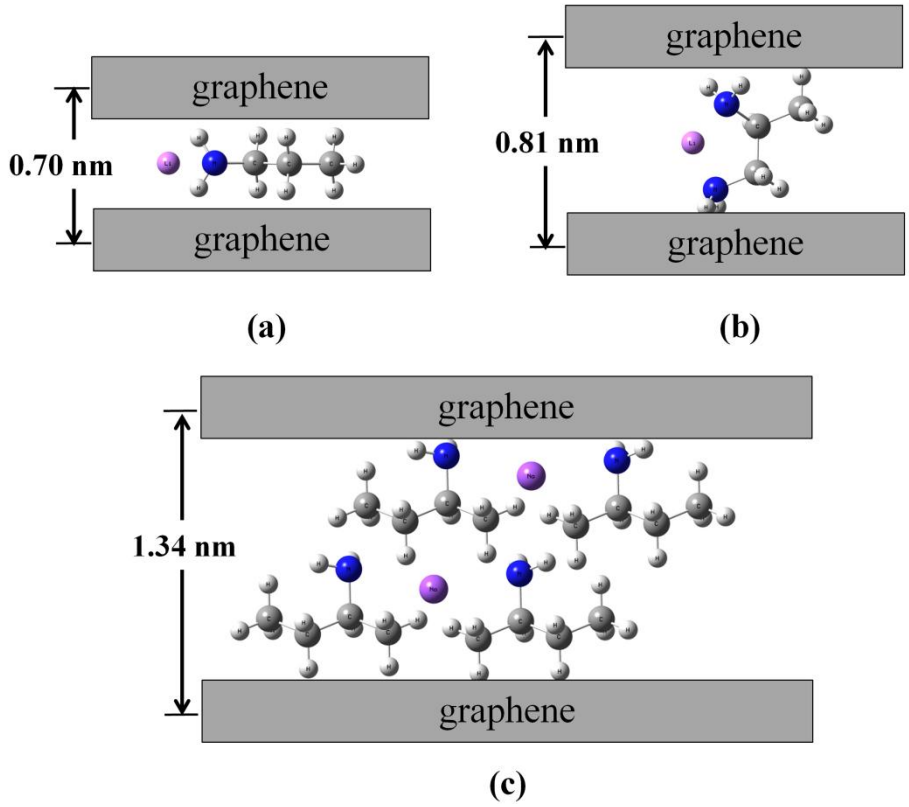

Figure 1.6 Structural arrangements of alkylamine in graphene sheets: (a) parallel monolayer, (b) perpendicular monolayer and (c) parallel bilayer.

Other polar organic molecules such as THF (tetrahydrofuran), furan, DMSO (dimethylsulfoxide) and DME (dimethoxyethane) are also known to form ternary GICs with alkali metals.[75–78] In some of these syntheses, polycyclic aromatic hydrocarbons such as naphthalene, phenanthracene, anthracene and biphenyl were added to assist in electron-transfer from metal to graphite.[79] The chemical and structural properties of $M(THF)_yC_x$ GICs have been investigated. They were prepared from the reaction of binary MC_x GICs either in liquid THF or under THF vapor. For example, $K(THF)_yC_{24}$

may show different orientations of $[K(THF)_y]^+$ intercalate complexes depending on the ratio of THF/K (y). THF molecules lie parallel to graphene sheets when the THF/K ratio was 1, yielding $K(THF)_1C_{24}$ with d_i of 0.716 nm. In $K(THF)_{2\text{-}3}C_{24}$, a perpendicular arrangement of THF was observed with a larger gallery height (d_i ~ 0.88 nm).[80] On the other hand, lithium formed a tetrahedral complex, $[Li(THF)_4]^+$, and required a larger gallery dimension (d_i ~ 1.24 nm).[81]

Ternary GICs that contains hydrocarbon molecules with a presence of alkali metal have also been described. These non-polar co-intercalates are incorporated via a reversible gas-solid physisorption reaction on binary MC_x GICs (M = alkali metal). For polar molecules, the driving force for intercalation is ion-dipole interactions that compensate for the electrostatic energy change due to gallery expansion. For non-polar cointercalates, weaker interactions between these cointercalates and ionic guests recur that driving force and lead to less expansion or stable ternary products. As a result, the intercalation process causes small increase of the gallery height compared to a starting binary MC_x GIC; i.e. $Cs(n\text{-pentane})_{1.0}C_{24}$ with d_i = 0.678 nm and $Cs(n\text{-hexane})_{0.9}C_{24}$ with d_i = 0.694 nm, (vs. stage-2 CsC_{24} with d_i = 0.594 nm).[82,83] Apparently, alkane cointercalates are only accommodated within confined galleries in a parallel orientation. A similar result was observed in the formation of stage-2 $Cs(ethylene)_{1.2}C_{24}$ with d_i of 0.675 nm.[84] However, in case of ternary GICs containing $[M(aromatic)_y]^+$ cations, the orientation of aromatic molecules was approximately perpendicular to the graphene sheets, which requires a large expansion. It was proposed that this structure is stabilized by ion-dipole interactions between negatively-charged graphene sheets and the aromatic

hydrocarbons. The compositions and gallery heights (in parentheses) of these stage-1 GICs are as follows; K(benzene)$_2$C$_{24}$ (0.931 nm), K(toluene)$_3$C$_{24}$ (0.908 nm) and K(o-xylene)$_2$C$_{24}$ (1.060 nm).[85–87]

1.4.2.4 Tetra-n-alkylammonium (NR_4^+ or TAA cations) GICs

This thesis primarily describes the intercalation of NR_4^+ cations into graphite. There are reports of this chemistry prior to the work described in this thesis. Those GICs were obtained by either electrochemical or chemical ion-exchange method. Following early work by Besenhard et al., the electrochemical reduction of graphite in DMSO-based electrolytes containing tetramethylammonium, $N(CH_3)_4^+$, salts was studied.[88–90] Cyclic voltammogram showed the reversible intercalation of solvated-$N(CH_3)_4^+$. The on-set potential of intercalation reduction is about -1.8 V (vs SCE). From a quantitative galvanostatic plot, the stoichiometric ratio of graphitic carbon (C_x) to $N(CH_3)_4^+$ intercalate was determined to follow a series of C_{24n}^-, where n is the stage number; C_{24}^- for stage-1, C_{48}^- for stage-2 and so on. The obtained GIC products were physically dull-black in color and extremely air-sensitive. Due to this instability, a phase mixture was usually obtained. The gallery dimension of $N(CH_3)_4C_{24n}\cdot\delta$DMSO was reported to be 1.25 nm, which could accommodate 6 DMSO-molecules per formula unit as estimated from the estimated area required per $N(CH_3)_4^+$, the observed gallery dimensions and the radius of $N(CH_3)_4^+$. Therefore, they authors proposed that the intercalate species was a regular octahedral complex of DMSO-solvated $N(CH_3)_4^+$.

Simonet et al. reported the electrochemical behavior of graphite in a DMF-based electrolyte using TAA salts.[91–95] A variety of TAA cations were used, including $(CH_3)_4N^+$, $(C_2H_5)_4N^+$, $(C_4H_9)_4N^+$, $(C_6H_{13})_4N^+$ and $(C_8H_{17})_4N^+$. The reversible charge-discharge reactions associated with intercalation and de-intercalation of TAA cations were clearly observed with a graphite reduction onset potential at -1.8 V (vs SCE). For larger cations, the volume of the graphite lattice was dramatically increased during intercalation and the chemical reversibility was lower owing to a large ion diffusion limit during de-intercalation. The step-wise galvanostatic charge plots suggested the formation of $(R_4N)C_x$ (R = methyl or butyl; x = 24, 48 and 96).

The formation of $(C_2H_5)_4N$-GIC has also been investigated in electrochemical capacitors with a graphite cathode. The graphite electrode exhibited a reversible$(C_2H_5)_4N^+$ intercalation/de-intercalation in both propylene carbonate (PC) and acetonitrile (AN)-based electrolytes containing $(C_2H_5)_4N$-salt.[96,97] The *in situ* PXRD showed disappearance of graphite phase and appearance of a new phase during reduction. However, the new reflection peaks were unindexed and the stage or gallery dimension of any GIC products obtained was not identified. In ionic liquid (IL)-based electrolytes containing trimethyl-n-hexylammonium cations, $(CH_3)(C_6H_{13})N^+$, the intercalation of cations into a graphite anode was suggested by *ex situ* PXRD and cyclic voltammetry.[98] PXRD results indicated the formation of a new GIC after reduction, with the appearance of a new peak at *d*-spacing ~0.37 nm. Interestingly, when the graphite electrode was oxidized, the new peak remained but decreased in intensity. This suggested that de-

intercalation of $(CH_3)(C_6H_{13})N^+$ was a slower reaction that did not proceed to completion.

Only few reports have described the formation of TAA-GICs via an ion-exchange reaction. Truong et al. demonstrated the ion exchange of stage 2+3 ternary Li-THF-GICs with TAA cations, such as $(CH_3)_4N^+$, $(C_2H_5)_4N^+$ and $(C_3H_7)_4N^+$, in THF.[99] However, the PXRD patterns of obtained products showed graphite, a remaining TAA salt, some impurity phases and a small broad peak ascribed to the TAA-GIC phase. The stage number and reflection indices of these GICs were not identified.

1.5 NR_4^+-INTERCALATION IN OTHER HOSTS

There are numerous studies on the intercalation of quaternary alkylammonium cations into layered hosts, especially in clay minerals, transition metal dichalcogenides, transition metal oxides, metal phosphates and graphite oxide. The major driving forces for intercalation include ion exchange reactions of interlayer exchangeable cations as well as host-guest and guest-guest interactions. X-ray diffraction has been used to demonstrate the interlayer expansion of host lattices and indicate the conformation and arrangement of intercalate species. Detailed structural and compositional characterizations are available for many of these compounds.

In clay minerals (e.g. smectites and vermiculites), a cation exchange reaction is typically conducted by mixing aqueous suspension of clay and TAA salt solution at a moderate temperature. An obtained product is called organoclay due to the development of organophilic properties. The general reaction can be expressed as follows:[100,101]

$$NR_4^+ + M^+\text{-clay} \rightleftharpoons NR_4^+\text{-clay} + M^+ \qquad (1.12)$$

where M^+ is an interlayer exchangeable cation, including proton (H^+). A quantitative ion exchange of the interlayer cations by NR_4^+ provides a method to determine layer charge density in a host lattice.[102] The arrangement of TAA cations within silicate layers depends on the ionic size of intercalate species and the surface layer charge density; alkylammonium cations with short-alkyl chain generally arrange in monolayers and those with longer alkyl chains arrange in bilayers parallel to silicate sheets, as shown in Figures 1.7(a) and (b). In highly-charged layer silicates, pseudo-trimolecular layers or paraffinic

structures of alkylammonium with long alkyl chains have been reported and can lead to very large interlayer expansions, as show in Figures 1.7(c) and (d).[103]

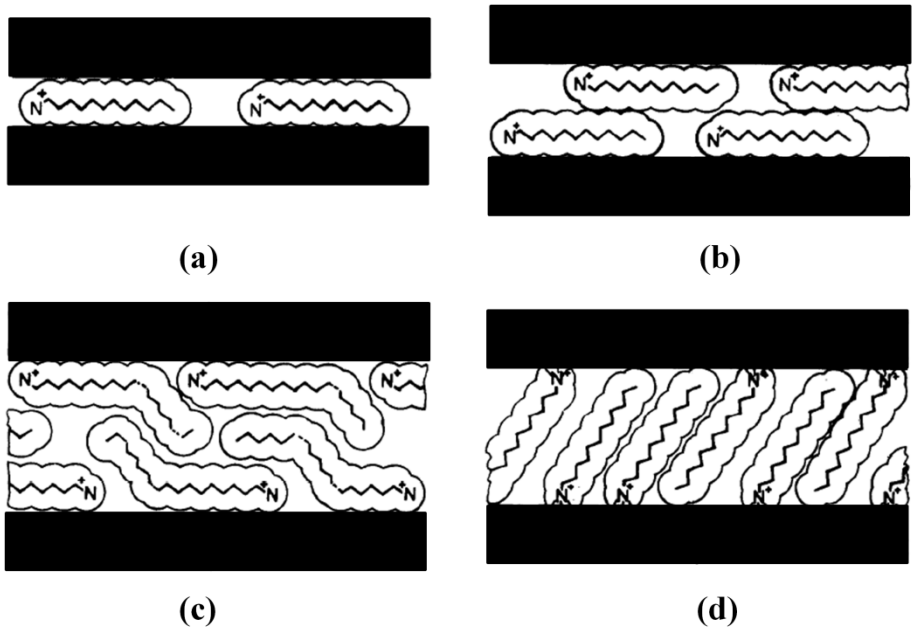

Figure 1.7 Arrangements of alkylammonium cations in the gallery of clay minerals: (a) monolayers, (b) bilayers and (c) pseudo-trimolecular layers and (d) paraffinic structures.

Several TAA cations, including symmetric and asymmetric alkyl groups such as $(C_nH_{2n+1})_4N^+$ (n = 1-8) and $[CH_3(CH_2)_{n-1}N(CH_3)_3]^+$ (n = 4, 8, 12, 16, 18), have been studied for intercalation.[104–107] Considering NR_4^+ with aliphatic alkyl chains, it is interesting to note that the gallery expansion of 0.4-0.5 nm for monolayers corresponds to a "flattened" conformation of the intercalates where the alkyl chains lie parallel to the clay sheet. The lattice enthalpy associated with a smaller lattice expansion should be

increased by such flattened intercalates. For a given charge density on silicate sheets, a monolayer-to-bilayer transition with 0.4-0.5 nm increments in the gallery thickness occurs when the area of TAA intercalates becomes larger than the equivalent area available in a monolayer arrangement. Besides offering more interlayer area, bilayer arrangements also provide van der Waals interactions between alkyl groups (chain-chain overlapping). For cations with very long alkyl chains (n > 8), the formation of pseudo-trimolecular layers and paraffinic structures has been observed with an interlayer expansion greater than 1 nm.

In the class of transition metal dichalcogenides, MoS_2 (which contains hexagonal MoS_2 sheets with a layer thickness of 0.62 nm) is a typical example for the study of TAA intercalation.[108] The general reaction involves MoS_2 reduction using a strong reductant such as n-butyllithium to form $LiMoS_2$, followed by cation exchange in aqueous TAA salt solution, as reported by Golub et al.[109] The arrangement of TAA cations between MoS_2 layers depends on the nature of the intercalate. As with the clay minerals, the observed interlayer expansion was about 0.5 nm in case of small TAA cations, $(C_nH_{2n+1})_4N^+$ (n = 1-3), indicating a monolayer arrangement with the compositions of $[(CH_3)_4N]_{0.29}MoS_2$, $[(C_2H_5)_4N]_{0.17}MoS_2$ and $[(C_3H_7)_4N]_{0.14}MoS_2$. For larger TAA cations ($n \geq 4$), bilayer and trilayer structures were formed with an interlayer expansion of 0.8 nm for $[(C_4H_9)_4N]_{0.15}MoS_2$ and $[(C_6H_{13})_4N]_{0.12}MoS_2$, and 1.2 nm for $[(C_{14}H_{29})(CH_3)_3N]_{0.19}MoS_2$, respectively. The paraffin-like structure, in which one long alkyl chain of the asymmetric TAA cations forms a bilayer perpendicular to the MoS_2

layers, was also observed with an interlayer expansion of 2.7 nm for $[(C_{16}H_{33})(CH_3)_3N]_{0.27}MoS_2$ and 2.9 nm for $[(C_{18}H_{37})(CH_3)_3N]_{0.25}MoS_2$.

Layered transition metal oxides provide another example of a host lattice known to intercalate TAA cations. Birnessite is two-dimensional layered manganese oxide that contains water molecules and alkali metal cations or protons in its interlayer space. The interlayer gallery dimension is about 0.7 nm for a hydrate monolayer.[110] TAA cations can be directly introduced into birnessite via an ion-exchange reaction. It is worth noting that aside from the TAA structure, as indicated above, the synthetic route and drying conditions can also impact the observed compositions and interlayer dimensions of the resulting products. Symmetric TAA cations, $(C_nH_{2n+1})_4N^+$ (n= 1-4), are typically employed to expand birnessite.[111–114] Unlike clay minerals and MoS_2, the organic cations intercalate with an undistorted conformation, resulting in a greater gallery expansion (0.46 nm for $(CH_3)_4N^+$, 0.67 nm for $(C_2H_5)_4N^+$, 0.84 nm for $(C_3H_7)_4N^+$ and 0.97 nm for $(C_4H_9)_4N^+$) and hydrate layers are retained in the products. $(CH_3)_4N^+$ exhibits the most hydrophilic nature and a stronger interaction with the negatively-charged manganese oxide layers as compared to the other intercalates. As a consequence, more $(CH_3)_4N^+$ cations and hydrate layers can intercalate into the host gallery. For the larger TAAs, the interaction is weaker due to an increase of hydrophobicity and only a monolayer of cations and mono- or bilayers of water molecules in the host gallery were observed.[115]

The layered titanates $H_{0.7}Ti_{1.825}\square_{0.175}O_4{\cdot}H_2O$ (□ is a vacant site) display a protonated lepidocrocite-type structure, and these can accommodate $(C_4H_9)_4N^+$ cations

into an interlayer gallery via the exchange of protons and $(C_4H_9)_4N^+$. An obtained product has an interlayer expansion about 0.81 nm, indicating the existence of a $(C_4H_9)_4N^+$ cation monolayer aligned along the C_2 rotational axis normal to titanate layers.[116] Likewise, $(C_4H_9)_4N^+$-intercalation compounds were also observed for layered protonic ruthenate, $H_{0.2}RuO_{2.1}{\cdot}nH_2O$, layered hexaniobate, $K_{4-x}H_xNb_6O_{17}$ and even protonated Ruddlesden-Popper tantalates and titanotantalates, $H_2[A_{x-1}B_xO_{3x+1}]$ (A = Na, Ca, Sr, La; B = Ta, Ti).[117–119]

Graphite oxide (GO) is a two-dimensional lamellar structure containing some functional groups such as hydroxyl, carbonyl and other groups with the interlayer dimension of 0.88 nm, including a hydrate monolayer of 0.27 nm. Similar to the other hosts described above, TAA-intercalated GO can be obtained via an ion-exchange reaction between acidic protons attached in the GO layers and TAA cations in aqueous solution. A systematic study of TAA intercalation, $(C_nH_{2n+1})_4N^+$ (n= 1-4), into GO showed that the interlayer expansion depends on the size of TAA cations. For example, $(CH_3)_4N$-intercalated GO provided an interlayer expansion of 0.95 nm, corresponding to monolayer of symmetric $(CH_3)_4N^+$ cations plus a water monolayer. In case of $(C_4H_9)_4N$-GO, monolayer of $(C_4H_9)_4N^+$ cations and hydrate bilayers can be accommodated into GO layers with the expansion of 1.2 nm.[120]

1.6 COMPARISON: NR_4^+ IN GRAPHITE AND IN OTHER HOSTS

As will be shown in this thesis, the synthesis of TAA-GICs via ion-exchange can proceed in stable organic solvents such as DMSO or DMF (*see* Chapters 2 and 3). Reactions in aqueous solution are not possible due to the very low chemical potential of donor-type GICs (which would reduce water), and reactions needs to be performed under inert atmosphere to prevent the oxidation by O_2 as well. The obtained TAA-GIC products show conformation changes and gallery arrangements that depend on ion size, as described above; i.e. monolayer for small TAA and bilayer for larger TAA, which is similar to intercalation of TAAs in clay minerals. No pseudo-trimolecular layers or paraffinic structures were observed in TAA-GICs, even in $(C_{18}H_{37})(CH_3)_3N^+$.

It is noteworthy that sheet charge densities on graphene layers may be variable, as in the layered metal dichalcogenides, and negative/positive charges can be delocalized over the pi-conjugated system. For example, $[(C_4H_9)_4N]C_{44}$ which has one negative charge per 44 carbon atoms (C_{44}^-) was prepared via the ion-exchange from $[Na(en)_{1.0}]C_{15}$ which has a higher charge density (C_{15}^-). In clays, sheet charge density is fixed and localized at a specific atom. As previously stated in Section 1.3, TAA-GICs show staging behaviors. For example, $[(C_5H_{11})_4N]C_x \cdot \delta$DMSO forms a stage-2 bilayer structure while other large TAAs provide stage-1 bilayer. Staging transitions may also limit the range of sheet charge densities by forming intercalate islands with a relatively constant extent of charge transfer.

1.7 CHARACTERIZATION TECHNIQUES

1.7.1 Powder X-ray diffraction (PXRD)

PXRD is a powerful tool for determining crystalline structures. Due to the preferred orientation of graphitic samples, only *(00l)* reflections are indexed in PXRD patterns of graphite and GIC samples are generally observed. The peak position (observed 2θ) directly provides a *d*-spacing value which can be used to determine the repeated distance (I_c) and the change of structural repeat dimensions due to an intercalation reaction. The PXRD data were collected on a Rigaku Miniflex II diffractometer with Ni-filtered Cu Kα radiation (0.1541 nm). Data were collected at 5°/min from 3° to 60° 2θ. The sample was prepared in an epoxy resin with a shallow cavity. The sample holder was sealed with cellotape to minimize air exposure and prevent sample decomposition during the X-ray measurement.

1.7.2 Thermalgravimetric analysis (TGA)

Thermal analysis is used to determine chemical characteristics of a sample based on mass loss due to volatilization and decomposition as a function of temperature. TGA data were obtained using a Shimadzu TGA-50 thermogravimetric analyzer under flowing Ar/O_2 (20 ml/min) at a heating rate of 10°C/min from ambient to 800°C. Samples were loaded in a Pt pan with approximate mass 7-10 mg. Step-wise data plotted were clearly

observed for TAA-GIC samples. Mass losses from each step were calculated to determine the amount of intercalate species.

The evolved gaseous products formed in TGA can be investigated by equipping the TGA with a mass spectrometer, a technique called TGA/MS. In this thesis, a TA Q-600 TGA equipped with a Hiden HPR-20 QIC mass spectrometer was employed to track the evolution of DMSO at m/z = 63 in flowing N_2 at a heating rate of 10°/min.

1.7.3 Capillary zone electrophoresis (CZE)

CZE is a useful tool to separate ionic or molecular species based on differences in their charge-to-mass ratio. The separation occurs in a homogeneous buffer solution and constant applied electric field throughout the length of a capillary. Our group developed this technique to analyze the identity and concentration of TAA cations, ethylenediamine (en) and Na^+ in solution after a displacement reaction (*see* equation 1.13).

$$[Na(en)_{1.0}]C_{15} + \underset{\text{(excess)}}{TAABr} \longrightarrow [TAA]_yC_x + \underbrace{Na^+ + en + (1\text{-}y)TAA^+}_{\text{CZE}} + Br^- \qquad (1.13)$$

Since the starting concentrations of each component are known, the extent of ion-exchange and composition of a solid $[TAA]_yC_x$ GIC product can be obtained. Although this constitutes an indirect measure, the obtained results are a valuable addition to TGA in determining GIC product compositions, especially where solvent co-intercalates are present.

CZE analyses were performed on an HP ^{3D}CE instrument equipped with a UV detector, using a 50 µm inner diameter, 56 cm long fused-silica capillary (47.5 cm to the detection window). A new capillary was sequentially conditioned by flushing with methanol (30 min), Milli-Q water (5 min), 1.0 M NaOH (30 min), Milli-Q water (5 min) and finally the background electrolyte (BGE) for 30 min. In order to remove an excess of Na ions remaining in a capillary after conditioned, the capillary was flushed with a copious amount of Milli-Q water, followed by a buffer solution until no Na^+ peak was detected prior to running a sample. And also, the capillary pre-treatment and post-treatment was set up as a sequence of Milli-Q water (3 min) and BGE (3 min) in between runs. Separation was accomplished using an applied voltage of +15 kV. The capillary was thermostatted at 30^{o}C and solutions were injected hydrodynamically at 50 mbar for 5 s. Indirect detection was employed with the detection wavelength set at 210 nm. The background electrolyte used was 15 mM imidazole, pH adjusted to 5.2 with glacial acetic acid.

A sample collected from the top phase solution was diluted into the appropriate concentration range. The diluted sample concentration was determined based on calibration curves of each component. The standard solutions were prepared using NaBr, TAABr and ethylenediamine as standard reagents and their concentrations range from 0.1 to 1.5 mM as shown in Figures 1.8.

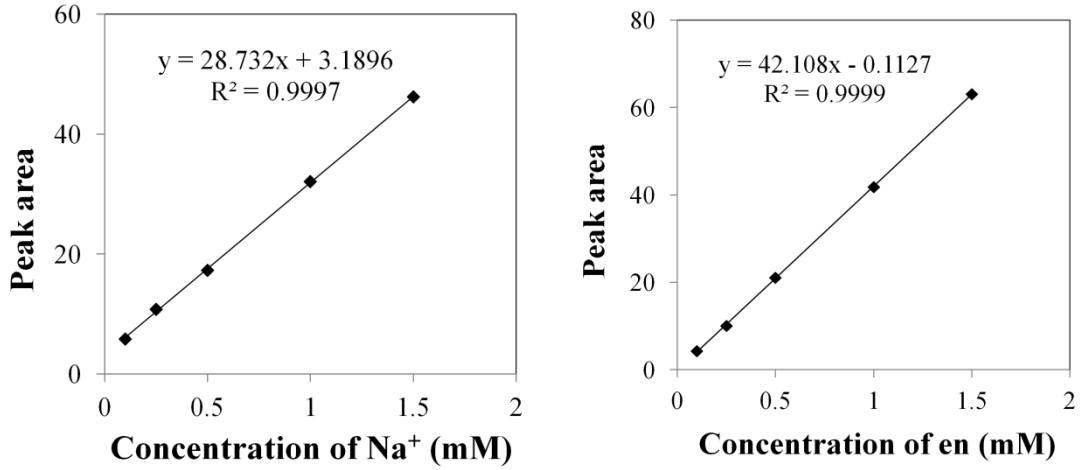

(a) (b)

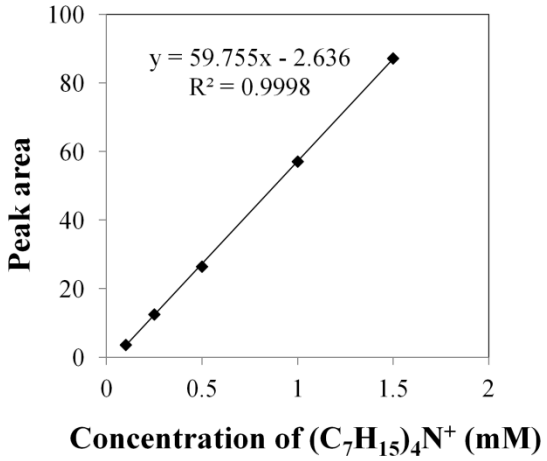

(c)

Figure 1.8 Typical calibration curves of the standard solution containing (a) Na^+, (b) ethylenediamine (en) and (c) $(C_7H_{15})_4N^+$.

1.7.4 Structural model calculations

The energy-minimized structures of intercalate species such as $(C_2H_5)_4N^+$, $(C_7H_{15})_4N^+$ and DMSO are calculated using the hybrid density functional method (B3LYP) with a 6-31G* basis set and the Gaussian 09W software. Due to the unusual flattened structure of TAA intercalates observed from the experimental result, energy minimization was applied only to the free ions. Calculations assumed that DMSO orients within graphite galleries to minimize gallery expansions and with the same conformation as for the isolate molecules.

One dimensional electron density maps for a centrosymmetric stage-1 bilayer $[(C_7H_{15})_4N]C_x{\cdot}\delta$DMSO cell were derived from the observed PXRD diffraction data using available 7 terms and the proposed structural model using 7 terms. The observed PXRD intensity data are used to generate structural factors after correction by a Lorentz-polarization (L_p) factor:

$$F_{obs}(00l) = \pm\left[I \times \left(\frac{\sin^2\theta\cos\theta}{1+\cos^2 2\theta} \right) \right]^{1/2} \tag{1.14}$$

where I is the integrated peak intensity from observed PXRD data.

For a model study, the calculated structural factors, F_{00l}, are obtained using:

$$F_{calc}(00l) = \sum f_i \cos(2\pi l Z_i) \tag{1.15}$$

where l is the Miller index,

Z_i is the fractional c-axis coordinate of each atom,

f_i is the angle-dependence scattering factor.

The electron density maps for both cases are then generated for z = 0-1, at increments of 0.004 using the following equation:

$$\rho(z) = \frac{1}{c}\left[F_0 + 2\sum F_{00l}\cos\left(\frac{2\pi}{z}\right)\right] \quad (1.16)$$

where z is the fractional coordinate of atoms along the c-axis,

c is the unit cell dimension,

F_o is the zeroth-order structural factor.

Structures are refined by minimizing the crystallographic R factor:

$$R = \frac{\sum\left|k|F_{00l}| - |F_{cal}(00l)\right|}{\sum k|F_{obs}(00l)|} \quad (1.17)$$

where k is an arbitrary scale factor.

It should be noted that the generated density maps are sufficient to confirm the existence of bilayer structures for many TAA cations, including cases where DMSO co-intercalates into the galleries. However, the compositional parameters (x and δ) of a $[(C_7H_{15})_4N]C_x{\cdot}\delta$DMSO GIC derived from structure refinements remained inconsistent with those obtained from CZE and TGA as described above. This mismatch may be due to the limited number of available PXRD peak intensities.

1.7.5 Other techniques

The surface morphology of graphite and obtained GICs is determined by a scanning electron microscope (SEM) recorded on a FEI QUANTA 600F environmental SEM fitted with tungsten filament. The operation voltage is 10 kV under high vacuum. The powder sample was spread on a carbon tape mounted on a SEM stub.

Raman spectroscopy is used to study a perturbation of the in-plane force constant on a graphite lattice when the GICs are formed. This phenomenon results in a G-band shift to higher frequency for reductive intercalation compared to 1582 cm^{-1} for G-band of pristine graphite. A Witech confocal Raman microscope was used to collect Raman spectra (resolution = 4 cm^{-1}) with a 514 nm laser source. A powder sample was simply deposited on a glass slide prior to measurement.

1.8 APPLICATIONS OF GICs

Most importantly for now, graphite intercalation chemistry is used as the negative electrode reaction in lithium ion batteries.[121] In these batteries, graphite is the active anode material and forms an intercalation compound with lithium during cell charge. The LiC_x product is kinetically stabilized by a solid electrolyte interphase (SEI) film derived from the controlled decomposition of organic electrolytes. In theory, the stage-1 LiC_6 compound formed generates a maximum Li storage capacity 372 mAh/g,[122] and in practical devices, reversible capacities (Q_{rev}) of about 340 mAh/g can be achieved. There is some loss due to SEI layer formation during the first charge, where some Li is irreversibly consumed.[123] The first charge and discharge potential curves for natural graphite in 1 M $LiClO_4$/EC+DEC are shown in Figure 1.9.

One interesting idea would be to reduce the charge loss by forming a protective surface layer on graphite prior to cell assembly. Recently, Verma et al. reported the chemical pretreatment on graphite (SFG6 from TIMCAL) surface by reacting with n-butyllithium. This modified graphite showed lower irreversible charge loss compared to untreated graphite, and avoided graphite exfoliation in a propylene carbonate (PC)-based electrolyte.[124]

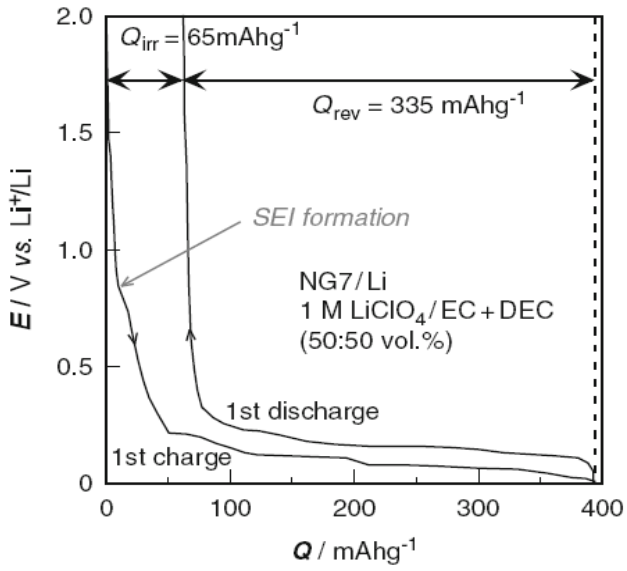

Figure 1.9 The first charge and discharge curves for natural graphite (NG7). (EC = ethylene carbonate, DEC = diethyl carbonate).[123]

Additionally, GICs are used as precursors in the syntheses of thermally exfoliated graphite and graphene nanosheets. Exfoliated graphite (EG) is used in several applications such as fire retardants, gas/oil adsorbents, thermal insulators, and gasket materials. A large-scale EG synthesis involves rapidly heating GICs, which causes the sudden vaporization or decomposition of intercalate species and the subsequent huge exfoliation of graphitic host in a perpendicular direction to the graphite sheets. The structure of obtained EG is a worm-like accordion that are expanded in thickness by up to 300 times from the initial GIC.[125] A wide variety of intercalates have been studied for thermal exfoliation of graphite such as H_2SO_4/HNO_3, Na-THF, K-THF, $FeCl_3$, $SbCl_5$, etc.[126–128] As recently reported by Truong et al., the exfoliation of natural graphite was also conducted on GICs containing TAA cations, $(C_nH_{2n+1})_4N^+$ (n = 1-3), using

microwave radiation.[99] They found that this GIC can expand to several mm particle thickness, especially $(CH_3)_4N$-GIC. However, their starting GICs were not single-phase compounds, and no structural and compositional data were reported.

Graphene is a two dimensional and one atom thick array of sp^2 carbon, and exhibits unique chemical and physical properties. Several synthetic strategies to scale up graphene production have been reported since 2004.[129] One promising method is the solution-phase exfoliation of GICs in polar organic solvents. Vallés et al. reported the use of ternary $K(THF)_xC_{24}$ as a precursor to produce a stable solution of negatively-charge graphene sheets by the sonication-free dissolution in *N*-methylpyrrolidone (NMP).[130] Another method involves the exfoliation of GICs by an electrochemical route. Graphite electrodes are markedly expanded in PC-based electrolytes containing Li salts under a high current density. This is ascribed to the incorporation of the Li^+-PC complex and formation of a ternary $Li(PC)_yC_x$ GIC. Few-layer graphene has been obtained by sonicating that expanded GIC in a DMF solvent.[131]

1.9 THESIS OVERVIEW

This thesis investigates the syntheses and characterization of donor-type graphite intercalation compounds (GICs) containing tetra-n-alkylammonium (TAA) cations. The central goal is to develop new synthetic routes via ion-exchange and to explore the structures of the obtained GICs. Electrochemical methods were also investigated to prepare new GICs and results compared to the chemical approach. A surface passivation model is proposed to describe the intercalation behavior and chemical properties observed for TAA-GICs.

Chapter 2 reports the synthesis of a new GIC containing tetra-n-butylammonium cation, $(C_4H_9)_4N^+$, using ion-exchange from a ternary Na-ethylenediamine (en)-GIC, $[Na(en)_{1.0}]C_{15}$. The single-phase stage-1 product is obtained with a gallery expansion (Δd) of 0.467 nm, requiring an unusual flattened orientation of $(C_4H_9)_4N^+$ intercalating species. The product composition is $[(C_4H_9)_4N]C_{44}$. In addition, the preliminary data of $(C_8H_{17})_4N^+$ intercalation is also reported.

Chapter 3 describes the preparation and characterization of a homologous series of TAA-GICs. The GICs are synthesized via the ion-exchange in dimethylsulfoxide (DMSO)-based solution. A wide variety of TAA cations were used such as symmetric $(C_nH_{2n+1})_4N^+$ (n = 1-8) and asymmetric $(C_{12}H_{25})(CH_3)_3N^+$, $(C_{18}H_{37})(CH_3)_3N^+$ and $(C_{18}H_{37})_2(CH_3)_2N^+$. The obtained stage-1 TAA-GICs contain either monolayer (Δd ~ 0.5 nm) or bilayer (Δd ~ 0.8 nm) of flattened TAA intercalates with a significant amount of DMSO co-intercalate for the bilayer arrangement. Additionally, the electron density map

was generated to show the existence of bilayer conformation of intercalate species by comparing the observed data vs. the proposed model.

Chapter 4 reports the electrochemical study of TAA-GICs using galvanostatic reduction and cyclic voltammetry in TAABr/DMSO electrolytes. The resulting products exhibit similar structures as reported in Chapter 3; $(C_4H_9)_4N^+$ forms a monolayer arrangement with the gallery expansion of 0.48 nm while the bilayer is found in larger TAA cations, $(C_nH_{2n+1})_4N^+$ (n = 5-8), with an expansion about 0.8 nm. Moreover, we also propose a passivation model to explain the enhanced stabilities of large TAA-GICs vs. small TAA-GICs.

In Chapter 5, we further investigate the effect of surface passivation on the preparation and stability of TAA-GICs. The GIC containing tetra-n-ethylammonium cations, $(C_2H_5)_4N^+$, was successfully prepared via chemical surface passivation of $[Na(en)_{1.0}]C_{15}$ with large TAA cations such as $(C_7H_{15})_4N^+$ or $(C_8H_{17})_4N^+$, followed by the ion-exchange to displace a $Na(en)^+$ complex with $(C_2H_5)_4N^+$. In addition, the enhanced stabilities of $(C_7H_{15})_4N$-GIC are also examined in different environmental conditions.

1.10 REFERENCES

(1) Whittingham, M. S.; Jacobson, A. J. *Intercalation Chemistry*; Academic Press: New York, 1982.

(2) Muller-Warmuth, W.; Schollhorn, R. *Progress in Intercalation Research*; Kluwer Academic Publishers: The Netherlands, 1994.

(3) Schollhorn, R. *Physica* **1980**, 99B, 89–99.

(4) Ouvrard, G.; Guyomard, D. *Curr. Opin. Solid State Mater. Sci.* **1996**, 1, 260–267.

(5) Schöllhorn, R. *Chem. Mater.* **1996**, 8, 1747–1757.

(6) Jacobson, A. J.; Nazar, L. F. Intercalation Chemistry. *Encycl. Inorg. Bioinorg. Chem.* **2011**, 1–37.

(7) O'Hare, D. In *Inorganic Materials*; Bruce, D. W.; O'Hare, D., Eds.; John Wiley & Sons, Ltd.: New York, 1992; pp. 165–235.

(8) Jacobson, A. J. In *Solid State Chemistry Compounds*; Cheetham, A. K.; Day, P., Eds.; Clarendon Press: Oxford, 1992; pp. 182–233.

(9) Barrer, R. M. *Zeolites and Clay Minerals*; Academic Press: New York, 1978.

(10) Gieseking, J. E. *Soil Sci.* **1938**, 47, 1–14.

(11) Sideris, P. J.; Nielsen, U. G.; Gan, Z.; Grey, C. P. *Science* **2008**, 321, 113–117.

(12) Kullberg, L.; Clearfield, A. *J. Phys. Chem.* **1981**, 85, 1585–1589.

(13) Clearfield, A.; Smith, G. D. *Inorg. Chem.* **1969**, 8, 431–436.

(14) Oriakhi, C. O.; Lerner, M. M. In *Handbook of Layered Materials*; Auerbach, S. M.; Carrado, K. A.; Dutta, P. K., Eds.; Marcel Dekker, Inc.: New York, 2004; pp. 509–539.

(15) Chung, D. D. L. *J. Mater. Sci.* **2002**, 37, 1475–1489.

(16) Enoki, T.; Suzuki, M.; Endo, M. *Graphite Intercalation Compounds and Applications*; Oxford University Press: New York, 2003.

(17) Boehm, H.; Setton, R.; Stumpp, E. *Pure Appl. Chem.* **1994**, 66, 1893–1901.

(18) Dresselhaus, M. S.; Dresselhaus, G. *Adv. Phys.* **2002**, 51, 1–186.

(19) Thomas, J. M.; Millward, G. R.; Schlogl, R. F.; Boehm, H. *Mat. Res. Bull.* **1980**, 15, 671–676.

(20) Ebert, L. B. *Annu. Rev. Mater. Sci.* **1976**, 6, 181–211.

(21) Metrot, A.; Fischer, J. E. *Synth. Met.* **1981**, 3, 201–207.

(22) Bottomley, M. J.; Parry, G. S.; Ubbelohde, A. R.; Young, D. A. *J. Chem. Soc.* **1963**, 5674–5680.

(23) Touzain, P. *Synth. Met.* **1979**, 1, 3–11.

(24) Savoskin, M. V.; Yaroshenko, A. P.; Whyman, G. E.; Mysyk, R. D. *J. Phys. Chem. Solids* **2006**, 67, 1127–1131.

(25) Horn, D.; Boehm, H. *Mater. Sci. Eng.* **1977**, 31, 87–89.

(26) Rüdorff, W.; Siecke, W.-F. *Chem. Ber.* **1958**, 91, 1348–1354.

(27) Sasa, T.; Takahashi, Y.; Mukaibo, T. *Carbon* **1971**, 9, 407–416.

(28) Mallouk, T.; Bartlett, N. *J. Chem. Soc. Chem. Commun.* **1983**, 103–105.

(29) Nakajima, T.; Watanabe, N.; Kameda, I.; Endo, M. *Carbon* **1986**, 24, 343–351.

(30) Hagiwara, R.; Tozawa, K.; Ito, Y. *J. Fluor. Chem.* **1998**, 88, 201–206.

(31) Clarke, R.; Elzinga, M.; Gray, J. N.; Homma, H.; Morelli, D. T.; Winokur, M. J.; Uher, C. *Phys. Rev. B* **1982**, 26, 5250–5253.

(32) Boolchand, P.; Bresser, W. J.; Mcdaniel, D.; Sisson, K.; Yeh, V.; Eklund, P. C. *Solid State Commun.* **1981**, 40, 1049–1053.

(33) Resing, H. A.; Vogel, F. L.; Wu, T. C. *Mater. Sci. Eng.* **1979**, 41, 113–119.

(34) Facchini, L.; Bouat, J.; Sfihi, H.; Legrand, A. P.; Furdin, G.; Melin, J.; Vangelisti, R. *Synth. Met.* **1982**, 5, 11–22.

(35) Okino, F.; Bartlett, N. *J. Chem. Soc. Dalt. Trans.* **1993**, 2081–2090.

(36) Bach, B.; Ubbelohde, A. R. *Proc. R. Soc. Lond. A. Math. Phys. Sci.* **1971**, 325, 437–445.

(37) Stumpp, E.; Wloka, K. *Synth. Met.* **1981**, 3, 209.

(38) Nicholls, J. T.; Speck, J. S.; Dresselhaus, G. *Phys. Rev. B* **1989**, 39, 10047–10055.

(39) Nakajima, T.; Matsui, T.; Motoyama, M.; Mizutani, Y. *Carbon* **1988**, 26, 831–836.

(40) Ravaine, D.; Boyce, J.; Hamwi, A.; Touzain, P. *Synth. Met.* **1980**, 2, 249–260.

(41) Mouras, S.; Hamwi, A.; Djurado, D.; Cousseins, J. C.; Fawal, Z.; Mohamad, A. H.; Dupuis, J. *J. Solid State Chem.* **1989**, 83, 115–120.

(42) Lerner, M.; Hagiwara, R.; Bartlett, N. *J. Fluor. Chem.* **1992**, 57, 1–13.

(43) Selig, H.; Vaknin, D.; Davidov, D.; Yeshurun, Y. *J. Chem. Soc. Chem. Commun.* **1985**, 1689–1690.

(44) Platzer, N.; de la Martiniere, B. *Bull. Soc. Chim. Fr.* **1961**, 1961, 177–180.

(45) Leung, S. Y.; Underhill, C.; Dresselhaus, G.; Krapchev, T.; Ogilvie, R.; Dresselhaus, M. S. *Solid State Commun.* **1979**, 32, 635–639.

(46) Underhill, C.; Krapchev, T.; Dresselhaus, M. S. *Synth. Met.* **1980**, 2, 47–55.

(47) Atkins, P.; Overton, T.; Rourke, J.; Weller, M.; Armstrong, F.; Hagerman, M. In *Shriver & Atkins' Inorganic Chemistry*; Oxford University Press: New York, 2010; pp. 3–33.

(48) Ohzuku, T.; Iwakoshi, Y.; Sawai, K. *J. Electrochem. Soc.* **1993**, 140, 2490–2498.

(49) Metrot, A.; Guerard, D.; Billaud, D.; Herold, A. *Synth. Met.* **1979**, 1, 363–369.

(50) Asher, R. C. *J. Inorg. Nucl. Chem.* **1959**, 10, 238–249.

(51) Boersma, M. A. M. *Catal. Rev. Sci. Eng.* **1974**, 10, 243–280.

(52) Kganyago, K. R.; Ngoepe, P. E.; Catlow, C. R. A. *Solid State Ionics* **2003**, 159, 21–23.

(53) Nobuhara, K.; Nakayama, H.; Nose, M.; Nakanishi, S.; Iba, H. *J. Power Sources* **2013**, 243, 585–587.

(54) Avdeev, V. V.; Nalimova, V. A.; Semenenko, K. N. *Synth. Met.* **1990**, 38, 363–369.

(55) Udod, I. A.; Orman, H. B.; Genchel, V. K. *Carbon* **1994**, 32, 101–106.

(56) Nalimova, V. A.; Guerard, D.; Lelaurain, M.; Fateev, O. V. *Carbon* **1995**, 33, 177–181.

(57) Makrini, M. E.; Guerard, D.; Lagrange, P.; Herold, A. *Physica* **1980**, 99B, 481–485.

(58) Guerard, D.; Chaabouni, M.; Lagrange, P.; Makrini, M. E.; Herold, A. *Carbon* **1980**, 18, 257–264.

(59) Makrini, M. E. L.; Gubrard, D.; Lagrange, P.; Herold, A. *Carbon* **1980**, 18, 203–209.

(60) Emery, N.; Hérold, C.; Lagrange, P. *J. Solid State Chem.* **2005**, 178, 2947–2952.

(61) Emery, N.; Hérold, C.; Lagrange, P. *Carbon* **2008**, 46, 72–75.

(62) Emery, N.; Hérold, C.; Bellouard, C.; Delcroix, P.; Mareche, J. F.; Lagrange, P. *J. Solid State Chem.* **2008**, 181, 2924–2929.

(63) Rida, H.; Cahen, S.; Hérold, C.; Lagrange, P. *Carbon* **2010**, 48, 3190–3195.

(64) Billaud, D.; Herold, A. *Bull. Soc. Chim. Fr.* **1978**, 3-4, 131–134.

(65) Hérold, A.; Mareche, J.-F.; Lelaurain, M. *Carbon* **2000**, 38, 1955–1963.

(66) Hérold, C.; Hérold, A.; Lagrange, P. *Solid State Sci.* **2004**, 6, 125–138.

(67) Enoki, T.; Miyajima, S.; Sano, M.; Inokuchi, H. *J. Mater. Res.* **1990**, 5, 435–466.

(68) Rudorff, W.; Schulze, E.; Rubisch, O. *Z. Anorg. Allg. Chem.* **1955**, 282, 232–240.

(69) Craven, W. E.; Ostertag, W. *Carbon* **1966**, 4, 223–226.

(70) Stumpp, E.; Alheid, H.; Schwarz, M.; Janssen, J.; Muller-Warmuth, W. *J. Phys. Chem. Solids* **1996**, 57, 925–930.

(71) Maluangnont, T.; Gotoh, K.; Fujiwara, K.; Lerner, M. M. *Carbon* **2011**, 49, 1040–1042.

(72) Maluangnont, T.; Bui, G. T.; Huntington, B. A.; Lerner, M. M. *Chem. Mater.* **2011**, 23, 1091–1095.

(73) Maluangnont, T.; Lerner, M. M.; Gotoh, K. *Inorg. Chem.* **2011**, 50, 11676–11682.

(74) Maluangnont, T.; Sirisaksoontorn, W.; Lerner, M. M. *Carbon* **2012**, 50, 597–602.

(75) Beguin, F.; Setton, R. *Carbon* **1975**, 13, 293–295.

(76) Jegoudez, J.; Mazieres, C.; Setton, R. *Carbon* **1986**, 24, 747–756.

(77) Okuyama, N.; Takahashi, T.; Kanayama, S.; Yasunaga, H. *Phys. B+C* **1981**, 105, 298–301.

(78) Duc, C. M.; Gole, J.; Mai, C.; Riviere, R. *J. Chim. Phys.* **1972**, 69, 991–&.

(79) Facchini, L.; Quinton, M. F.; Legrand, A. P. *Physica* **1980**, 99B, 525–530.

(80) Beguin, F.; Setton, R.; Hamwi, A.; Touzain, P. *Mater. Sci. Eng.* **1979**, 40, 167–173.

(81) Beguin, F.; Gonzalez, B.; Conard, J.; Estrade-szwarckopf, H.; Guerard, D. *Synth. Met.* **1985**, 12, 187–193.

(82) Beguin, F.; Pilliere, H. *Carbon* **1998**, 36, 1759–1767.

(83) Pilliere, H.; Goldmann, M.; Beguin, F. *J. Mater. Res.* **1993**, 8, 2288–2298.

(84) Takahashi, Y.; Oi, K.; Terai, T.; Akuzawa, N. *Carbon* **1991**, 29, 283–284.

(85) Beguin, F.; Setton, R.; Facchini, L.; Legrand, A. P.; Merle, G.; Mai, C. *Synth. Met.* **1980**, 2, 161–170.

(86) Isaev, Y. V.; Novikov, Y. N.; Vol'pin, M. E. *Synth. Met.* **1982**, 5, 23–30.

(87) Isaev, Y. V.; Novikov, Y. N.; Vol'pin, M. E.; Rashkov, I.; Panayotov, I. *Synth. Met.* **1983**, 6, 9–14.

(88) Besenhard, J. O.; Fritz, H. P. *J. Electroanal. Chem.* **1974**, 53, 329–333.

(89) Besenhard, J. O. *Carbon* **1976**, 14, 111–115.

(90) Besenhard, J. O.; Mohward, H.; Nickl, J. J. *Carbon* **1980**, 18, 399–405.

(91) Simonet, J.; Lund, H. *J. Electroanal. Chem.* **1977**, 75, 719–730.

(92) Bernard, G.; Simonet, J. *J. Electroanal. Chem.* **1979**, 96, 249–253.

(93) Bernard, G.; Simonet, J. *J. Electroanal. Chem.* **1980**, 112, 117–125.

(94) Berthelot, J.; Jubault, M.; Simonet, J. *J. Chem. Soc. Chem. Commun.* **1982**, 759–760.

(95) Simonet, J. *Electrochem. commun.* **2013**, 30, 17–20.

(96) Ruch, P. W.; Hahn, M.; Rosciano, F.; Holzapfel, M.; Kaiser, H.; Scheifele, W.; Schmitt, B.; Novak, P.; Kotz, R.; Wokaun, A. *Electrochim. Acta* **2007**, 53, 1074–1082.

(97) Wang, H.; Yoshio, M. *J. Power Sources* **2012**, 200, 108–112.

(98) Zheng, H.; Jiang, K.; Abe, T.; Ogumi, Z. *Carbon* **2006**, 44, 203–210.

(99) Truong, Q. T.; Pokharel, P.; Song, G. S.; Lee, D. S. *J. Nanosci. Nanotechnol.* **2012**, 12, 4305–4308.

(100) Weiss, A. *Angew. Chem. Int. Ed.* **1963**, 2, 134–144.

(101) Ogawa, M.; Kuroda, K. *Bull. Chem. Soc. Jpn.* **1997**, 70, 2593–2618.

(102) Lagaly, G. *Clay Miner.* **1981**, 16, 1–21.

(103) Lagaly, G. *Solid State Ionics* **1986**, 22, 43–51.

(104) Mercier, L.; Detellier, C. *Clays Clay Miner.* **1994**, 42, 71–76.

(105) Chun, Y.; Sheng, G.; Boyd, S. A. *Clays Clay Miner.* **2003**, 51, 415–420.

(106) Tamura, K.; Nakazawa, H. *Clays Clay Miner.* **1996**, 44, 501–505.

(107) Jaynes, W. .; Boyd, S. A. *Soil Sci. Soc. Am. J.* **1991**, 55, 43–48.

(108) Golub, A. S.; Protsenko, G. A.; Gumileva, L. V.; Buyanovskaya, A. G.; Novikov, Y. N. *Russ. Chem. Bull.* **1993**, 42, 632–634.

(109) Golub, A. S.; Zubavichus, Y. V.; Slovokhotov, Y. L.; Novikov, Y. N.; Danot, M. *Solid State Ionics* **2000**, 128, 151–160.

(110) Liu, J.; Durand, J. P.; Espinal, L.; Garces, L. J.; Gomez, S.; Son, Y. C.; Villegas, J.; Suib, S. L. In *Handbook of Layered Materials*; Auerbach, S. M.; Carrado, K. A.; Dutta, P. K., Eds.; Marcel Dekker, Inc.: New York, 2004; pp. 475–508.

(111) Brock, S. L.; Sanabria, M.; Suib, S. L.; Urban, V.; Thiyagarajan, P.; Potter, D. *J. Phys. Chem. B* **1999**, 103, 7416–7428.

(112) Nakayama, M.; Konishi, S.; Tagashira, H.; Ogura, K. *Langmuir* **2005**, 21, 354–359.

(113) Liu, Z.; Ooi, K.; Kanoh, H.; Tang, W.; Tomida, T. *Langmuir* **2000**, 16, 4145–4164.

(114) Omomo, Y.; Sasaki, T.; Wang, L.; Watanabe, M. *J. Am. Chem. Soc.* **2003**, 125, 3568–3575.

(115) Gao, Q.; Giraldo, O.; Tong, W.; Suib, S. L. *Chem. Mater.* **2001**, 13, 778–786.

(116) Sasaki, T.; Watanabe, M. *Mol. Cryst. Liq. Cryst.* **1998**, 311, 417–422.

(117) Fukuda, K.; Kato, H.; Sato, J.; Sugimoto, W.; Takasu, Y. *J. Solid State Chem.* **2009**, 182, 2997–3002.

(118) Shiguihara, A. L.; Bizeto, M. A.; Constantino, V. R. L. *Colloids Surfaces A* **2007**, 295, 123–129.

(119) Schaak, R. E.; Mallouk, T. E. *Chem. Mater.* **2000**, 12, 3427–3434.

(120) Liu, Z.; Wang, Z. M.; Yang, X.; Ooi, K. *Langmuir* **2002**, 18, 4926–4932.

(121) Ogumi, Z.; Wang, H. In *Lithium-Ion Batteries*; Yoshio, M.; Kozawa, A.; Brodd, R. J., Eds.; Springer: New York, 2009; pp. 49–73.

(122) Noel, M.; Santhanam, R. *J. Power Sources* **1998**, 72, 53–65.

(123) Ue, M. In *Lithium-Ion Batteries*; Yoshio, M.; Kozawa, A.; Brodd, R. J., Eds.; Springer: New York, 2009; pp. 75–115.

(124) Verma, P.; Sasaki, T.; Novak, P. *Electrochim. Acta* **2012**, 82, 233–242.

(125) Celzard, A.; Mareche, J. F.; Furdin, G. *Prog. Mater. Sci.* **2005**, 50, 93–179.

(126) Wei, T.; Fan, Z.; Luo, G.; Zheng, C.; Xie, D. *Carbon* **2009**, 47, 337–339.

(127) Falcao, E. H. L.; Blair, R. G.; Mack, J. J.; Viculis, L. M.; Kwon, C. W.; Bendikov, M.; Kaner, R. B.; Dunn, B. S.; Wuld, F. *Carbon* **2007**, 45, 1367–1369.

(128) Fu, W.; Kiggans, J.; Overbury, S. H.; Schwartz, V.; Liang, C. *Chem. Commun.* **2011**, 47, 5265–5267.

(129) Rao, C. N. R.; Sood, A. K.; Subrahmanyam, K. S.; Govindaraj, A. *Angew. Chem. Int. Ed.* **2009**, 48, 7752–7777.

(130) Valles, C.; Drummond, C.; Saadaoui, H.; Furtado, C. A.; He, M.; Roubeau, O.; Ortolani, L.; Monthioux, M.; Penicaud, A. *J. Am. Chem. Soc.* **2008**, 130, 15802–15804.

(131) Wang, J.; Manga, K. K.; Bao, Q.; Loh, K. P. *J. Am. Chem. Soc.* **2011**, 133, 8888–8891.

CHAPTER 2

PREPARATION AND CHARACTERIZATION OF A TETRABUTYL-AMMONIUM GRAPHITE INTERCALATION COMPOUND

Weekit Sirisaksoontorn, Adeniyi A. Adenuga,

Vincent T. Remcho and Michael M. Lerner

Department of Chemistry,

Oregon State University

Corvallis, OR 97331-4003, USA

J. Am. Chem. Soc. **2011**, 133, 12436-12438.

2.1 ABSTRACT

The intercalation of tetrabutylammonium (TBA) cations into graphite by cation exchange from a sodium-ethylenediamine graphite intercalation compound yields a single-phase first-stage product, C_{44}TBA, with a gallery expansion of 0.47 nm. The gallery dimension requires an anisotropic “flattened” cation conformation.

2.2 INTRODUCTION

Both anions and cations, including their solvated forms, can intercalate between graphene sheets via oxidation or reduction reactions, respectively, forming graphite intercalation compounds (GICs). A variety of applications for GICs have been proposed or realized, including use as gas physiosorbers,[1] battery electrodes,[2] highly conductive materials,[3] and exfoliation precursors.[4] The syntheses, compositions, and properties of a broad range of GICs containing different intercalate species have been studied. There are many practical and potentially scalable methods for synthesizing GICs from graphite involving chemical oxidants or reductants;[5-8] however, there are relatively few reports on the use of ion exchange or displacement reactions to form new GICs.[9]

The report of monolayer graphene by Geim *et al.* in 2004,[10] has spurred the search for a scalable route to graphene by solution-phase exfoliation of GICs. A likely strategy involves finding methods to intercalate large and low-charge-density ions into graphite. Tetraalkylammonium cations (TAAs) have been used extensively to modify or delaminate layered hosts,[11-14] including expanded graphite sulfate.[15]

The intercalation of TAAs in graphite has been previously described using electrochemical reduction in polar aprotic organic solvents which are stable against cathodic reduction,[16-20] e.g. DMF (*N*,*N*-dimethylformamide), 1,2-dimethoxyethane, dimethylsulfoxide (DMSO), or propylene carbonate. Besenhard *et al.* reported a first-stage GIC with DMSO-solvated tetramethylammonium (TMA) cations, $C_{24}TMA(DMSO)_6$, with a basal repeat distance of 1.582 nm.[16] The material was dull

black and highly air sensitive. Simonet *et al.* reported the electrochemical intercalation of TAAs in graphite, but did not obtain product structures or compositions.[19] Based on electroanalytical estimates, those GICs exhibited low intercalate contents, e.g. $C_{400-100}NR_4$.

In the following report, we describe a new exchange reaction where TBA cations rapidly displace a sodium-ethylenediamine $Na(en)_y^+$ cationic complex within graphene galleries. The resulting GIC shows increased gallery expansion, and the product composition is determined using thermogravimetric analysis (TGA) and capillary zone electrophoresis (CZE).

2.3 EXPERIMENTAL

Initially, the first-stage GIC was synthesized by combining Na metal (0.050 g) and graphite powder (0.250 g, SP-1 grade, average particle diameter 100 μm) in ethylenediamine (3 ml). The reaction mixture was continuously stirred at 60^{o}C for 24 h under an inert atmosphere. After separating the supernatant solution by centrifugation, the blue solid product was dried *in vacuo* at room temperature for 12 h. The exchange reaction was subsequently performed by addition of 0.1 M TBA bromide (0.064 g) to $C_{15}Na(en)_{1.0}$ (0.070 g) in DMF (2 ml). The reaction mixture was stirred at 60^{o}C for 1.5 h under an inert atmosphere. The black solid was separated from the supernatant solution by centrifugation and then dried *in vacuo* at 60^{o}C for 6 h. The top phase solution was diluted into DI water for CZE analysis (*see* Section 1.7.3)**.**

2.4 RESULTS AND DISCUSSION

Powder XRD patterns for the products obtained are shown in Figure 2.1. $C_{15}Na(en)_{1.0}$ (Figure 2.1b) exhibits the characteristic pattern of first-stage GICs with a basal repeat distance (I_c) of 0.671 nm. Subtracting the graphene sheet thickness (0.335 nm) gives an expansion (Δd) along the *c*-direction of 0.336 nm due to the intercalation of the Na-en cationic complex. We will later report further details on this GIC structure and composition. After the displacement reaction, the product is transformed into a GIC with I_c = 0.802 nm (Figure 2.1c), corresponding to a first-stage product with Δd = 0.467 nm.

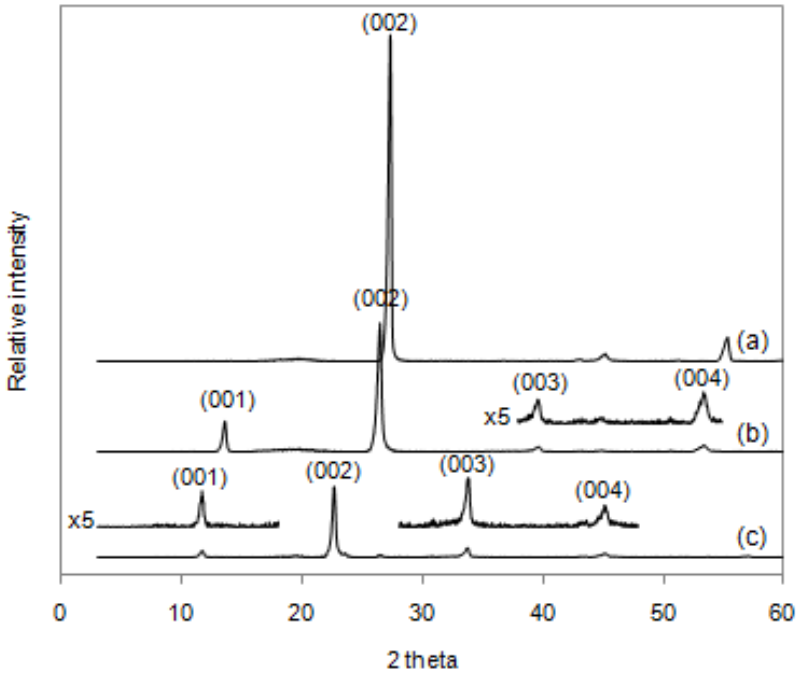

Figure 2.1 Powder XRD patterns of (a) graphite, (b) $C_{15}Na(en)_{1.0}$ and (c) $C_{44}TBA$.

Scanning electron micrographs (SEM) of graphite, $C_{15}Na(en)_{1.0}$, and $C_{44}TBA$ show the layered morphology retained for both GIC products, with the latter case showing evidence of increased particle delamination and curved edges. (Figure 2.2)

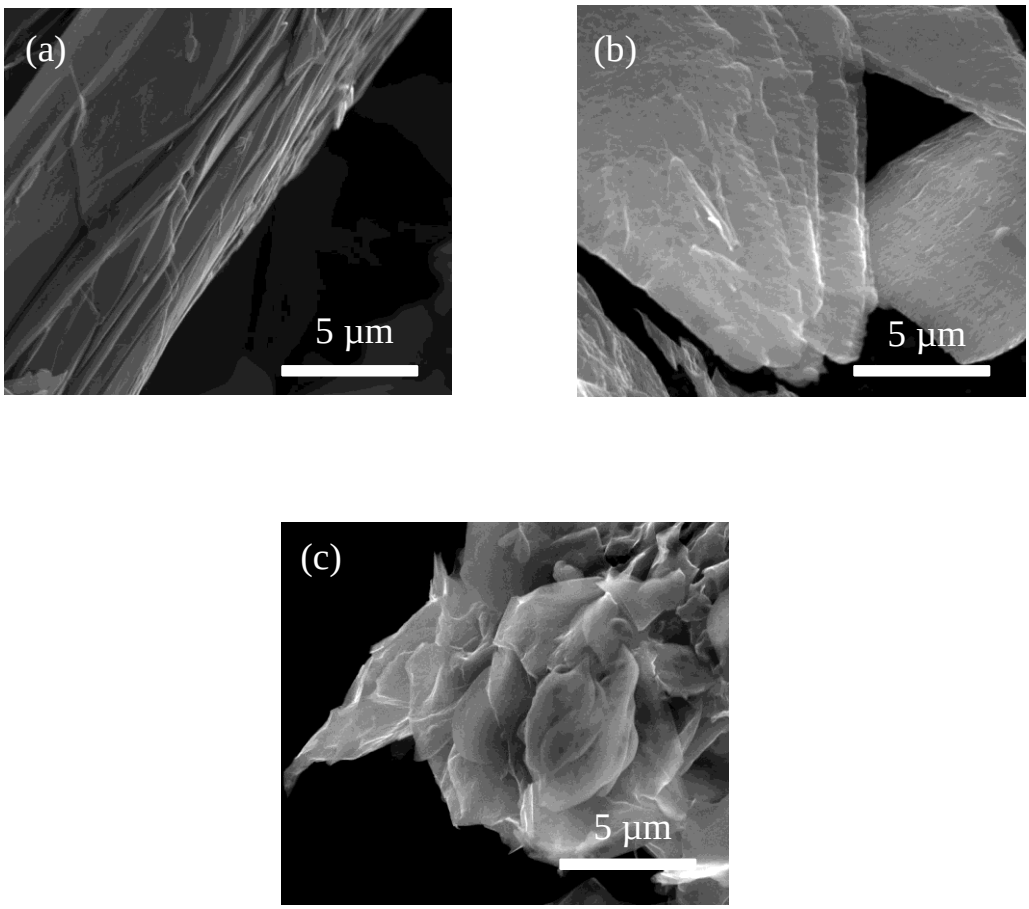

Figure 2.2 SEM images for (a) graphite, (b) $C_{15}Na(en)_{1.0}$ and (c) $C_{44}TBA$.

It is interesting to note that obtained $C_{44}TBA$ does not hydrolyze readily in air, or even in water (Figure 2.3). Because of this stability, it was not possible to fully digest

C_{44}TBA to graphite in order to obtain sample compositions. Instead, compositions were determined by following TBA displacement of $Na(en)^+$. Figure 2.4 shows the capillary electropherogram of the top phase solution following the displacement reaction. Three major solute components are separated by migration time; ethylenediamine, Na and TBA. The recoveries of en and Na from the starting GIC are approximately quantitative, 110 and 93 %, respectively (variation from 100% likely stems from a variability in starting GIC composition). The depletion of TBA from solution provides a product composition of C_{43}TBA. This closely agrees with thermogravimetric data as indicated below.

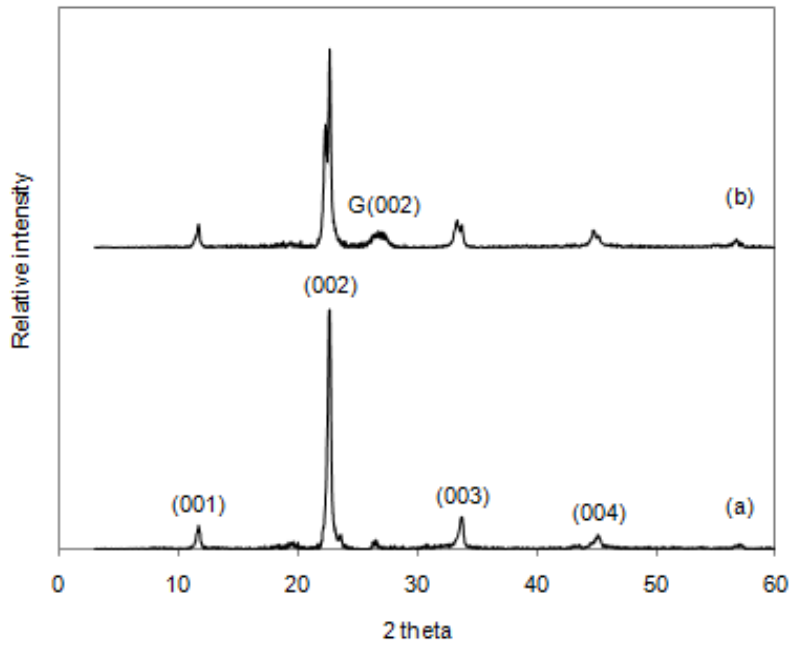

Figure 2.3 Powder XRD patterns of TBA-GIC (a) before and (b) after digestion in water at 50°C for 72 h.

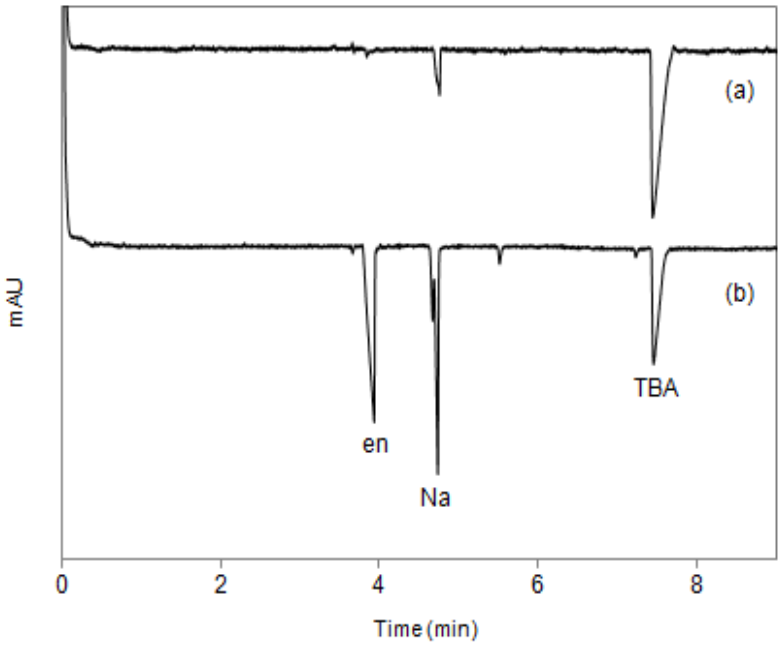

Figure 2.4 Capillary electropherograms of (a) the TBA solution before displacement and (b) the top phase solution following the displacement of TBA for $Na(en)^+$.

In order to further evaluate GIC compositions, thermal decomposition curves were obtained (Figure 2.5). Data obtained for graphite and TBA bromide are provided for comparison. $C_{15}Na(en)_{1.0}$ shows a mass loss at 50-150^oC (17.4 %) which is attributed to the volatilization of en (Figure 2.5b). $C_{44}TBA$ (Figure 2.5c) shows two prominent mass losses at 150-300^oC and 350-500^oC (total loss = 31.5 %) ascribed to the two-step thermolysis of the TBA intercalate. The two step mass loss has been observed previously for TBA[33] and for GICs with large intercalates.[6] These mass losses yield a product composition of $C_{44}TBA$. Graphite and all GICs begin to lose graphitic carbon mass above 600°C due to combustion by trace O_2 in the flow gas.

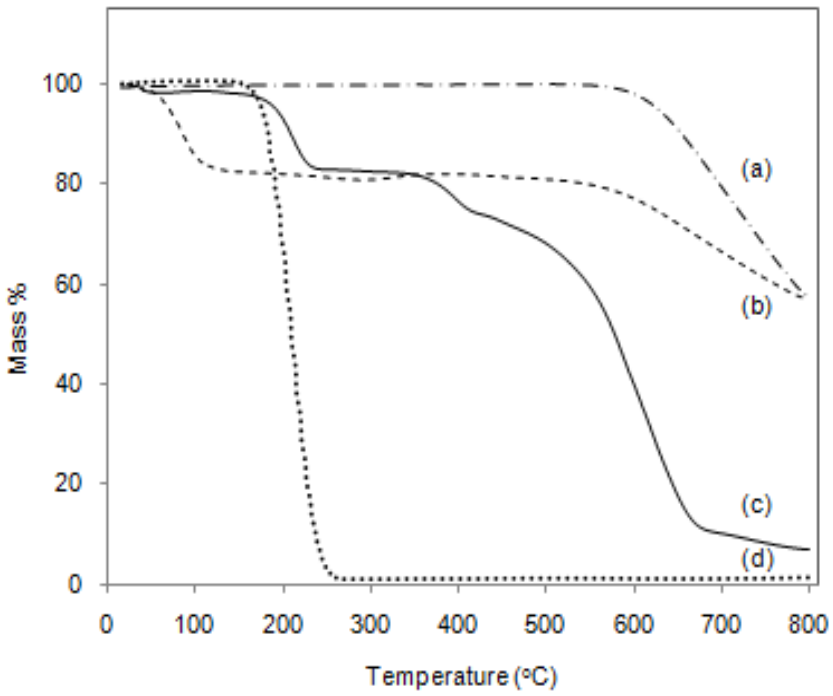

Figure 2.5 TGA curves of (a) graphite, (b) $C_{15}Na(en)_{1.0}$, (c) $C_{44}TBA$, and (d) TBA bromide salt.

As noted above, the gallery expansion associated with TBA intercalation is 0.467 nm. In clay minerals,[21-24] e.g. montmorillonite, smectite, or in metal oxide/sulfide layered structures,[25-32] e.g. MnO_2, $H_{0.2}RuO_{2.1}{\cdot}Nh_2O$, $Na_2Si_{14}O_{29}{\cdot}Xh_2O$, $H_{0.7}Ti_{1.825}\square_{0.175}O_4{\cdot}H_2O$, NbS_2, TiS_2, or TaS_2, the intercalation of TBA results in an expansion in the range of 0.72-0.91 nm. For example, Sasaki *et al.* showed that TBA intercalates in layered protonic MnO_2 align with C_2 axis normal to the host layers with a gallery expansion 0.84 nm.[11] Considering the crystallographic ionic diameter of TBA (≈0.99 nm),[31] an expansion of >0.8 nm requires only some nestling of intercalate into host sheet surfaces or minor distortion of the TBA conformation.

However, there are some previous reports of TBA intercalation with expansions comparable to those observed here for C_{44}TBA. Akçay reported a gallery expansion in montmorillonite of 0.49 nm,[33] and Golub *et al.* found that TBA uptake into MoS_2 under acidic conditions resulted in Δd = 0.52 nm.[34] Figure 2.6 compares an energy-minimized TBA conformation retaining high symmetry, and requiring a gallery expansion of ≈0.8-0.9 nm (a), and a lower-symmetry conformation requiring an expansion of only ≈0.4 nm. Gas-phase ion energy calculations show a relatively small difference for these conformations (<5 kJ/mol), in agreement with Luzhkov *et al.* who report a 3 kJ/mol difference for symmetric vs distorted TBA conformations.[35] These conformation energy differences can be offset by a greater lattice enthalpy associated with smaller lattice expansion. Two factors may tip the energetics in favor of less expansion for TBA in graphite, (1) the delocalization of charge density on graphene sheets, and (2) van der Waals interactions between the graphene sheets and nonpolar intercalates.

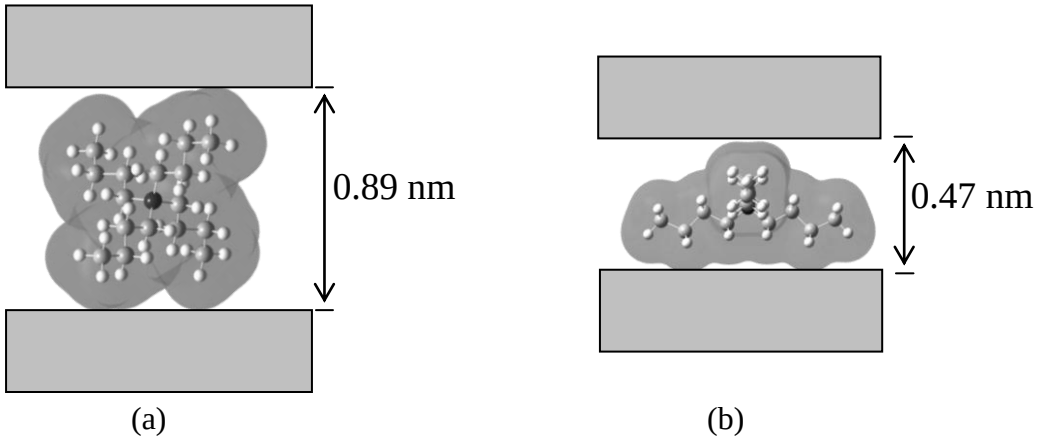

Figure 2.6 Different TBA conformations inside the graphene layers; (a) fully-tetrahedral and (b) flattened. The B3LYP with a 6-31G* basis set was used for energy optimization of the gas-phase cations.

The displacement method can be employed to prepare other new C_xNR_4 compounds. Using a displacing tetraoctylammonium (TOA) cation and similar procedures albeit longer reaction time, we have obtained a 2nd-stage C_xTOA (Figure 2.7). The gallery expansion is 0.44 nm, indicating that a flattened cation conformation is also adopted for TOA cations.

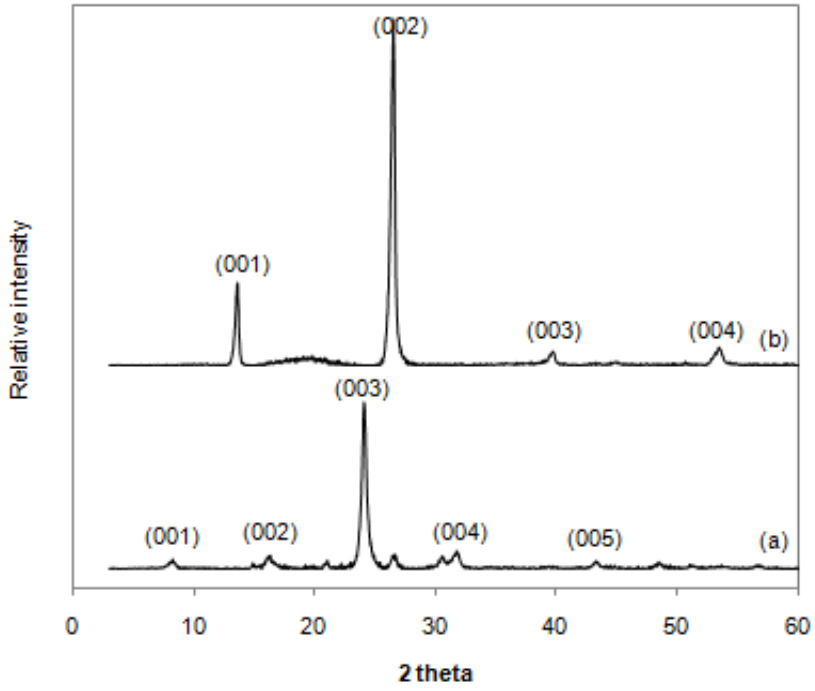

Figure 2.7 Powder XRD patterns of (a) 2nd-stage C_xTOA and (b) $C_{15}Na(en)_{1.0}$.

2.5 REFERENCES

(1) Purewal, J. J.; Keith, J. B.; Ahn, C. C.; Fultz, B.; Brown C. M.; Tyagi, M. *Phys. Rev. B.* **2009**, 79, 054305.

(2) Watanabe, N. *J. Fluorine Chem.* **1983**, 22, 205-230.

(3) Tsukamoto, J.; Matsumura, K.; Takahashi, T.; Sakoda, K. *Synth. Met.* **1986**, 131, 255-264.

(4) Malik, S.; Vijayaraghavan, A.; Erni, R.; Ariga, K.; Khalakhan, I.; Hill, J. P. *Nanoscale* **2010**, 2, 2139-2143.

(5) Özmen-Monkul, B.; Lerner, M. M.; Hagiwara, R. *J. Fluorine Chem.* **2009**, 130, 581-585.

(6) Maluangnont, T.; Bui, G. T.; Huntington, B. A.; Lerner, M. M. *Chem Mater.* **2011**, 23, 1091-1095.

(7) Katinonkul, W.; Lener, M. M. *Carbon* **2007**, 45, 2672-2677.

(8) Vallés, C.; Drummond, C.; Saadaoui, H.; Furtado, C. A.; He, M.; Roubeau, O.; Ortolani, L.; Monthioux, M.; Pénicaud, A. *J. Am. Chem. Soc.* **2008**, 130, 15802-15804.

(9) Isaev, Y. V.; Lenenko, N. D.; Gumileva, L. V.; Buyanovskaya, A. G.; Novikov, Y. N.; Stumpp, E. *Carbon* **1997**, 35, 563-566.

(10) Novoselov, K. S.; Geim, A. K.; Morozov, S. V.; Jiang, D.; Zhang, Y.; Dubonos, S. V.; Grigorieva, I. V.; Firsov, A. A. *Science* **2004**, 306, 666-669.

(11) Omomo, Y.; Sasaki, T.; Wang, L.; Watanabe, M. *J. Am. Chem. Soc.* **2003**, 125, 3568-3575.

(12) Tamura, K.; Nakazawa, H. *Clays Clay Miner.* **1996**, 44, 501-505.

(13) Shiguihara, A. L.; Bizeto, M. A.; Constantini, V. R. L. *Colloids Surf. A* **2007**, 295, 123-129.

(14) Liu, Z.; Wang, Z.; Yang, X.; Ooi, K. *Langmuir* **2002**, 18, 4926-4932.

(15) Li, X.; Zhang, G.; Bai, X.; Sun, X.; Wang, X.; Wang, E.; Dai, H. *Nature Nanotech.* **2008**, 3, 538-542.

(16) Besenhard, J.O.; Möhwald, H.; Nickl, J. J. *Carbon* **1980**, 18, 399-405.

(17) Besenhard, J. O. *Carbon* **1976**, 14, 111-115.

(18) Besenhard, J. O.; Fritz, H. P. *J. Electroanal. Chem.* **1974**, 53, 329-333.

(19) Simonet, J.; Lund, H. *J. Electroanal. Chem.* **1977**, 75, 719-730.

(20) Noel, M.; Santhanam, R. *J. Power Sources* **1995**, 56, 101-105.

(21) Ogawa, M.; Handa, T.; Kuroda, K.; Kato, C. *Chem Lett.* **1990**, 71-74.

(22) Chun, Y.; Sheng, G.; Boyd, S. A. *Clays Clay Miner.* **2003**, 52, 415-420.

(23) Mercier, L.; Detellier, C. *Clays Clay Miner.* **1994**, 42, 71-76.

(24) Nakayama, M.; Fukuda, M.; Konishi, S.; Tonosaki, T. *J. Mater Res.* **2006**, 21, 3152-3160.

(25) Nakayam, M.; Konishi, S.; Tagashira, H.; Oruga, K. *Langmuir* **2005**, 21, 354-359.

(26) Gao, Q.; Giraldo, O.; Tong, W.; Suib, S. L. *Chem. Mater.* **2001**, 13, 778-786.

(27) Fukuda, K.; Kato, H.; Sato, J.; Sugimoto, W.; Takasu, Y. *J. Solid State Chem.* **2009**, 182, 2997-3002.

(28) Sasaki, T.; Watanabe, M. *Mol. Cryst. Liq. Cryst.* **1998**, 311, 417-422.

(29) Sasaki, T.; Watanabe, M. *J. Am. Chem. Soc.* **1998**, 120, 4682-4689.

(30) Peng, S.; Gao, Q.; Du, Z.; Shi, J. *Apply Clay Sci.* **2006**, 31, 229-237.

(31) Rao, B. L. M.; Halbert, T. R. *Mat. Res. Bull.* **1981**, 16, 919-922.

(32) Kanzaki, Y.; Konuma, M.; Matsumuto, O. *J. Phys. Chem. Solids* **1980**, 41, 525-529.

(33) Akçay, M. *J. Colloid Interface Sci.* **2006**, 296, 16-21.

(34) Golub, A. S.; Zubavichus, Y. V.; Yu, L.; Novikov, Y. N.; Danot, M. *Solid State Ionics* **2000**, 128, 151-160.

(35) Luzhkov, V.B.; Österberg, F.; Acharya, P.; Chattopadhyaya, J.; Åqvist, J. *Phys. Chem. Chem. Phys.* **2002**, 4, 4640-4647.

CHAPTER 3

PREPARATION OF A HOMOLOGOUS SERIES OF TETRAALKYL-AMMONIUM GRAPHITE INTERCALATION COMPOUNDS

Weekit Sirisaksoontorn and Michael M. Lerner

Department of Chemistry

Oregon State University

Corvallis, OR 97331-4003, USA

Inorg. Chem. **2013**, 52, 7139-7144.

3.1 ABSTRACT

Graphite intercalation compounds (GICs) of a series of symmetric or asymmetric tetraalkylammonium (TAA) intercalates are obtained from stage-1 $[Na(en)_{1.0}]C_{15}$ via cation exchange. The prepared dull-black TAA-GICs contain either flattened monolayer or bilayer galleries, with significant cointercalation of the dimethylsulfoxide (DMSO) solvent in the bilayer galleries. The TAA-GIC products obtained are characterized by X-Ray diffraction and related structural modeling, compositional analyses, and Raman spectroscopy. $[(C_4H_9)_4N]C_{43}$ is obtained as a pure stage-1 GIC with the flattened monolayer structure. The larger symmetric TAA cations; $(C_6H_{13})_4N$, $(C_7H_{15})_4N$, $(C_8H_{17})_4N$, and the asymmetric TAA cations; $(C_{12}H_{25})(CH_3)_3N$, $(C_{18}H_{37})(CH_3)_3N$, $(C_{18}H_{37})_2(CH_3)_2N$ all form pure stage-1 GICs with flattened bilayer conformations. Thermogravimetric analyses combined with mass spectrometry and elemental analyses indicate the presence of ~1-2 DMSO cointercalates per bilayer cation. The intercalate layers in these TAA-GICs have expansions along the stacking direction of ~0.40 nm. Raman data confirm the low graphene sheet charge densities in the obtained TAA-GICs

3.2 INTRODUCTION

Graphite has been long studied as an intercalation host and shows some unique aspects.[1-3] Graphite intercalation compounds (GICs) consist of host graphene layers and intercalate guests; either donor or acceptor-type compounds can be prepared by reduction or oxidation of the graphene sheets, respectively.[4-11] This redox intercalation can be performed by either chemical or electrochemical methods, and a wide range of atomic or molecular ions, often accompanied by neutral co-intercalate molecules, are known to act as intercalate guests.[12-17] The ordered sequencing of intercalate and graphene sheets perpendicular to the stacking direction is known as "staging" in common for GICs,[18,19] and while known, it is rarely observed with other layered hosts.[20] The highest intercalate contents are for stage-1 GICs, where all graphene sheets are separated by intercalate layers. Important applications for GICs and the associated chemistries include reversible energy storage in Li-ion battery anodes,[21,22] use as reducing agents[23] or gas/liquid absorbers,[24-26] and as precursors to exfoliated graphite or graphene.[27-31]

Our group has previously reported new donor-type GICs containing a wide range of alkali metal-amine intercalate complexes.[32-35] These GICs were prepared using a direct chemical approach where alkali metals and amines are simply combined with graphite under appropriate conditions. The arrangements and orientations of intercalates in the resulting GICs depend on both the alkali metal cation and the amine. For example, in $[Na(n\text{-}C_3H_7NH_2)_{0.7}]C_{16}$ the intercalate complexes are arranged as a monolayers with long molecular axes parallel to the encasing graphene layers.[32] Amine intercalates with longer alkyl substituents, such as in $[Na(s\text{-}C_4H_9NH_2)_{1.6}]C_{18}$, form intercalate bilayers, again with

long molecular axes parallel to the graphene sheets.[32] Earlier studies on alkylammonium intercalation in graphite have employed electrochemical reduction in aprotic polar solvents.[16, 36-41] Recently, our group reported a new chemical method for the preparation of a GIC containing tetrabutylammonium cations, by reaction in *N*,*N*-dimethylformamide (DMF) to displace the $Na(en)^+$ intercalate in $[Na(en)_{1.0}]C_{15}$ (en = ethylenediamine).[42] In that study, a stage-1 $[(C_4H_9)_4N]C_{44}$ GIC was obtained with a highly-flattened intercalate monolayer and gallery expansion of 0.47 nm. We proposed that this cation conformation results from the large lattice enthalpies in GICs that strongly favor minimal expansion upon intercalation. No other tetraalkylammonium (TAA) GICs could be obtained using this approach.

The intercalation of alkylammonium ions via ion exchange has been widely studied for several layered hosts, along with detailed structural characterization of the resulting materials.[43-47] Highly flattened conformations have been observed previously. [48-51] For example, in smectite clays, a structural evolution from monolayer to bilayer to pseudo-trilayer galleries is observed for increasing size of symmetric alkylammonium cations.[52,53] The intercalate monolayers showed an interlayer expansion of ~0.5 nm relative to the anhydrous host, requiring that the alkyl chain substituents lie parallel to the clay layers and that the cations have a flattened conformation. The interlayer spacing increases by an additional 0.4-0.5 nm for each added cation layer. Flattened monolayers of ~0.5 nm thickness were also observed in MoS_2, rectorite and montmorillonite compounds with asymmetric alkylammonium intercalates.[54-56] These very small interlayer dimensions are at the steric limit of an alkylammonium headgroup.

In the present work, we report the first preparation of a homologous series of symmetric or asymmetric tetra-*n*-alkylammonium GICs (TAA-GICs) by adapting the previously reported method, and characterize structures and compositions of the GICs obtained.

3.3 EXPERIMENTAL

Materials. Graphite powder (SP-1 grade, average diameter 100 μm) was used as received from Union Carbide, Inc. Ethylenediamine (99%), dimethylsulfoxide (AR grade, 99.9%), acetonitrile (HPLC grade, 99.9%) and anhydrous methanol (99.9%) were dried over a 4 Å molecular sieve prior to use. All tetraalkylammonium cations were obtained as bromide salts with a purity >98% and were used as received.

Syntheses. $[Na(en)_{1.0}]C_{15}$ (en = ethylenediamine) was prepared according to a previously reported reaction:[33] 20 mmol of graphite (240 mg) and 2 mmol of sodium metal (50 mg) were added to 3 ml of ethylenediamine and continuously stirred at 60°C for 24 h under an inert atmosphere. After separating the supernatant solution by centrifugation, a blue solid product was dried *in vacuo* overnight at room temperature. The product was characterized by PXRD and TGA, and used as a reagent for subsequent reactions.

For the ion exchange reactions with smaller TAA cations (e.g. $(CH_3)_4N$, $(C_2H_5)_4N$, $(C_3H_7)_4N$, $(C_4H_9)_4N$, and $(C_{12}H_{25})(CH_3)_3N$), 2 ml of dimethylsulfoxide (DMSO) was added to a reaction tube containing 0.30 mmol of $[Na(en)_{1.0}]C_{15}$ and 0.20 mmol of the alkylammonium bromide salt. The exchange was carried out at 60°C for 10 min under an inert atmosphere. Next, the mixture was centrifuged for 5 min and the top liquid phase removed by syringe. The wet product was washed with acetonitrile and then anhydrous methanol to remove soluble byproducts and excess alkylammonium salt. The GIC product was dried *in vacuo* overnight at ambient temperature. The reactant solution and

rinse solvents were collected, combined and later analyzed to quantify the extent of the exchange.

The same synthetic procedure was employed for the larger TAA cations (e.g. $(C_5H_{11})_4N$, $(C_6H_{13})_4N$, $(C_7H_{15})_4N$, $(C_8H_{17})_4N$, $(C_{18}H_{37})(CH_3)_3N$, and $(C_{18}H_{37})_2(CH_3)_2N$), except that the products were rinsed only with anhydrous methanol, and were dried at 60°C for 6 h.

Characterization. Powder X-ray diffraction (PXRD) patterns were recorded using a Rigaku Miniflex II diffractometer with Ni-filtered Cu K_α radiation (λ = 0.15406 nm). All measurements were collected in the 2θ range from 3° to 60° at a scan speed of 5°/min. The relationship of the gallery height (d_i), repeat distance along c-axis (I_c), and stage number (n) is given by:

$$I_c = d_i - 0.335(n-1) \qquad (3.1)$$

where 0.335 nm corresponds to the thickness of a single graphene sheet. The interlayer expansion (Δd) refers to the difference between the gallery height of the GIC and the thickness of a single graphene sheet (i.e. $\Delta d = d_i - 0.335$ nm).

A Shimadzu TGA-50 thermogravimetric analyzer (TGA) was used to study the thermal behavior of GICs under flowing Ar/O_2 (20 ml/min) at a heating rate of 10°C/min from ambient up to 800°C. A TA Q-600 TGA equipped with a Hiden HPR-20 QIC mass spectrometer was employed to track the evolution of DMSO at m/z = 63 in flowing N_2 at the same heat heating rate. CHN and S elemental analyses were performed by Micro-Analysis, Inc. (Wilmington, DE). A Witech confocal Raman microscope was used to

collect Raman spectra (resolution = 4 cm^{-1}) with a 514 nm laser source. Capillary zone electrophoresis (CZE) analyses were performed on a HP ^{3D}CE instrument according to a previously-described method.[42]

Energy-minimized structural models and mapped electron density surfaces for the "flattened" and "undistorted" conformations of the selected $(C_7H_{15})_4N$ cation and DMSO molecule were calculated using the hybrid density functional method (B3LYP) with a 6-31G basis set and the Gaussian 09W software.

One-dimensional electron density maps were generated from a centrosymmetric stage-1 cell in comparison between the observed PXRD data sets and the calculated structure models. The methodology has been described in detail previously.[11]

3.4 RESULTS AND DISCUSSION

For larger TAA cations, the generation of a series of single-phase, stage-1 TAA-GICs can be accomplished via cation exchange as illustrated in Figure 3.1, where the $Na(en)^+$ cationic complex is displaced by TAA cations. For most of these reactions, the cation exchange occurs rapidly at moderate temperatures in a DMSO solvent. The color of all the obtained GICs is dull black, as compared to the bright blue $[Na(en)_{1.0}]C_{15}$ reactant.

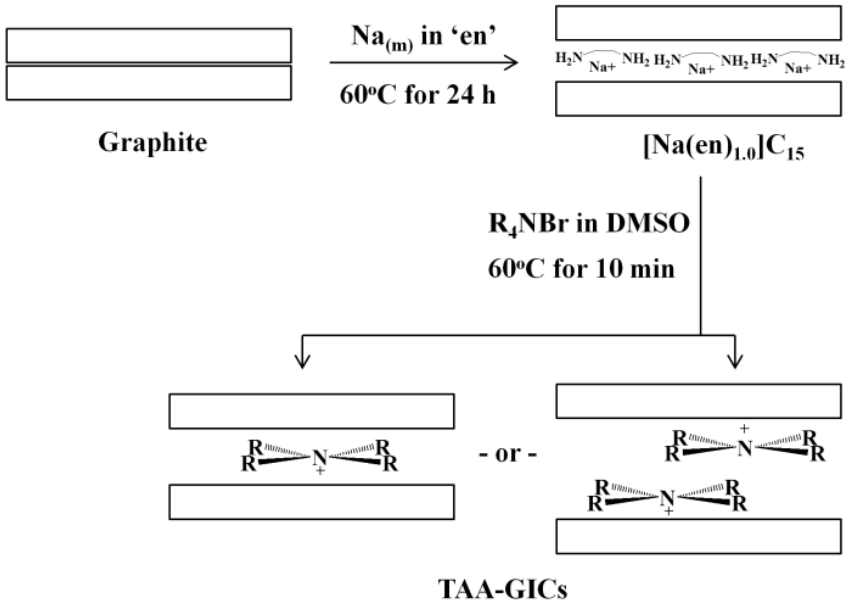

Figure 3.1 Synthetic route to TAA-GICs.

The PXRD patterns obtained for the reactant $[Na(en)_{1.0}]C_{15}$ and the TAA-GIC products are shown in Figure 3.2. $[Na(en)_{1.0}]C_{15}$ (Figure 3.2a) displays a highly-ordered stacking arrangement with d_i = 0.691 nm. As reported previously, this gallery expansion is consistent with a monolayer arrangement of $Na(en)^+$ in which ethylenediamine forms a chelate structure oriented parallel to the graphene sheets.[33] Figure 3.2e shows the stage-1 $[(C_4H_9)_4N]C_{43}$ product obtained, with d_i = 0.813 nm. This product is similar to that obtained previously using exchange in DMF, and the interlayer expansion (Δd) of only 0.478 nm sterically requires the $(C_4H_9)_4N^+$ intercalates to form monolayers with a highly flattened conformation.[42]

Figure 3.2g-i shows the formation of several new, well-ordered, single-phase TAA-GICs. In each case, the observed reflections can be indexed as stage-1 GICs with d_i ~ 1.14 nm. No residual $[Na(en)_{1.0}]C_{15}$ is seen, although a very small graphite*(002)* reflection at 2θ~27° is often present, most notably in Figure 3.2g. The larger interlayer expansion (Δd ~ 0.80 nm), coupled with structure modeling and compositional data (described below) indicate that these large TAA intercalates form novel bilayer, rather than monolayer, galleries, again with the steric requirement that each layer contains highly flattened cations.

Exchange with $(C_5H_{11})_4N^+$ (Figure 3.2f) does not result in either the ordered monolayer or bilayer arrangement, but yields instead a poorly ordered structure with only two strong reflections observed. These are consistent with a stage-2 TAA-GIC with a bilayer gallery (Δd = 0.79 nm). Compositional analyses also show a lower intercalate content for this product (Table 3.1). The high angle shoulder on the *(003)* reflection after

exchange with $(C_6H_{13})_4N^+$ (Figure 3.2g) may also be ascribed to a minor component of the stage-2 GIC.

Interestingly, attempts to exchange $[Na(en)_{1.0}]C_{15}$ with smaller TAA cations by the same route were unsuccessful; the products obtained after reaction with $(CH_3)_4N^+$ and $(C_2H_5)_4N^+$ cation-containing solutions show only broadened graphite reflections (Figure 3.2b,c), and the $(C_3H_7)_4N^+$ exchange reaction (Figure 3.2d) results in a mix of disordered graphite and a high-stage GIC. In these reactions, therefore, the oxidation of $[Na(en)_{1.0}]C_{15}$ to graphite or to a high-stage GIC must be accompanied by reduction of the reactant solution. Because $[Na(en)_{1.0}]C_{15}$ is oxidized to graphite by exposure to neat DMSO under similar conditions, we can restate these observations as the stabilization effect of the larger, but not the smaller, TAA cations that promotes ion exchange over GIC oxidation.

Although the products obtained after reaction with the larger TAA cations are stage-1GICs, the charge densities do decrease on the graphene sheets during these reactions, as will be shown below in the increased *x* value in the composition $[TAA]C_x$. This indicates a partial oxidation of the graphene sheets during the exchange process.

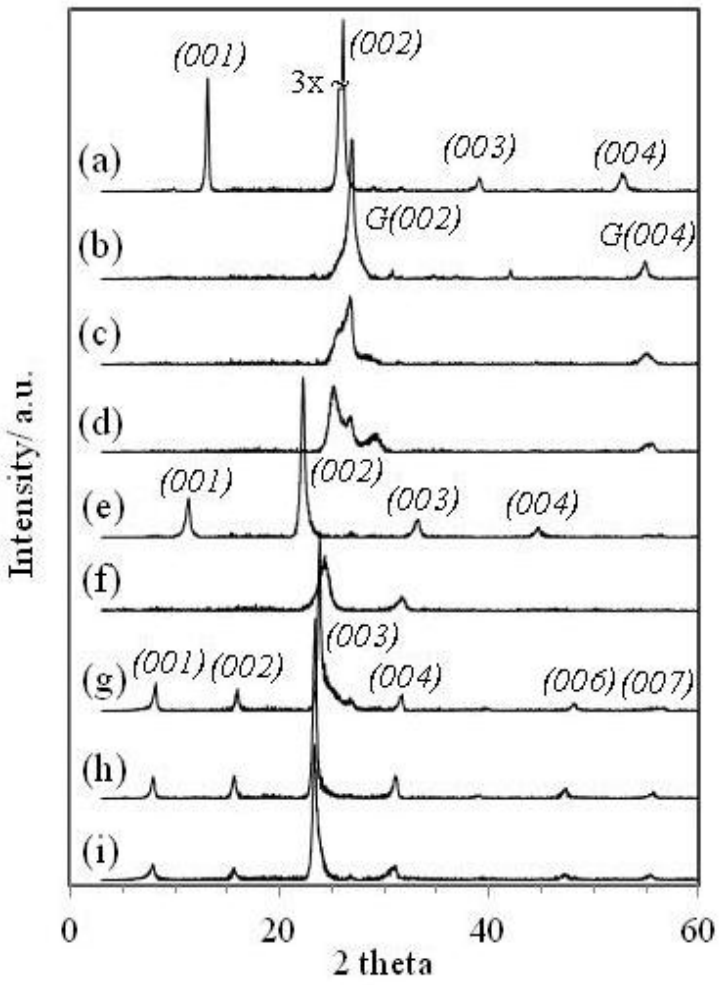

Figure 3.2 PXRD patterns of the (a) $[Na(en)_{1.0}]C_{15}$ reactant and GIC products containing (b) $(CH_3)_4N$, (c) $(C_2H_5)_4N$, (d) $(C_3H_7)_4N$, (e) $(C_4H_9)_4N$, (f) $(C_5H_{11})_4N$, (g) $(C_6H_{13})_4N$, (h) $(C_7H_{15})_4N$, and (i) $(C_8H_{17})_4N$. The assigned indices of obtained GICs and of graphite are denoted as *(00l)* and G*(00l)*, respectively.

Figure 3.3a-c shows the PXRD patterns obtained following exchange with asymmetric TAA cations. All of the products obtained are single-phase, stage-1 GICs with d_i ~ 1.12 nm, indicating again a bilayer arrangement of flattened TAA cations. The

structural data obtained for $[Na(en)_{1.0}]C_{15}$ and the TAA-GICs are summarized in Table 3.1.

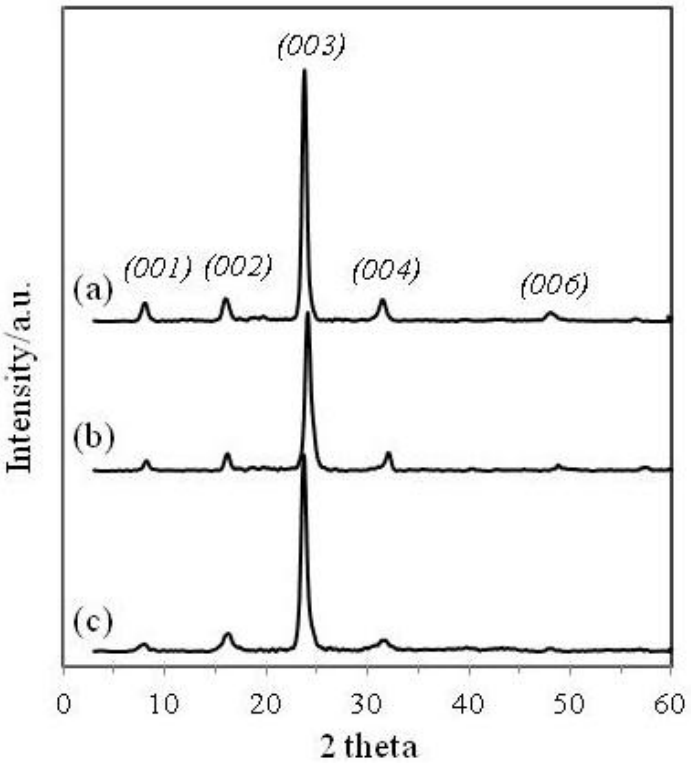

Figure 3.3 PXRD patterns of products obtained after exchange by asymmetric TAA cations (a) $(C_{12}H_{25})(CH_3)_3N$, (b) $(C_{18}H_{37})(CH_3)_3N$, and (c) $(C_{18}H_{37})_2(CH_3)_2N$.

Table 3.1 Structural and compositional data of $[Na(en)_{1.0}]C_{15}$ and obtained TAA-GICs.

Cation	Stage	d_i (nm)	Δd (nm)	Intercalate arrangement	Total intercalate (Mass %)	Composition	Packing fraction
$Na(en)_{1.0}$[a]	1	0.691	0.356	monolayer	30.4	$[Na(en)_{1.0}]C_{15}$	0.51
$(C_3H_7)_4N$	high-stage + graphite	0.760	0.425	monolayer	11.8	n/a	n/a
$(C_4H_9)_4N$	1	0.813	0.478	monolayer	31.8	$[(C_4H_9)_4N]C_{43}$	0.55
$(C_5H_{11})_4N$	2	1.123	0.793	bilayer	27.5	n/a	n/a
$(C_6H_{13})_4N$	1	1.122	0.787	bilayer	38.2	$[(C_6H_{13})_4N]C_{59}\cdot 1.1DMSO$	0.42
$(C_7H_{15})_4N$	1	1.144	0.809	bilayer	40.8	$[(C_7H_{15})_4N]C_{63}\cdot 1.4DMSO$	0.45
$(C_8H_{17})_4N$	1	1.148	0.813	bilayer	41.4	$[(C_8H_{17})_4N]C_{76}\cdot 1.9DMSO$	0.46
$(C_{12}H_{25})(CH_3)_3N$	1	1.109	0.774	bilayer	38.8	$[(C_{12}H_{25})(CH_3)_3N]C_{44}\cdot 1.4DMSO$	0.43
$(C_{18}H_{37})(CH_3)_3N$	1	1.126	0.791	bilayer	37.5	$[(C_{18}H_{37})(CH_3)_3N]C_{60}\cdot 1.6DMSO$	0.40
$(C_{18}H_{37})_2(CH_3)_2N$	1	1.118	0.783	bilayer	41.4	$[(C_{18}H_{37})_2(CH_3)_2N]C_{85}\cdot 2.2DMSO$	0.48

[a] Data from Ref 33.

Capillary zone electrophoretic (CZE) analyses can be used to quantitate soluble species during and after reactions, and here were used to monitor reaction progress and to determine GIC composition by the appearance of Na^+ and en and the disappearance of TAA cations from the reactant solution according to:

$$[Na(en)_{1.0}]C_{15} \xrightarrow{\text{excess TAA+}} [TAA]C_x + aNa^+ + b(en) \qquad (3.2)$$

where a, b and x in the products can be derived directly from CZE data. Quantitative displacement of the sodium complex will result in a=b=1.0. For exchanges using symmetric TAA cations larger than $(C_3H_7)_4N^+$, and for the asymmetric TAA cations, the exchange is nearly complete for both Na cations and en (the a and b values obtained are close to 1 in Table 3.2). Additionally, the TAA cation contents for the GICs derived from CZE (x) are consistent with TGA results (Table 3.2).

Table 3.2 Stoichiometric ratios for displacement reaction (3.2) as determined by CZE.[a]

Obtained GICs	CZE			TGA
	a	b	x	x
$[(C_4H_9)_4N]C_x$	0.97	1.0	41	43
$[(C_6H_{13})_4N]C_x$	1.0	0.98	56	59
$[(C_7H_{15})_4N]C_x$	1.0	1.0	58	63
$[(C_8H_{17})_4N]C_x$	1.0	0.99	63	72
$[(C_{12}H_{25})(CH_3)_3N]C_x$	0.97	0.93	40	44

[a] $[TAA]C_x$ values derived from TGA are also provided.

The thermal behavior of two TAA-GICs and graphite are shown in Figure 3.4. $[(C_4H_9)_4N]C_{43}$ shows two mass loss regions (130–250, 250-500 ºC) attributed to the thermolysis of the TAA cation. $[(C_7H_{15})_4N]C_{63}\cdot 1.4DMSO$ shows a much larger total mass loss, and an additional low-temperature mass loss at 95-110 ºC. The latter is ascribed to volatilization of a DMSO co-intercalate, and this is confirmed by both the corresponding DMSO mass peak at m/z = 63 in the same temperature range, and the subsequent elemental analysis for sulfur (3.5% S *vs* 3.4% S_{calc} from the actual composition in Table 3.1). Significant DMSO co-intercalation was observed for all the bilayer GICs, but neither the DMSO mass loss peak, nor any appreciable sulfur content, were identified in the monolayer gallery structure of $[(C_4H_9)_4N]C_{43}$. Mass loss above 550 ºC for all samples including graphite is due to the combustion of a graphitic carbon by O_2 in the flow gas. On the basis of the CZE, TGA, and sulfur content analyses, the structural compositions of all resulting TAA-GICs are reported in Table 3.1 for the single-phase, or nearly single-

phase, products. The exchanged products with $(C_3H_7)_4N^+$ and $(C_5H_{11})_4N^+$ are not included as they are multiphase. Again, it is interesting to note that only the TAA-GICs with bilayers incorporate DMSO into the intercalate galleries.

The packing fractions of these intercalate galleries can be calculated from the structural and compositional data reported above, and then compared to those in other GICs. Packing fraction is defined here as:

$$\text{Packing Fraction} = \frac{V_i}{V_h} \qquad (3.3)$$

where V_i is the van der Waals volume of intercalates per formula unit, which is estimated by the VABC (Atomic and Bond Contributions of van der Waals Volume) method,[57] and V_h is the available volume per formula unit due to the lattice expansion obtained from the surface area per graphitic carbon (0.0261 nm^3), product composition, and the observed Δd. The resulting packing fractions are provided in Table 3.1, and show a range of 0.40-0.55, with the monolayer gallery in $[(C_4H_9)_4N]C_{43}$ showing more dense intercalate packing than any of the bilayer arrangements.

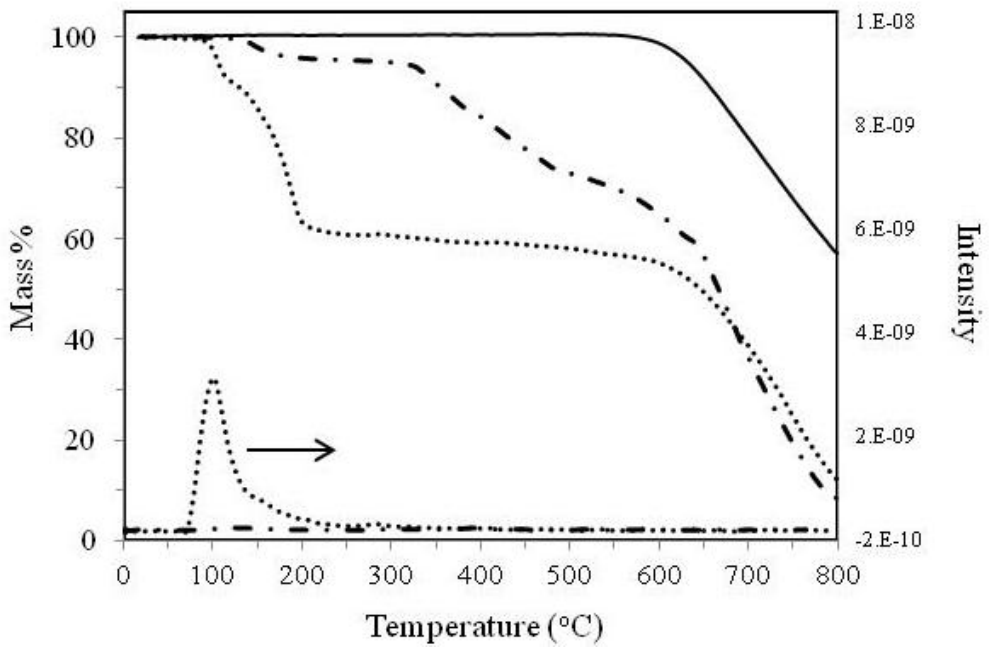

Figure 3.4 TGA mass loss data for $[(C_7H_{15})_4N]C_{63}{\cdot}1.4DMSO$ (·····), $[(C_4H_9)_4N]C_{43}$ (— · — ·), and unreacted graphite (——). At the bottom, m/z = 63 peak intensities from TGA/MS are shown for $[(C_7H_{15})_4N]C_{63}{\cdot}1.4DMSO$ (·····) and $[(C_4H_9)_4N]C_{43}$ (— · — ·).

To model the bilayer arrangement of flattened intercalates and DMSO cointercalates, a 1D electron density map along the *c*-axis direction was generated from the PXRD *(00l)* peak intensities. The calculated profile for a structure model of $[(C_7H_{15})_4N]C_x{\cdot}1.4DMSO$ is compared with that obtained from observed PXRD peak intensities (Figure 3.5). In the model, the flattened TAA conformations are generated using Gaussian, and bilayers are formed with these cations oriented with long axes parallel to the graphene sheets. The DMSO co-intercalates are positioned with H and S atoms nestled into the graphene sheets by 0.038 and 0.032 nm, respectively. The relative

concentrations of TAA and DMSO within galleries were fixed by the known product compositions. The close agreement of model and observed profiles obtained can be seen in Figure 3.5. Multiple models were tested, and we conclude that the double peak of electron density from the observed data is only consistent with a bilayer intercalate model. However, the best fit model indicates an *x* value considerably lower than that observed (37 *vs* 63). The origin of this mismatch is under investigation.

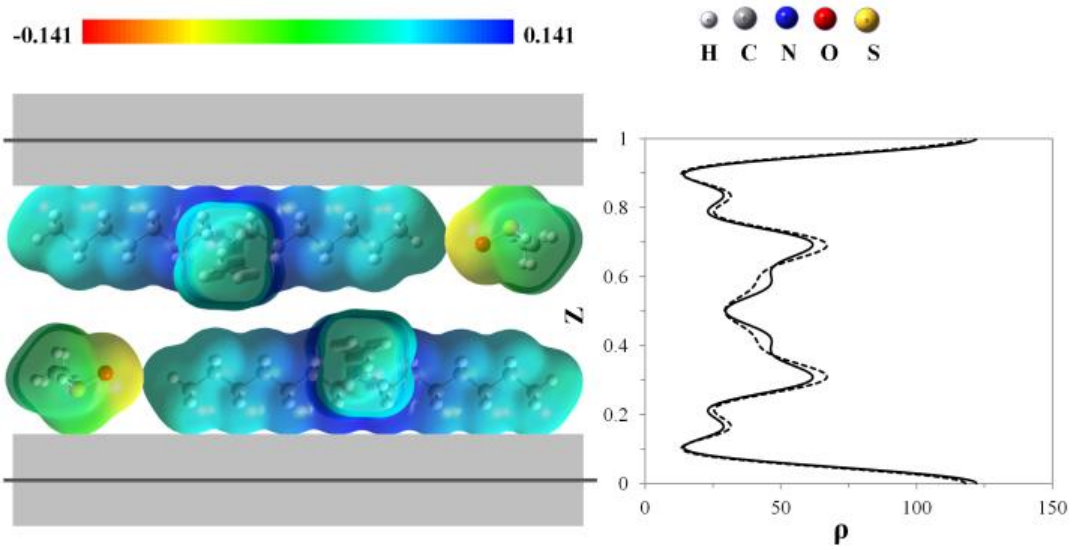

Figure 3.5 Structure model and 1D-electron density profiles for $[(C_7H_{15})_4N]C_x$·1.4DMSO showing the bilayer intercalate ar-rangement. The dashed line and solid line represent the pro-files derived from observed data and from the structure model, respectively (the crystallographic *R* factor = 0.11).

The Raman spectrum of pristine graphite (Figure 3.6a) exhibits a strong G-band at 1584 cm^{-1} (E_{2g}) involving intralayer atomic motion. Reductive intercalation into the graphitic host causes a perturbation of the in-plane force constant, resulting in a G-band

shift to higher frequency. The magnitude of the shift has been shown to depend on the degree of reduction, and therefore the stage, of the GIC formed.[58-60] $[Na(en)_{1.0}]C_{15}$ (Figure 3.6b) shows a significant shift to a peak maximum at 1605 cm^{-1}. The G-band peak positions for $[(C_4H_9)_4N]C_{43}$ and $[(C_7H_{15})_4N]C_{63}\cdot 1.4DMSO$ (Figure 3.6c,d) are both at 1586 cm^{-1}. These peak positions agree with conclusion drawn from the compositional data, that these GICs have very low charge densities for stage-1 GICs.

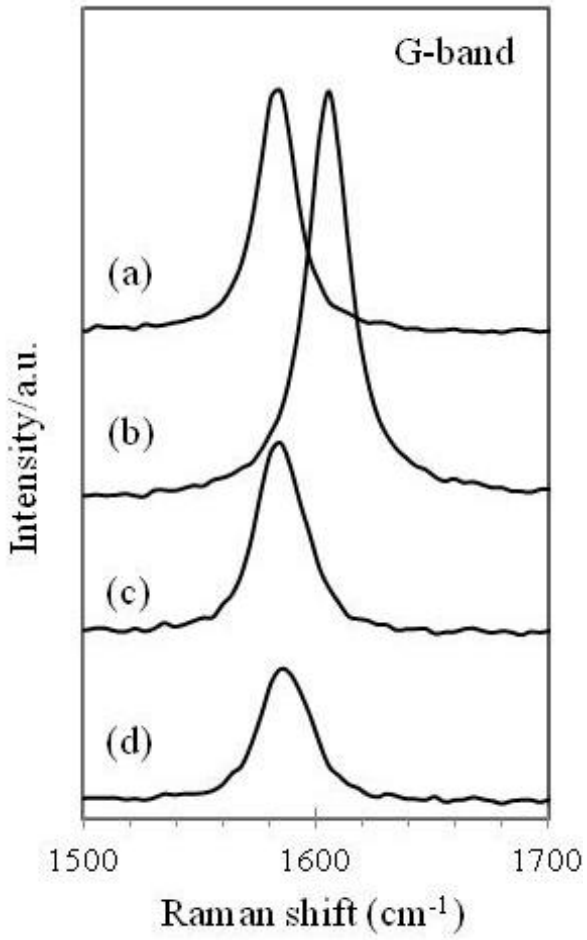

Figure 3.6 Raman spectra for (a) pristine graphite, (b) $[Na(en)_{1.0}]C_{15}$, (c) $[(C_4H_9)_4N]C_{43}$, and (d) $[(C_7H_{15})_4N]C_{63}\cdot 1.4DMSO$.

To our knowledge, the observed range of *x* from 41 to 85 in these TAA-GICs indicates the lowest charge densities for any stage-1 reduced GICs.[1] The very low charge densities are required by the steric demands (i.e., large footprints) of the monovalent, flattened TAA cations. Thus, designed intercalation of large deformable cations provides a degree of steric control over the sheet charge densities in GICs. Sterics may also help explain the observed monolayer to bilayer transition, as the high packing fractions for

$[(C_4H_9)_4N]C_{43}$ would necessarily increase even further if larger TAA cations adopted a monolayer arrangement. In future, the intercalation of even larger cations may generate tri- or multilayer galleries, or perhaps produce stable materials containing fully disordered (delaminated) graphene sheets.

3.5 REFERENCES

(1) Enoki, T.; Suzuki, M.; Endo, M. *Graphite Intercalation Compounds and Applications*; Oxford University Press: New York, 2003.

(2) Dresselhaus, M. S.; Dresselhaus, G. *Adv. Physics* **2002**, 51, 1-186.

(3) Chung, D. D. L. *J. Mater. Sci.* **2002**, 37, 1475-1489.

(4) Parry, G. S.; Nixon, D. E.; Lester, K. M.; Levene, B. C. *J. Phys. C* **1969**, 2, 2156-2158.

(5) Parry, G. S.; Nixon, D. E. *Nature* **1967**, 216, 909-910.

(6) Jones, J. E.; Cheshire, M. C.; Casadonte, D. J.; Phifer, C. C. *Org. Lett.* **2004**, 6, 1915-1917.

(7) Goutfer-Wurmser, F.; Herold, C.; Lagrange, P. *Carbon* **1996**, 34, 821-823.

(8) Akuzawa, N.; Ikeda, M.; Amemiya, T.; Takahashi, Y. *Synth. Met.* **1983**, 7, 65-72.

(9) Inagaki, M.; Ohira, M. *Carbon* **1993**, 31, 777-781.

(10) Shornikova, O. N.; Sorokina, N. E.; Maksimova, N. V.; Avdeev, V. V. *Inorg. Mater.* **2005**, 41, 120-126.

(11) Zhang, X.; Lerner, M. M. *Chem. Mater.* **1999**, 11, 1100-1109.

(12) Mizutani, Y.; Abe, T.; Ikeda, K.; Ihara, E.; Asano, M.; Harada, T.; Inaba, M.; Ogumi, Z. *Carbon* **1997**, 35, 61-65.

(13) Takenaka, A.; Tsumura, T.; Toyoda, M. *Synth. Met.* **2010**, 160, 1247-1251.

(14) Özmen-Monkul, B.; Lerner, M. M.; Pawelke, G.; Willner, H. *Carbon* **2009**, 47, 1592-1597.

(15) Moissette, A.; Fuzellier, H.; Burneau, A.; Dubessy, J.; Lelaurain, M. *Carbon* **1995**, 33, 123-128.

(16) Bensenhard, J. O.; Möhwald, H.; Nickl, J. J. *Carbon* **1980**, 18, 399-405.

(17) Okuyama, N.; Takahashi, T.; Kanayama, S.; Yasunaga, H. *Physica B&C* **1981**, 105, 298-301.

(18) Thomas, J. M.; Millward, G. R.; Schlögl, R. F.; Boehm, H. P. *Mat. Res. Bull.* **1980**, 15, 671-676.

(19) Sethuraman, V. A.; Hardwick, L. J.; Srinivasan, V.; Kostecki, R. *J. Power Sources* **2010**, 195, 3655-3660.

(20) Solin, S. A. *Annu. Rev. Mater. Sci.* **1997**, 27, 89-115.

(21) Santhanam, R.; Noel, M. *J. Power Sources* **1998**, 72, 53-65.

(22) Ogumi, Z.; Inaba, M. *Bull. Chem. Soc. Jpn.* **1998**, 71, 521-534.

(23) Rashkov, I. B.; Panayotov, I. M.; Shishkova, V. C. *Carbon* **1979**, 17, 103-108.

(24) Takahashi, Y.; Akuzawa, N.; Béguin, F. *Synth. Met.* **1995**, 73, 45-48.

(25) Skowronski, J. M.; Krawczyk, P. *Solid State Ion.* **2010**, 181, 653-658.

(26) Toyoda, M.; Inagaki, M. *Carbon* **2000**, 38, 199-210.

(27) Kwon, O. -Y.; Choi, S. -W.; Park, K. -W.; Kwon, Y. -B. *J. Ind. Eng. Chem.* **2003**, 9, 743-747.

(28) Inagaki, M.; Tashiro, R.; Washino, Y.; Toyoda, M. *J. Phys. Chem. Solids* **2004**, 65, 133-137.

(29) Viculis, L. M.; Mack, J. J.; Kaner, R. B. *Science* **2003**, 299, 1361.

(30) Makotchenko, V. G.; Grayfer, E. D.; Nazarov, A. S.; Kim, S. -J.; Fedorov, V. E. *Carbon* **2011**, 49, 3233-3241.

(31) Geng, Y.; Zheng, Q.; Kim, J. -K. *J. Nanosci. Nanotechnol.* **2011**, 11, 1084-1091.

(32) Maluangnont, T.; Sirisaksoontorn, W.; Lerner, M. M. *Carbon* **2012** 50, 597-602.

(33) Maluangnont, T.; Lerner, M. M.; Gotoh, K. *Inorg. Chem.* **2011**, 50, 11676-11682.

(34) Maluangnont, T.; Bui, G. T.; Huntington, B. A.; Lerner, M. M. *Chem. Mater.* **2011**, 23, 1091-1095.

(35) Maluangnont, T.; Gotoh, K.; Fujiwara, K.; Lerner, M. M. *Carbon* **2011**, 49, 1040-1042.

(36) Santhanam, R.; Noel, M. *J. Power Sources* **1995**, 56, 101-105.

(37) Simonet, J.; Lund, H. *J. Electroanal. Chem.* **1977**, 75, 719-730.

(38) Simonet, J. *Electrochem. Commun.* **2013**, 30, 17-20.

(39) Katayama, Y.; Yukumoto, M.; Miura, T. *Electrochem. Solid-State Lett.* **2003**, 6, A96-A97.

(40) Zheng, H.; Li, B.; Fu, Y.; Abe, T.; Ogumi, Z. *Electrochim. Acta* **2006**, 52, 1556-1562.

(41) Zheng, H.; Jiang, K.; Abe, T.; Ogumi, Z. *Carbon* **2006**, 44, 203-210.

(42) Sirisaksoontorn, W.; Adenuga, A. A.; Remcho, V. T.; Lerner, M. M. *J. Am. Chem. Soc.* **2011**, 133, 12436-12438.

(43) Liu, Z. -H.; Ooi, K.; Kanoh, H.; Tang, W. -P.; Tomida, T. *Langmuir* **2000**, 16, 4154-4164.

(44) Kanzaki, Y.; Konuma, M.; Matsumoto, O. *J. Phys. Chem. Solids* **1980**, 41, 525-529.

(45) Sasaki, T.; Watanabe, M. *Mol. Cryst. Liq. Cryst.* **1998**, 311, 417-422.

(46) Letaief, S.; Detellier, C. *Clays Clay Miner.* **2009**, 57, 638-648.

(47) Liu, Z. -H.; Wang, Z. -M.; Yang, X.; Ooi, K. *Langmuir* **2002**, 18, 4926-4932.

(48) Xi, Y.; Frost, R. L.; He, H.; Kloprogge, T.; Bostrom, T. *Langmuir* **2005**, 21, 8675-8680.

(49) Peng, S.; Gao, Q.; Du, Z.; Shi, J. *Appl. Clay Sci.* **2006**, 31, 229-237.

(50) Nakayama, M.; Konishi, S.; Tagashira, H.; Ogura, K. *Langmuir* **2005**, 21, 354-359.

(51) Jaynes, W. F.; Boyd, S. A. *Soil Sci. Soc. Am. J.* **1991**, 55, 43-48.

(52) Mercier, L.; Detellier, C. *Clays Clay Miner*. **1994**, 42, 71-76.

(53) Chun, Y.; Sheng, G.; Boyd, S. A. *Clays Clay Miner*. **2003**, 51, 415-420.

(54) Li, Z.; Jiang, W. T. *Thermochim. Acta* **2009**, 483, 58-65.

(55) Golub, A. S.; Zubavichus, Ya. V.; Slovokhotov, Yu. L.; Novikov, Yu. N.; Danot, M. *Solid State Ionics* **2000**, 128, 151-160.

(56) He, H.; Frost, R. L.; Bostrom, T.; Yuan, P.; Duong, L.; Yang, D.; Xi, Y.; Kloprogge, J. T. *Appl. Clay Sci.* **2006**, 31, 262-271.

(57) Zhao, Y. H.; Abraham, M. H.; Zissimos, A. M. *J. Org. Chem.* **2003**, 68, 7368-7373.

(58) Doll, G. L.; Eklund, P. C.; Fischer, J. E. *Phys. Rev. B* **1987**, 36, 4940-4945.

(59) Vora, P.; York, B. R.; Solin, S. A. *Synth. Met.* **1983**, 7, 355-360.

(60) Dresselhaus, M. S.; Dresselhaus, G. *Top. Appl. Phys.* **1982**, 51, 3-57.

CHAPTER 4

THE ELECTROCHEMICAL SYNTHESIS OF THE GRAPHITE INTERCALATION COMPOUNDS CONTAINING TETRA-n-ALKYLAMMONIUM CATIONS

Weekit Sirisaksoontorn and Michael M. Lerner

Department of Chemistry

Oregon State University

Corvallis, OR 97331-4003, USA

ECS J. Solid Sci. Technol. **2013**, 2(9), M28-M32.

4.1 ABSTRACT

The electrochemical intercalation of tetra-n-alkylammonium (TAA) cations into graphite is investigated using galvanostatic reduction and cyclic voltammetry in TAABr/ dimethylsulfoxide (DMSO) electrolytes. Structural and compositional analyses by X-ray diffraction, thermogravimetric and elemental analyses show that stable graphite intercalation compounds (GICs) are formed with highly-flattened TAA cation bilayers for $(C_5H_{11})_4N^+$, $(C_6H_{13})_4N^+$, $(C_7H_{15})_4N^+$, $(C_8H_{17})_4N^+$, with gallery expansions of 0.81 nm. $(C_4H_9)_4N^+$ forms a mixed-phase product including a stable GIC with monolayer TAA arrangement and a gallery expansion of 0.48 nm. The GICs with bilayer galleries incorporate 0.7-1.2 DMSO co-intercalate molecules per cation; the monolayer galleries contain relatively little DMSO. Although cyclic voltammetry shows that TAA cations smaller than $(C_4H_9)_4N^+$ do intercalate into graphite, they do not form stable GICs. The GICs obtained by galvanostatic reduction are compared to those prepared using chemical ion-exchange reactions. A surface passivation model is introduced to explain the relative stabilities of GICs formed with larger TAA cation intercalates.

4.2 INTRODUCTION

Graphite exhibits a unique intercalation chemistry, and undergoes a wide range of reduction or oxidation reactions to form donor and acceptor-type graphite intercalation compounds (GICs), respectively.[1-3] Both chemical and electrochemical methods have been employed in the preparation of GICs.[4-7] Depending on the nature of the GICs and synthetic conditions, the intercalate ions (cations for donor-type, anions for acceptor-type GICs) may be accompanied by neutral co-intercalate molecules.[8] GICs display structural ordering perpendicular to the graphene sheet stacking direction; regular sequences of intercalate galleries and graphene layers arise in a phenomenon known as staging.[9,10] Stage-1 GICs have a single graphene sheet encased by intercalate galleries; stage-2 GICs have each bilayer of graphene sheets encased, and etc. Gallery expansion, Δd, is used to indicate the increased distance between graphene layer surfaces when separated by an intercalate gallery. Important applications of GICs to date include use as anodes in reversible lithium ion batteries,[11] as precursors to exfoliated graphite,[12-15] and in environmental oil absorption.[16]

Our group recently reported the first preparation of a series of symmetric or asymmetric tetra-n-alkylammonium GICs (TAAGICs) that were obtained via the quantitative displacement of the cationic complex, $Na(en)^+$, in $[Na(en)]C_{15}$ (square brackets indicate intercalates, x in C_x is the number of graphene carbons per negative charge, en is ethylenediamine) by TAA cations in an aprotic organic solvent such as dimethylsulfoxide (DMSO) or *N*,*N*-dimethylformamide (DMF).[17,18] Depending on the TAA cation employed, the TAAGIC products had Δd of either 0.47 nm or 0.8 nm,

associated with the intercalation of either monolayers or bilayers of cations with highly-flattened conformations. These same gallery dimensions were obtained over the wide range of TAA cation diameters, from about 0.4-0.5 nm for $(C_4H_9)_4N^+$ to ~1.4 nm in $(C_8H_{17})N^+$. The monolayer arrangement was only observed in $[(C_4H_9)_4N]C_{43}$, and only this TAAGIC showed no solvent co-intercalation. The larger TAA cations form bilayer structures with significant DMSO co-intercalation, e.g. $[(C_7H_{15})_4N\cdot 1.4DMSO]C_{63}$ or $[(C_{18}H_{37})(CH_3)_3N\cdot 1.6DMSO]C_{60}$. Attempts to exchange TAA cations smaller than $(C_4H_9)_4N^+$ resulted only in high-stage GICs or graphite.

Earlier studies on the intercalation of TAA cations into graphite employed electrochemical reduction in organic electrolytes. Besenhard et al.[19] reported a dull-black, stage-1 GIC with Δd = 1.25 nm and approximate composition $[(CH_3)_4N\cdot 6.0DMSO]C_{24}$ by the reduction of graphite in $(CH_3)_4NCl$/DMSO. The product was highly air sensitive and found to partially decompose during characterization. Simonet[20] reported the reversible intercalation/deintercalation of TAA cations by cyclic voltammetry on graphite in DMF-based electrolytes containing TAA cations. A galvanostatic charge plot showed the step-wise formation of $[(CH_3)_4N]C_x$, x = 96, 24, and 12. Zheng et al.[21] reported a new X-ray diffraction peak at 23.5° 2θ (d = 0.378 nm) after reducing graphite at different potentials in an ionic liquid electrolyte containing $(CH_3)_3(C_6H_{13})N^+$, suggesting the formation of a new TAAGIC at 0.7 V vs. Li/Li^+. The appearance and disappearance of this single peak during cyclic voltammetry suggested reversible intercalation/de-intercalation of the asymmetric TAA cation.

We are not aware of the electrochemical preparation, isolation, and characterization of any stable TAAGICs to date. In this work, we will describe a series of stable TAAGICs obtained by reduction in DMSO-based electrolytes. The products obtained are isolated and then characterized by X-ray diffraction, and thermogravimetric and elemental analyses. In addition, the electrochemical reactions are evaluated using cyclic voltammetry.

4.3 EXPERIMENTAL

TIMREX SLP50 Graphite powder (TIMCAL America Inc., average particle diameter 50 μm) and all tetra-n-alkylammonium bromide (TAABr) salts with a purity >98% were used as received. The abbreviation TnA will be used for these symmetric cations, where n is the number of carbons per alkyl group, thus $(C_4H_9)_4N^+$ will be listed as T4A. DMSO (AR grade, 99.9 %) and acetonitrile (HPLC grade, 99.9 %) were dried over a 4 Å molecular sieve prior to use.

Galvanostatic reductions were performed in a two-compartment cell with a fritted glass separator, and were maintained under an inert atmosphere at ambient temperature. Working electrodes were prepared by painting a cyclohexane slurry containing graphite powder (20-25 mg) and 5 wt% polymer binder (EPDM) onto a stainless steel (SS) mesh flag (geometric area ~1 cm^2). Coated electrodes were dried at 50°C. Counter and reference electrodes were SS mesh and wire. Repeated tests on the SS wire reference in the same electrolytes, both as prepared and after the reduction reaction, returned a potential of -0.03(1) V vs. SCE, and potentials reported below have been converted to V vs. SCE. Electrolyte solutions were 0.1 M TAABr in DMSO, except for T1ABr/DMSO which was found to saturate at a lower concentration. Graphite electrodes were reduced at a current density of 3.3 mA/g for 22 h. If the graphite reduction is fully efficient, the applied charge corresponds to a negative charge on graphene sheets of $x = 32$ in C_x^-. From previous results on the chemical intercalation of TAA cations, this is a significantly higher charge than required to form the stage-1 products.[17] Reductions for longer times were also tried in some cases, with no change in the products obtained. Following

reduction, the working electrodes were immediately removed from the cell, rinsed briefly with 3-4 ml of acetonitrile, and then dried overnight under vacuum. Cyclic voltammetry was conducted at 1.0 mV/s, from 0 to -2.5 V vs. SCE, for one or more cycles. Electrode preparation was similar to that described above but utilized ~2 mg of graphite on a 9 mm^2 SS flag.

Powder X-ray diffraction (PXRD) studies used a Rigaku Miniflex II diffractometer with Ni-filtered Cu K_α radiation. PXRD data were collected at 5°/min from 3° to 60° 2θ. Only *(00l)* reflections were indexed in the obtained PXRD patterns due to preferred orientation in the samples. The relationship between the gallery expansion (Δd), repeat distance along the c-direction (I_c), and the GIC stage number (n) is $I_c = \Delta d + 0.335n$, where 0.335 nm corresponds to the thickness of a single graphene sheet. Thermal analyses used a Shimadzu TGA-50 thermogravimetric analyzer (TGA) under flowing Ar/O_2 (20 ml/min) at a heating rate of 10°C/min from ambient to 800°C. Sulfur elemental analyses were performed by Micro-Analysis, Inc. (Wilmington, DE).

4.4 RESULTS AND DISCUSSION

Three representative potential-charge curves are shown in Figure 4.1a-c. For all these curves, a sharp potential drop occurs at the outset, followed by a voltage increase and then a long, negatively-sloping plateau. A similar voltage decrease and recovery feature has been observed at the initial stage of electrode reduction for a range of chemistries, and is sometimes termed the "voltage delay".[22-24] The feature is generally ascribed to the formation of a passivation layer at the electrode surface. The appearance, voltage profile, and duration of the voltage delays depend on several factors including the electrode and electrolyte chemistry. In Figure 4.1, the charge associated with these voltage delays is seen to be 5-10 mAh/g. For comparison, the formation of a passivation layer on graphite anodes in Li-ion batteries, known as the solid electrolyte interface, requires ~20-60 mAh/g.[25-27] After the surface passivation and voltage recovery, a subsequent intercalation reaction occurs with a gradually decreasing potential. No distinct potential steps are observed to indicate staging transitions; although a broad potential step was noted at 60-70 mAh/g for many cells (see arrow in Figure 4.1). The absence or broadening of potential steps is likely associated with a relatively slow intercalation rate into the electrode bulk, resulting in a heterogeneous intercalate distribution and the formation and maintenance of a stage-1 TAAGIC at the electrode surface at the applied current density. Lower current densities were tested, but always resulted in high-stage GIC products due to the inefficiency of the overall reduction reaction.

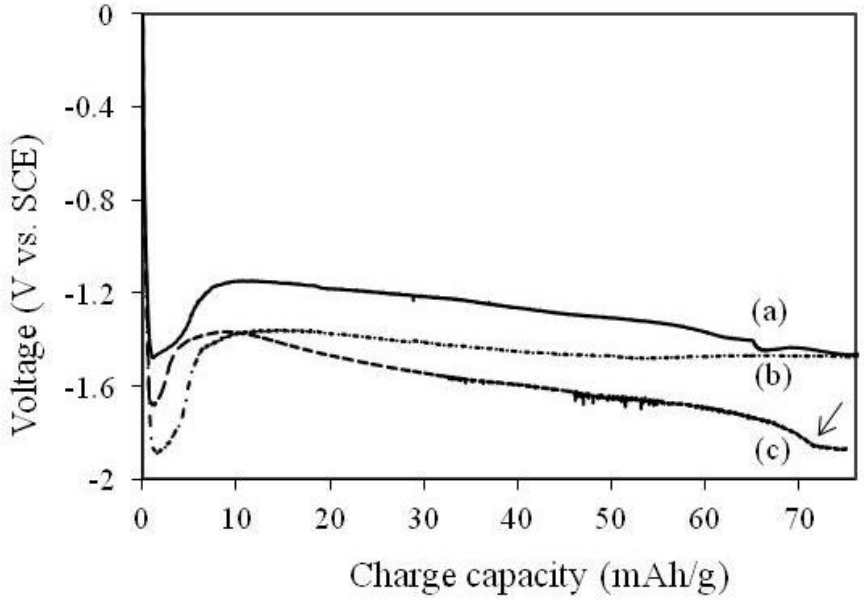

Figure 4.1 Galvanostatic potential-charge curves for graphite in (a) sat. T1ABr/DMSO, (b) 0.1 M T5ABr/DMSO and (c) 0.1 M T7ABr/DMSO electrolytes.

Figure 4.2 shows PXRD data for the obtained TAAGICs, and derived structural data are summarized in Table 4.1. With the larger TAA cations (Figure 4.2b-e), the reactions generate stage-1 products with Δd = 0.81 nm; all these patterns show the same structure and (*00l*) peak indices, as indicated above Figure 4.2e. The stage and gallery dimensions correspond to those obtained for the chemically-derived TAAGICs reported previously.[17] These gallery dimensions require sterically that the TAA cations are present in a highly-flattened conformation as shown in Figure 4.3. T4AGIC (Figure 4.2a) alone forms monolayers, with Δd = 0.48 nm, again in agreement with the chemically-derived TAAGICs. The starred peak at 23.4° 2θ in Figure 4.2a might either be ascribed to a stage-2 monolayer phase or a stage-1 bilayer phase, in both cases the strongest reflection

is *(003)*, with a calculated position of 23.2 or 23.3° 2θ, for these respective alternatives. Given the compositional data analysis, described below, the assignment of this impurity phase as a stage-1 bilayer is more reasonable. Additionally, a small *G(002)* peak from unreacted graphite is observed for all samples.

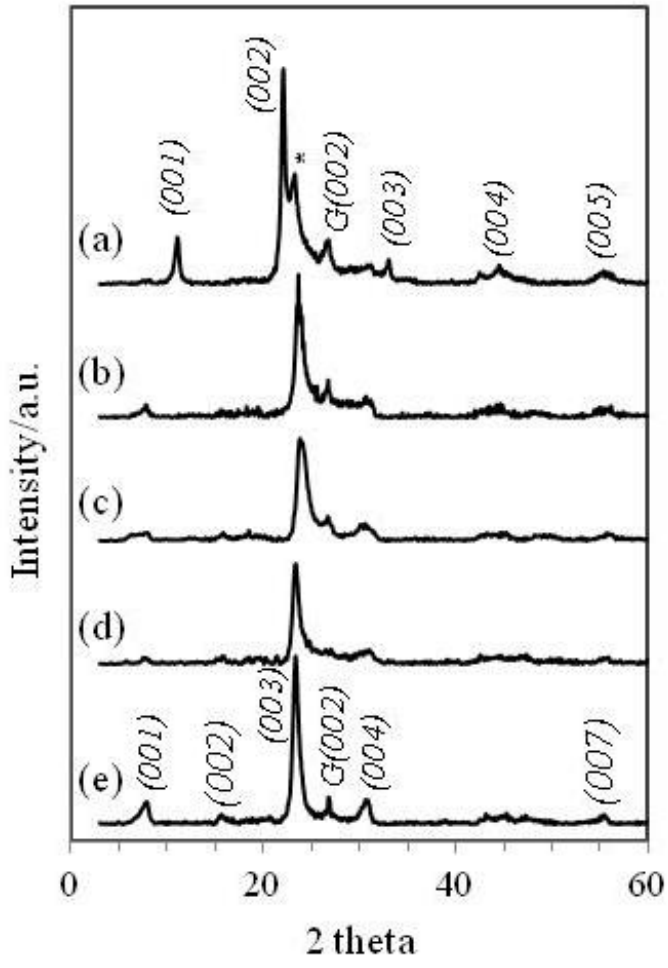

Figure 4.2 PXRD patterns of products obtained after galvanostatic reduction in 0.1 M (a) T4ABr/DMSO, (b) T5ABr/DMSO, (c) T6ABr/DMSO, (d) T7ABr/DMSO and (e) T8ABr/DMSO. The *(00l)* indices all refer to stage-1 GIC products. The starred peak corresponds to an impurity phase (see text). G*(002)* denotes unreacted graphite.

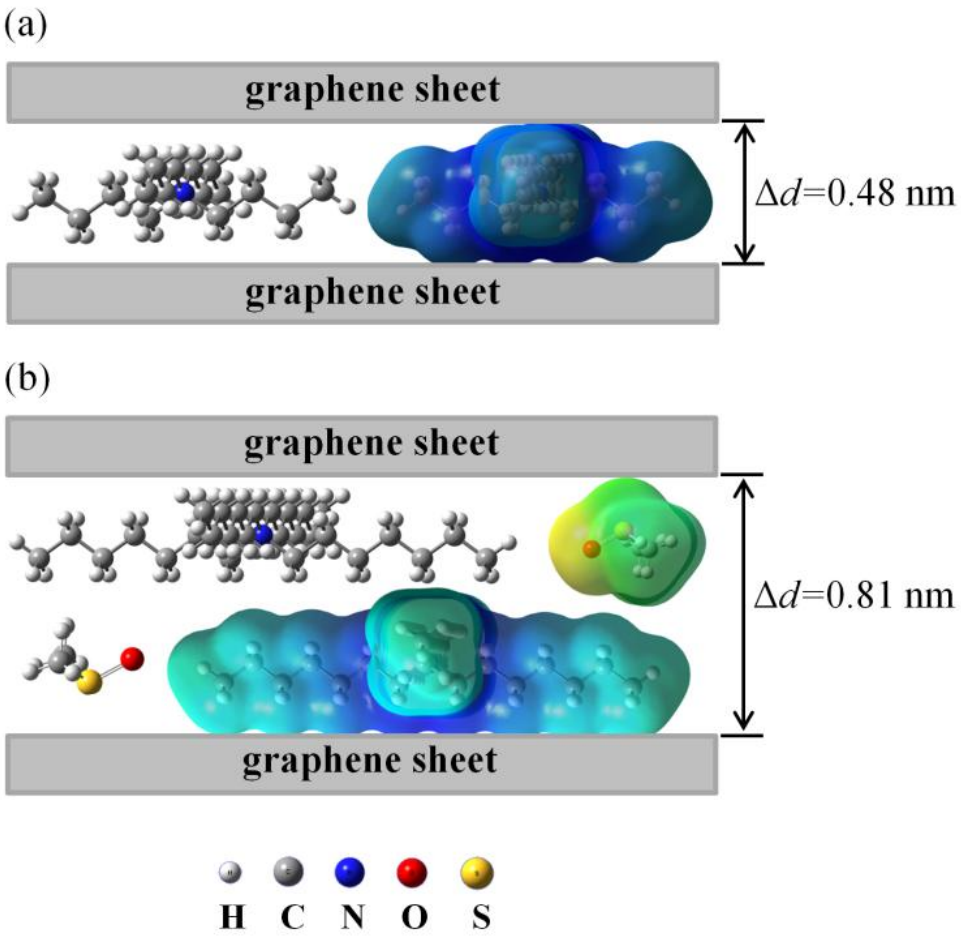

Figure 4.3 Schematic of intercalate conformations for (a) monolayer T4AGIC and (b) bilayer T7AGIC, including the DMSO co-intercalate for the bilayer phase. Both ball-and-stick (left) and space-filling representations (right) of the intercalates are shown.

As shown in Figure 4.4, it is notable that TAA cations smaller than T4A did not generate low-stage GICs. This was also observed for the chemical exchange reactions, and seems at first counter-intuitive. Smaller cations might be expected to show higher diffusion rates into graphene galleries and therefore more readily generate GICs. In Figure 4.4, the T1A and T2A cations show only a broadened graphitic reflection, whereas

T3A generates a high-stage GIC along with graphite. The data and trend suggest that, as was observed earlier by Besenhard et al.,[19] a reaction does occur, GICs with the smaller TAA cations do form, but they are highly unstable and rapidly oxidize back to graphite, either *in situ* or during product workup.

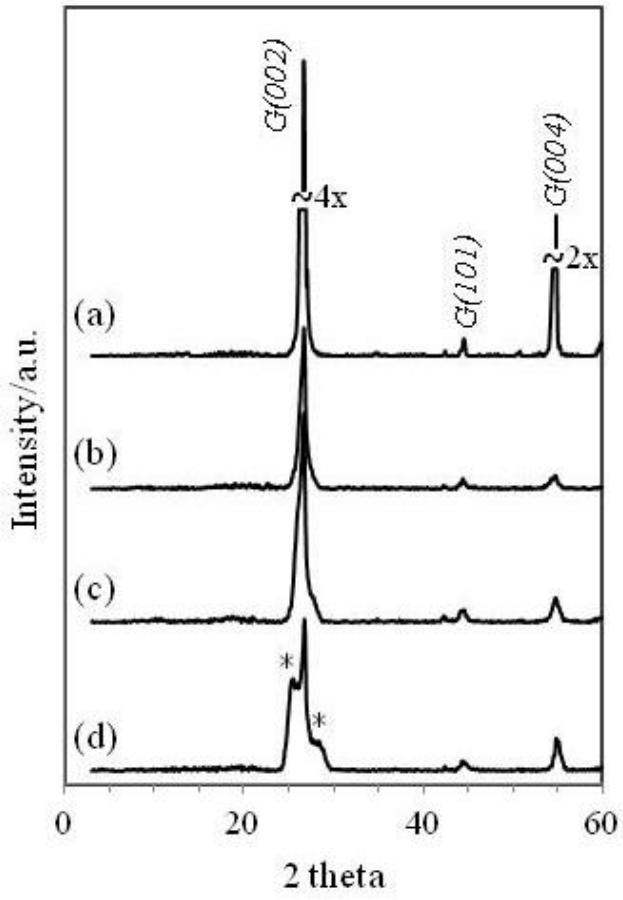

Figure 4.4 PXRD patterns of (a) pristine graphite, and after galvanostatic reduction in (b) sat. T1ABr/DMSO, (c) 0.1 M T2ABr/DMSO and (d) 0.1 M T3ABr/DMSO. G*(hkl)* denotes unreacted graphite reflections, and the starred peaks are from a high-stage GIC.

We propose a passivation model to explain the increase in TAAGIC stability with increasing TAA size. TAA cations are known to generate alkyl radicals upon reductive decomposition at the potentials applied in these experiments,[28-30] according to:

$$(C_7H_{15})_4N^+ + e^- \rightarrow (C_7H_{15})_3N + C_7H_{15}\cdot \quad (4.1)$$

The fate of these alkyl radicals depends on the species present and reaction conditions. In the aprotic and reductively-stable DMSO solvent, we propose that both small and large alkyl formed from TAA cations react to alkylate the graphene sheet edges:

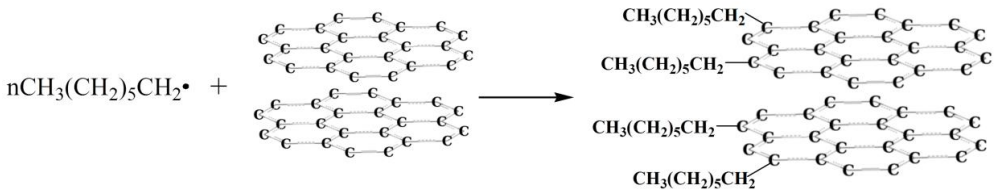

(4.2)

The exact nature of the surface chemistry during this reaction is not currently understood, and may be complex, however, the significant point for this model is that surface alkylation results. Then, only the longer surface alkyl groups can combine to form an effective passivation layer that stabilizes and permits isolation of a stable TAAGIC.

In Li-ion batteries, decomposition of the organic/Li salt electrolyte results in the formation of a protective solid electrolyte interphase (SEI) layer on the graphite surface.

The insoluble SEI layer is about 20 nm thick, appears to consist predominantly of Li_2CO_3 and LiF, and permits rapid transfer of desolvated Li^+ ions.[31] Our proposed surface layer from TAA decomposition is likely to be thinner and more flexible, and, interestingly, permits the rapid transport of large TAA cations. This surface passivation and transport will be further described in a subsequent publication.

The TGA mass losses of selected TAAGICs are shown in Figure 4.5. The unreacted electrodes (Figure 4.5a) show a small loss at 300-450°C due to binder degradation, and the onset of graphite degradation is at 600°C. The binder content obtained by TGA (3.5 mass pct) is comparable to that used in the electrode formation slurry (5 pct). T4AGIC and T7AGIC (Figure 4.5b and c) show multiple mass loss steps ascribed to thermolysis of the TAA cations at 120-580°C, polymer binder at 300-450°C, and graphite above 600°C. T7AGIC also exhibits a prominent mass loss below 120°C, ascribed to DMSO evaporation. The thermal decomposition of TAA cations in the TAAGICs begins at a lower temperature, and requires a wider temperature range, than the corresponding bromide salts. The decreased thermal stability of TAA cations has been attributed to the catalytic effect of graphene sheets.[32,33]

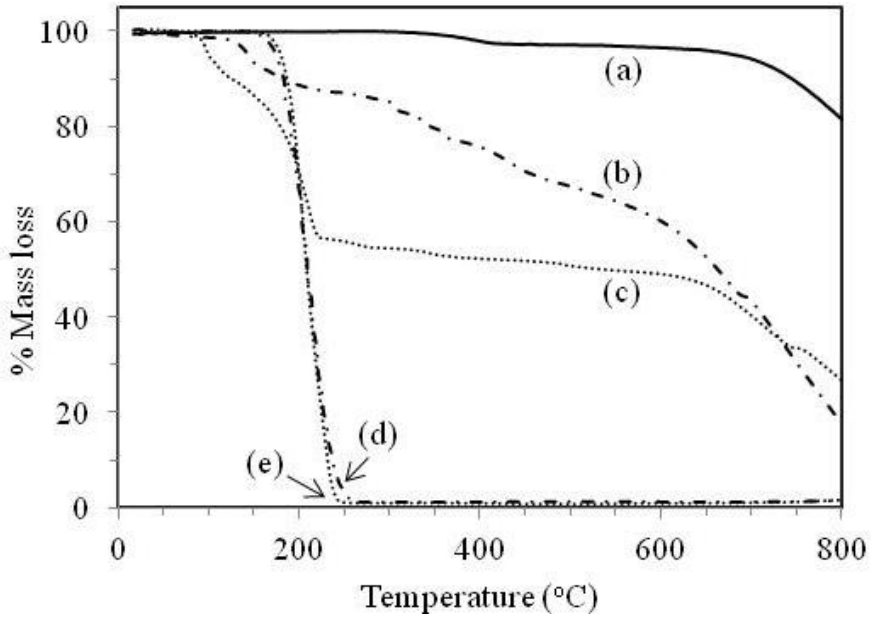

Figure 4.5 TGA plots for (a) graphite with EPDM binder, (b) T4AGIC, (c) T7AGIC, (d) T4ABr and (e) T7ABr.

After correcting for binder content, the TAAGIC compositions obtained by the above TGA assignments are shown in Table 4.1. Compared with the x = 43 value obtained in the chemically-derived product, the T4AGIC with x = 37 has a relatively high intercalate content, consistent with an impurity bilayer phase (that will have a higher intercalate content) rather than an impurity stage-2 phase (that will be poorer in intercalate). Also, the T4AGIC product obtained does contain a small DMSO co-intercalate content, unlike the chemically-derived product. DMSO mass contents in T4AGIC and T7AGIC from TGA were calculated at 1.5 and 8.7 mass pct, respectively, consistent with sulfur elemental analyses for these samples, which yielded 1.7 mass pct DMSO for T4AGIC and 9.8 mass pct DMSO for T7AGIC. Again, a bilayer impurity

phase, but not a stage-2 phase, is more appropriate to explain the minor presence of DMSO.

Lattice enthalpies for GICs generally decrease for larger gallery expansions, and in the simplest electrostatic model might be expected to scale with $1/\Delta d$. However, bilayer galleries can be favored over monolayers when larger ion monolayers cannot compensate the host sheet charge densities. The formation of monolayers vs. multilayers for different intercalates is well-known for other charged host structures.[34-36] In order to further evaluate these effects, the packing fraction of intercalate galleries was calculated for the obtained TAAGICs. This fraction was determined by taking the ratio of the intercalate volume, estimated using the VABC (Atomic and Bond Contributions of van der Waals volume) method,[37] to the gallery volume, obtained from the observed TAAGIC gallery expansions, product compositions, and a surface area for graphene sheets of 0.0261 nm^2 / C atom. The derived packing fractions are indicated in Table 4.1, and show that the monolayer arrangement (with some bilayer impurity phase) to be the most densely packed gallery. The maximum achievable packing fraction from geometric considerations is not apparent for these irregularly-shaped, flattened TAA cations, but the transition to an exclusively bilayer arrangement is consistent with the greater spatial requirements to accommodate the larger TAA cations. Additionally, it is notable that the *x* values obtained for the bilayer GICs, from 47 to 56, indicate that unusually-low sheet charge densities are obtained for stage-1 GICs with these large TAA cation intercalates. Since lattice enthalpies also depend on sheet charge densities, and the chemical and electrochemical properties, including delamination, depend on lattice enthalpies, the

ability to control sheet charge densities on GICs by selection of intercalate cation size could be a significant step towards producing GICs with novel properties.

The electrochemical behavior of graphite electrodes in TAABr/DMSO electrolytes was also investigated by cyclic voltammetry. As shown in Figure 4.6a and d, the electrolytes themselves are stable to about -2.3 to -2.6 V on a Pt foil electrode. Previous reports indicate the irreversible reduction of T2A and T7A at similar potentials to yield the corresponding amines.[28] Our evaluation of a 0.1 M $LiN(SO_2CF_3)_2$/DMSO electrolyte under similar scans from 0 to -2.8 V shows no cathodic decomposition, demonstrating the stability of the DMSO solvent at low potentials (data not shown).

Graphite electrodes in 0.1 M TAABr/DMSO electrolytes exhibit a new broad cathodic reaction with onset at -1.6 V and current peak near -2.2 V. This cathodic feature is ascribed to reductive TAA intercalation, and the very broad and sometimes multiple anodic peaks from -2.0 to -0.5 V in the case of T2A, are ascribed generally as oxidative de-intercalation of the GIC. The round-trip coulombic efficiency for the first voltammetric cycle was 96% for T2A; this efficiency decreases with increased cation size down to 26% for T7A. The lower chemical reversibility for larger cations suggests a diffusion-limited de-intercalation process. The graphite sheet charge density, expressed as x in C_x^-, is 35 for T2A as compared with 37 for T4AGIC (Table 4.1), indicating that a stage-1 T2AGIC was formed *in situ* during cyclic voltammetry. As described above, this T2AGIC is unstable and cannot be isolated after galvanostatic reduction.

Table 4.1 The structural and compositional data for obtained TAAGICs.

Product	Stage	Δd_i (nm)	Intercalate arrangement	Total intercalate (mass pct)	Composition	Packing fraction
T4AGIC	1[a]	0.48	monolayer	36.5	$[(C_4H_9)_4N]C_{37}\cdot 0.1DMSO$	0.67
T5AGIC	1	0.81	bilayer	40.9	$[(C_5H_{11})_4N]C_{47}\cdot 0.7DMSO$	0.42
T6AGIC	1	0.81	bilayer	41.0	$[(C_6H_{13})_4N]C_{56}\cdot 0.8DMSO$	0.42
T7AGIC	1	0.82	bilayer	47.4	$[(C_7H_{15})_4N]C_{54}\cdot 1.2DMSO$	0.51
T8AGIC	1	0.81	bilayer	49.3	$[(C_8H_{17})_4N]C_{56}\cdot 1.2DMSO$	0.56

[a] impurity ascribed to bilayer phase

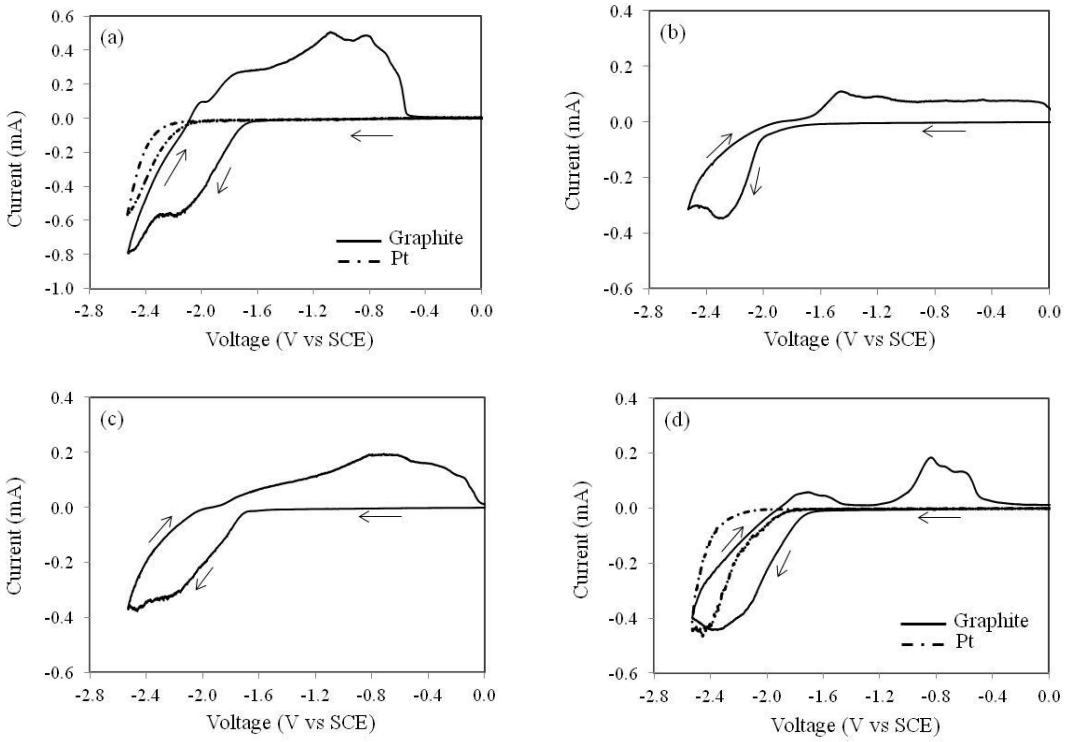

Figure 4.6 Cyclic voltammograms of graphite in 0.1 M (a) T2ABr/DMSO, (b) T3ABr/DMSO, (c) T5ABr/DMSO and (d) T7ABr/DMSO at a scan rate of 1 mV/s.

Since galvanostatic methods show that TAA cations smaller than T4A do not form stable low-stage GICs, whereas cyclic voltammetry shows the characteristic features of intercalation/de-intercalation for these cations, and even suggests more rapid diffusion and more efficient processes for the smaller TAA cations. By putting these results together we can conclude that the smaller TAAs readily form GICs but they are unstable and rapidly decompose back to graphite or high-stage GICs, as noted by Besenhard et al. previously,[19] and that the stability of the larger TAAGICs is consistent with the formation of a more effective passivation layer as proposed above.

Figure 4.7 displays the first and third voltammetric cycles for graphite in 0.1 M T7ABr/DMSO. The first cycle exhibits reversible electrochemical intercalation/de-intercalation along with the irreversible decomposition of T7A cations at lower potential. The charges associated with cathodic and anodic scans were 0.32 and 0.082 C, respectively. The ratio suggests that only a minor fraction of the TAA intercalates are released from the galleries after intercalation. This indicates the slow diffusion of DMSO-solvated T7A cations within the galleries. The second cycle (not shown) shows lower currents with greater separation of cathodic and anodic peak potentials. For the third cycle (shown), this trend continues, with the cathodic sweep dominated by the TAA reduction rather than intercalation. Slow TAA diffusion results in dampened intercalation/de-intercalation on cycling even at the low sweep rate employed. Large TAA cations would not appear to be interesting as reversible insertion/de-insertion guests, such as for use directly in rechargeable electrodes. On the other hand, these cations might be introduced and retained within graphene galleries, and thereby modify the gallery chemistry and structure for accommodation of other guests.

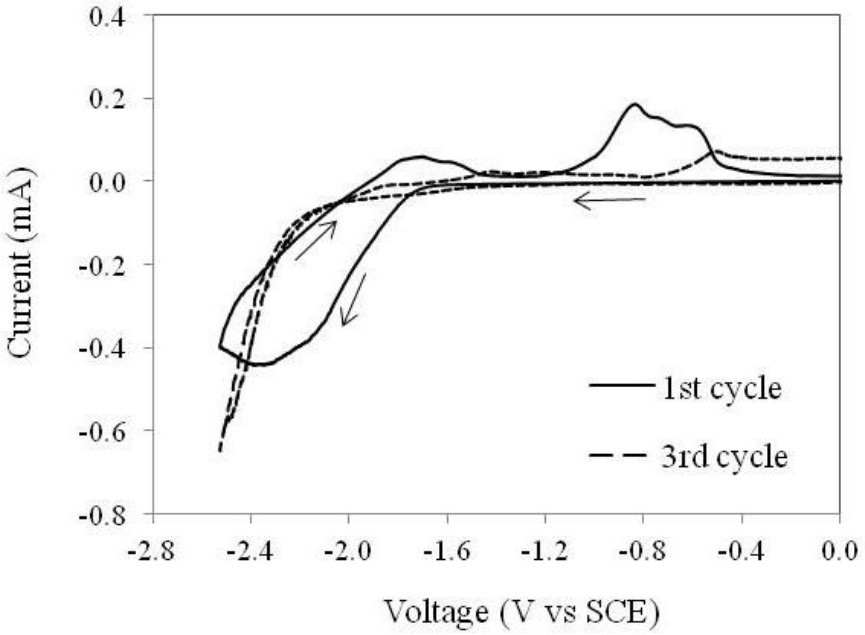

Figure 4.7 Cyclic voltammetry of graphite in 0.1 M T7ABr/DMSO at a scan rate of 1 mV/s.

4.5 REFERENCES

(1) Dresselhaus, M. S.; Dresselhaus, G. *Adv. Phys.* **2002**, 51, 1-186.

(2) Ebert, L. B. *Annu. Rev. Mater. Sci.* **1976**, 6, 181-211.

(3) Forsman, W. C.; Dziemianowicz, T.; Leong, K.; Carl, D. *Synth. Met.* **1983**, 5, 77-100.

(4) Maluangnont, T.; Sirisaksoontorn, W.; Lerner, M. M. *Carbon* **2012**, 50, 597-602.

(5) Mizutani, Y.; Abe, T.; Ikeda, K.; Ihara, E.; Asano, M.; Harada, T.; Inaba M.; Ogumi, Z. *Carbon* **1997**, 35, 61-65.

(6) Abe, T.; Fukuda, H.; Iriyama Y.; Ogumi, Z. *J. Electrochem. Soc.* **2004**, 151, A1120-A1123.

(7) Besenhard, J. O. *Carbon* **1976**, 14, 111-115.

(8) Enoki, T.; Suzuki, M.; Endo, M. *Graphite Intercalation Compounds and Applications*; Oxford University Press: New York, 2003.

(9) Thomas, J. M.; Millward, G. R.; Schlögl R. F.; Boehm, H. P. *Mater. Res. Bull.* **1980**, 15, 671-676.

(10) Sethuraman, V. A.; Hardwick, L. J.; Srinivasan V.; Kostecki, R. J. *J. Power Sources* **2010**, 195, 3655-3660.

(11) Ogumi, Z.; Inaba, M. *Bull. Chem. Soc. Jpn.* **1998**, 71, 521-534.

(12) Fukada, S.; Shintani, Y.; Shimomura, M.; Tahara F.; Yagi, R. *Jpn. J. Appl. Phys.* **2012**, 51, 085101-085104.

(13) Mukherjee, A.; Kang, J.; Kuznetsov, O.; Sun, Y.; Thaner, R.; Bratt, A. S.; Lomeda, J. R.; Kelly K. F.; Billups, W. E. *Chem. Mater.* **2011**, 23, 9-13.

(14) Truong, Q. T.; Pokharel, P.; Song G. S.; Lee, D. S. *J. Nanosci. Nanotechnol.* **2012**, 12, 4305-4308.

(15) Wei, T.; Fan, Z.; Luo, G.; Zheng C.; Xie, D. *Carbon* **2009**, 47, 337-339.

(16) Toyoda, M.; Inagaki, M. *Carbon* **2000**, 38, 199-210.

(17) Sirisaksoontorn, W.; Lerner, M. M. *Inorg. Chem.* **2013**, 52, 7139-7144.

(18) Sirisaksoontorn, W.; Adenuga, A. A.; Remcho, V. T.; Lerner, M. M. *J. Am. Chem. Soc.* **2011**, 133, 12436-12438.

(19) Besenhard, J. O.; Möhwald H.; Nickl, J. J. *Carbon* **1980**, 18, 399-405.

(20) Simonet, J. *J. Electrochem. Commun.* **2013**, 30, 17-20.

(21) Zheng, H.; Jiang, K.; Abe T.; Ogumi, Z. *Carbon* **2006**, 44, 203-210.

(22) Ko, Y.; Lee, C. T. *J. Ind. Eng. Chem.* **2012**, 18, 726-730.

(23) Besenhard, J. O.; Theodoridou, E.; Möhwald H.; Nickl, J. J. *Synth. Met.* **1982**, 4, 211-223.

(24) Leef, A.; Gilmour, A. *J. Appl. Electrochem.* **1979**, 9, 663-670.

(25) Smart, M. C.; Ratnakumar, B. V.; Surampudi, S.; Wang, Y.; Zhang, X.; Greenbaum, S. G.; Hightower, A.; Ahn, C. C.; Fultz, B. *J. Electrochem. Soc.* **1999**, 146, 3963-3969.

(26) Yuqin, C.; Hong, L.; Lie, W.; Tianhong, L. *J. Power Sources* **1997**, 68, 187-190.

(27) Matsumura, Y.; Wang S.; Mondori, J. *J. Electrochem. Soc.* **1995**, 142, 2914-2918.

(28) Dahm, C. E.; Peters, D. G. *J. Electroanal. Chem.* **1996**, 402, 91-96.

(29) Eggert, G.; Heitbaum, J. *Electrochim. Acta* **1986**, 31, 1443-1448.

(30) Mayell, J. S.; Bard, A. J. *J. Am. Chem. Soc.* **1963**, 85, 421-425.

(31) Xu, K.; Cresce, A. *J. Mater. Res.* **2012**, 27, 2327-2341.

(32) Muradov, N.; Smith, F.; T-Raissi, A. *Catal. Today* **2005**, 102, 225-233.

(33) Sun, R. Q.; Sun, L. B.; Chun, Y.; Xu, Q. H. *Carbon* **2008**, 46, 1757-1764.

(34) Mercier, L.; Detellier, C. *Clays Clay Miner.* **1994**, 42, 71-76.

(35) Chun, Y.; Sheng, G.; Boyd, S. A. *Clays Clay Miner.* **2003**, 51, 415-420.

(36) Li, Z.; Jiang, W.T. *Thermochim. Acta* **2009**, 483, 58-65.

(37) Zhao, Y. H.; Abraham, M. H.; Zissimos, A. M. *J. Org. Chem.* **2003**, 68, 7368-7373.

CHAPTER 5

THE EFFECT OF SURFACE PASSIVATION ON THE PREPARATION AND STABILITY OF THE GRAPHITE INTERCALATION COMPOUNDS CONTAINING TETRA-n-ALKYLAMMONIUM CATIONS

Weekit Sirisaksoontorn and Michael M. Lerner

Department of Chemistry

Oregon State University

Corvallis, OR 97331-4003, USA

Carbon, doi:10.1016/j.carbon.2013.12.070

5.1 ABSTRACT

The kinetic stability of graphite intercalation compounds (GICs) is markedly increased by a surface passivation reaction that occurs under strong reducing conditions in the presence of long-chain tetra-n-alkylammonium cations. A simple alkylation model is proposed. Surface alkylation allows the formation of a stable, isolable, graphite intercalation compound of tetra-n-ethylammonium, $(C_2H_5)_4N^+$ for the first time, by chemical surface passivation of $[Na(en)_{1.0}]C_{15}$ (en = ethylenediamine) with NR_4^+, R = C_6H_{13}, C_7H_{15} or C_8H_{17}, followed by an ion exchange reaction to displace the $Na(en)^+$ complex with $(C_2H_5)_4N^+$. One GIC thus obtained using dimethylsulfoxide (DMSO) as solvent has composition $[(C_2H_5)_4N]C_{57}\cdot 0.5DMSO$, and is a stage-1 compound with a gallery expansion of 0.47 nm. This relatively small expansion indicates a monolayer of intercalate and additionally requires an unusually flattened cation conformation. Electrophoretic analyses indicate that the ion exchange within the graphene galleries goes to completion. Additionally, the passivated GIC surfaces afford a dramatic increase in the stability of GICs, in protic solvents, aqueous media, and the ambient environment.

5.2 INTRODUCTION

Graphite intercalation compounds (GICs) contain graphene sheets as layered host and intercalate guests located between the host sheets. The graphene sheets themselves are either reduced or oxidized, and accommodate cation or anion intercalates, respectively, to form donor-type or acceptor-type GICs.[1-5] Chemical and electrochemical methods can produce a wide range of GICs.[6-9] Depending on synthetic conditions, neutral molecules may co-intercalate along with ions.[10-13] Uniquely for GICs, ordered stacking of host sheets and intercalates can result in a "staging" phenomenon; in stage-1 all individual graphene sheets are encased by intercalate galleries, in stage-2, two graphene sheets are encased, and etc.[14,15] GICs are important in several applied technologies, including Li-ion batteries and the production of thermally exfoliated graphite.[16-18]

Our group recently reported a homologous series of tetra-n-alkylammonium (TAA) GICs that can be prepared by either the chemical exchange of the $Na(en)^+$ complex from $[Na(en)_{1.0}]C_{15}$ (en = ethylenediamine) or by the electrochemical reduction of graphite in a TAABr/dimethylsulfoxide (DMSO) electrolyte.[19-21] Stage-1 GIC products were obtained with TAA cations larger than $(C_3H_7)_4N^+$. The $(C_4H_9)_4N^+$ cation intercalates to form monolayers with a gallery expansion of 0.47 nm and no solvent co-intercalation. The larger TAA cations, e.g. $(C_6H_{13})_4N^+$, $(C_7H_{15})_4N^+$ or $(C_8H_{17})_4N^+$, form intercalate bilayers with gallery expansions of approx. 0.76 nm and with significant DMSO co-intercalation. All these GICs must contain TAA cations with highly-flattened conformations in order to fit within the confined gallery dimensions observed.

When the same chemical exchange method is employed with the smaller symmetric TAA cations, $(CH_3)_4N^+$, $(C_2H_5)_4N^+$ and $(C_3H_7)_4N^+$, only graphite or high-stage GICs were obtained.[20] On first impression, this is a surprising result. The reductive stabilities of small and large TAA cations, e.g. $(CH_3)_4N^+$, $(C_2H_5)_4N^+$, $(C_4H_9)_4N^+$ and $(C_6H_{13})_4N^+$, as measured by linear sweep voltammetry in the $TAABF_4$/propylene carbonate (PC) electrolyte, are similar and all are between -3.00 and -3.10 V vs SCE.[22] The kinetics of exchange with smaller cations should be, if anything, more favorable. Additionally, electrochemical reduction of graphite in a $(C_2H_5)_4NBr$/ DMSO electrolyte indicated that the intercalation of $(C_2H_5)_4N^+$ occurs *in situ*. However, as noted above, and also in these electrochemical syntheses, the GIC products with smaller TAA cations were not sufficiently stable enough to be isolated and characterized.

This observation agrees well with many previous reports that describe the *in situ* generation of $(CH_3)_4N$- and/or $(C_2H_5)_4N$-GICs by electrochemical reduction in aprotic organic electrolytes, including acetonitrile, PC, *N*,*N*-dimethylformamide (DMF), DMSO and *N*-methyl-2-pyrrolidone.[23-28] In these studies, linear sweep or cyclic voltammetry indicates a reversible redox process associated with intercalation/deintercalation. However, well-ordered or single-phase GIC products are very difficult to isolate and structurally or compositionally characterize. Foundational studies by Besenhard et al,[27] indicated that electrochemically-prepared $(CH_3)_4N$-GIC exhibits multiple phases owing to its instability and self-decomposition. They reported a gallery expansion of 1.25 nm, and proposed the intercalate guest may be an octahedral $[(CH_3)_4N(DMSO)_6]^+$ complex.

The product composition obtained from the potential/charge curve was $[(CH_3)_4N]C_{24n}$ (*n* is the stage number), in agreement with a more recent report by Simonet.[25]

Ruch et al reported the disappearance of *(002)* graphite reflection during reduction at around 1 V vs Li/Li^+ in a $(C_2H_5)_4N^+$- containing electrolyte, and the appearance of weak un-indexed reflections.[23] Wang et al similarly reported that a graphite electrode held at a low potential in TAA salt/PC electrolytes lost the native graphite phase and new broad peaks appeared at *d*-spacings at 0.37 and 0.29 nm.[24] Cooper et al similarly observed the native graphite diffraction reflection to broaden and disappear and a number of new diffraction peaks to appear after reduction in PC electrolytes containing TAA salts.[28]

We have postulated that larger TAA cations can alkylate graphene sheet edges to form effective passivation layers that permit the isolation of low-stage GIC products with dramatically enhanced stabilities. A typical surface alkylation reaction would proceed as follows;

$$(C_7H_{15})_4N^+ + e^- \longrightarrow (C_7H_{15})_3N + CH_3(CH_2)_5CH_2^{\cdot} \qquad (5.1)$$

$$GIC + CH_3(CH_2)_5CH_2^{\cdot} \longrightarrow GIC\text{---}CH_3(CH_2)_5CH_2 \qquad (5.2)$$

$(C_7H_{15})_4N^+$ cations are first reduced by reaction of the starting GIC, $[(Na(en)_{1.0}]C_{15}$, yielding an amine and alkyl radical. The electrochemical reduction of TAA cations to

form alkyl radicals has been reported previously.[29-31] The radical species then alkylates functional groups present on the graphene sheet edges to form a passivation layer.

In this article, we describe the first synthesis, isolation and characterization of single-phase $(C_2H_5)_4N$-GIC by using this surface passivation by larger TAA cations to stabilize the subsequent GIC products, and also explore how such passivation leads to increased stability for TAA-GICs under a range of oxidizing conditions.

5.3 EXPERIMENTAL

5.3.1 Synthesis of $(C_2H_5)_4N$-GIC

$[Na(en)_{1.0}]C_{15}$ was prepared by a previously reported method with minor modifications:[32] 240 mg (20 mmol) of SP-1 graphite (Union Carbide, average diameter = 100 μm) was mixed with 57 mg (2.5 mmol) of sodium metal and 3 ml of ethylenediamine (en). The reactants were continuously stirred at 60 °C for 24 h under an inert atmosphere. The mixture was then centrifuged and the solution phase removed via syringe. The blue solid product was dried *in vacuo* overnight at room temperature. The product was characterized by PXRD and TGA, and then used in the subsequent reactions.

Next, surface passivation of $[Na(en)_{1.0}]C_{15}$ was accomplished by combining 12 mg (0.024 mmol) of tetra-n-heptylammonium bromide, $(C_7H_{15})_4NBr$, and 79 mg (0.30 mmol) of $[Na(en)_{1.0}]C_{15}$ in 2 ml of DMSO. The reactants were stirred under an inert atmosphere at 20°C for 2 min. After centrifuging, the solution phase was removed via syringe and a dull-black and wet solid was obtained.

Ion exchange was accomplished by adding a 0.1 M solution of tetra-n-ethylammonium bromide, $(C_2H_5)_4NBr$, in 2 ml of DMSO, to the black solid product obtained from the previous step and reacting at 60°C for 10 min under an inert atmosphere. The top phase solution was separated by syringe after centrifuging. The wet product was washed with acetonitrile and then dried *in vacuo* overnight at ambient temperature. For other trials, the solvents DMF or n-hexanol were employed for the ion exchange reactions.

All reactant solutions and rinse solvents were collected and combined for electrophoretic analyses. The extent of ion exchange was evaluated from the known masses of $[Na(en)_{1.0}]C_{15}$ and TAA cations in reactant and those found in the residual solutions. Solid products were characterized as described below.

5.3.2 Stability of $(C_7H_{15})_4N$-GIC

$(C_7H_{15})_4N$-GIC was synthesized via the chemical exchange reaction from $[Na(en)_{1.0}]C_{15}$ as indicated above. The synthesis, structure and composition of $(C_7H_{15})_4N$-GIC have been reported in our previous work.[20] Stability tests were carried out by exposing the GIC to the following conditions; (1) distilled water, (2) 1 M HCl (pH = 0), (3) 0.1 M $FeCl_3$ in 1 M HCl, and (4) in 0.01 M I_2 in $CHCl_3$. All stability tests were conducted at 20 °C for 24 h. After each test, the solid sample was collected and dried at ambient temperature *in vacuo* overnight.

5.3.3 Characterization

A Rigaku Miniflex II diffractometer with Ni-filtered Cu K_α radiation was used for powder X-ray diffraction (PXRD) studies. PXRD patterns were collected at a scan speed of 5° /min from 3 - 60° 2θ. Due to preferred orientation, mainly *(00l)* reflections are observed and indexed. The relationship between the observed repeat distance along the stacking c-direction (I_c), the stage number (n) and the gallery expansion is expressed as;

gallery expansion = I_c – 0.335n, where 0.335 nm corresponds to the thickness of a single graphene sheet. The thermal behaviors of obtained GICs were investigated on a Shimadzu TGA-50 thermogravimetric analyzer (TGA) under flowing Ar/O_2 (20 ml/min) at a heating rate of 10 °C/min from ambient to 800°C. The extent of ion exchange; the appearance of Na^+ and en, and the depletion of the TAA cation used for passivation and of the $(C_2H_5)_4N^+$ intercalate, was studied by using the capillary zone electrophoresis (CZE) analyses. Measurements were performed on a HP ^{3D}CE instrument equipped with a UV detector, using fused-silica capillaries. The experimental details for CZE have been described previously.[19] CZE calibration curves are provided in Supplementary Data.

5.4 RESULTS AND DISCUSSION

Figure 5.1 shows diffraction patterns of obtained solid products, including native graphite (Figure 5.1a) for comparison. Following reaction with Na(m) in en solution, graphite is reduced to form a stage-1 $[Na(en)_{1.0}]C_{15}$ with gallery expansion of 0.36 nm as reported previously (Figure 5.1b).[32] In this GIC, en forms a chelate complex with Na^+ oriented parallel to the graphene sheets. Following surface treatment by $(C_7H_{15})_4N^+$ and subsequent ion exchange with $(C_2H_5)_4N^+$, (Figure 5.1c) a new series of Bragg reflections up to *(001-005)* indicates a new stage-1 GIC with gallery expansion of 0.47 nm. This dimension is similar to that observed previously for $(C_4H_9)_4N$-GIC,[19] and corresponds to the flattened monolayer arrangement of TAA cations, presented in Figure 5.2. However, when the surface passivation step is omitted (Figure 5.1d), the obtained product is a mixture of a high-stage GIC and a disordered graphite with broadened *(00l)* reflections.

As noted above, we ascribe the isolation of a stable $(C_2H_5)_4N$-GIC following surface treatment to the passivation afforded by alkylation of graphene sheet edges. More specifically, all the GICs obtained are thermodynamically unstable with respect to oxidation by the solvents employed. Shorter alkyl chains do not provide a sufficient barrier to that surface reaction, but when alkyl chains longer than butyl are employed for passivation the decomposition reaction slows dramatically. Presumably, surface alkylation increases the surface hydrophobicity, or more generally decreases surface wetting by polar species, and thus decreases any oxidative decomposition by polar species. The reaction model suggests that even without an explicit passivation step,

$(C_2H_5)_4N$-GIC will undergo surface ethylation, but these short alkyl chains do not afford an isolable product.

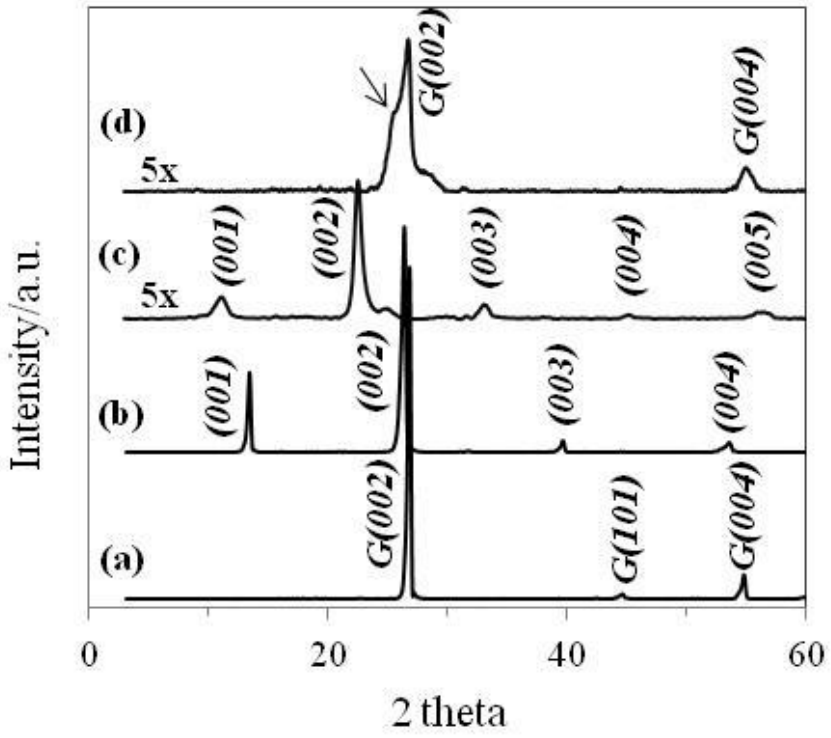

Figure 5.1 PXRD patterns of (a) SP-1 graphite, (b) $[Na(en)_{1.0}]C_{15}$, (c) $(C_2H_5)_4N$-GIC and (d) the product obtained without using surface passivation. Intensities of (c) and (d) are 5x. Reflection indices are indicated, and native graphite reflections are labeled with a G. The arrow above 1d points at a high-stage GIC reflection.

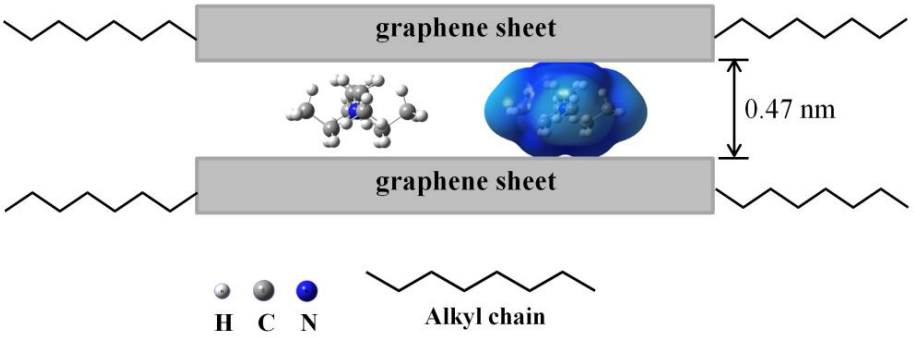

Figure 5.2 The flattened monolayer arrangement of intercalate encased by graphene sheets with alkylated surface. Both ball-and-stick (left) and mapped-surface (right) depictions of $(C_2H_5)_4N^+$ are shown.

Figure 5.3 shows PXRD patterns of products obtained following surface passivation of $[Na(en)_{1.0}]C_{15}$ with different TAA cations. The major product following passivation with $(C_4H_9)_4N^+$ is graphite (Figure 5.3a). The larger TAA cations, $(C_6H_{13})_4N^+$, and $(C_8H_{17})_4N^+$ act similarly to $(C_7H_{15})_4N^+$ and resulted in a predominantly stage-1 $(C_2H_5)_4N$-GIC with a gallery expansion of 0.47 nm (Figure 5.3c and d). A broadened strongest reflection indicates the presence of some high-stage GICs in these products. Passivation with $(C_5H_9)_4N^+$ results in a disordered product (broad and weak diffraction) containing a high-stage GIC (Figure 5.3b). These results confirm that only the larger TAA cations can form effective passivation layers that permit the isolation of $(C_2H_5)_4N$-GIC.

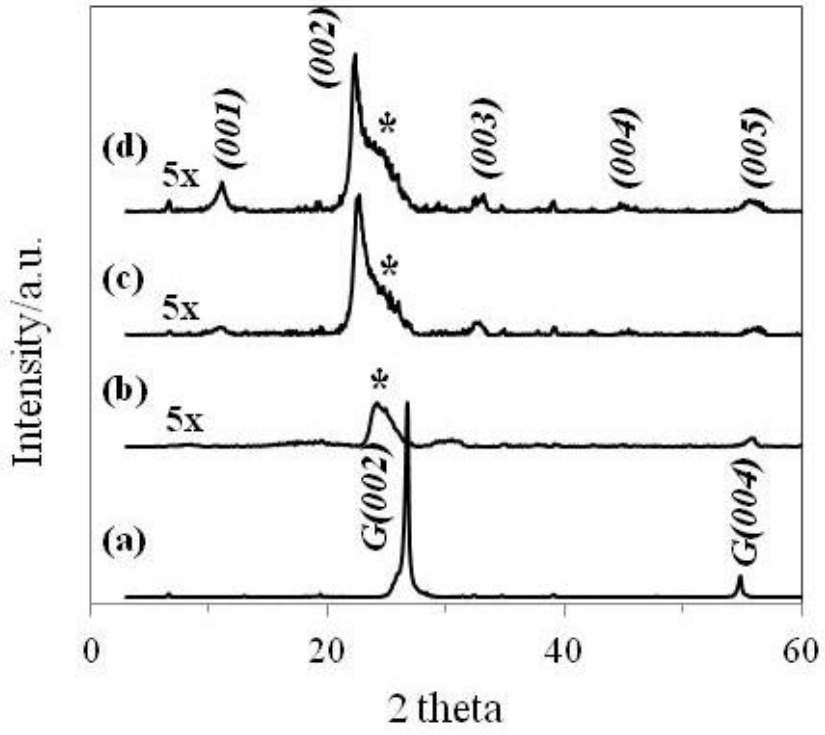

Figure 5.3 PXRD patterns of products obtained using the following TAA cations for surface passivation; (a) $(C_4H_9)_4N^+$, (b) $(C_5H_{11})_4N^+$, (c) $(C_6H_{13})_4N^+$ and (d) $(C_8H_{17})_4N^+$. Intensities of (b), (c) and (d) intensities are 5x. Asterisks indicate reflections from a high-stage GIC.

Previously, we reported that DMSO does not co-intercalate with $(C_4H_9)_4N^+$, but does co-intercalate with the larger TAA cations.[20,21] The selection of reaction solvents for reductive interaction or exchange of donor-type GICs has been limited by the requirement that such solvents be reductively stable with respect to the reducing agents employed and the GIC products. In this study, DMF was also evaluated as the exchange solvent and a stage 1 GIC obtained with a gallery expansion similar to that obtained in DMSO (Figure 5.4a). Surprisingly, we observed that the exchange can even be carried

out in n-hexanol. This is a good solvent for the TAA salt employed in the exchange, but as a protic solvent, is highly susceptible towards reduction by a donor-type GIC. As far as we are aware this is an unprecedented result – the generation of a donor-type GIC by exchange in a protic solvent. The observed product (Figure 5.4b) displays reflections corresponding to a stage-2 GIC with gallery expansion of 0.48 nm.

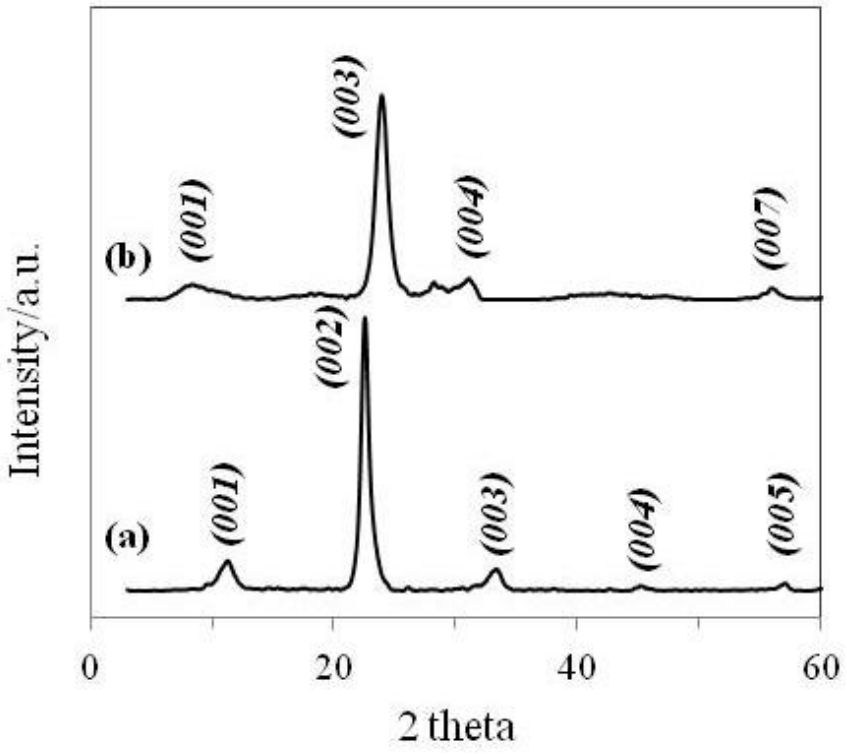

Figure 5.4 PXRD patterns of obtained $(C_2H_5)_4N$-GIC with the surface passivation by $(C_7H_{15})_4N^+$ and subsequent ion exchange in (a) *N*,*N*-dimethylformamide (DMF) and (b) n-hexanol.

The thermal behavior of $(C_2H_5)_4N$-GIC was used to evaluate composition. As seen in Figure 5.5, the mass loss for $(C_2H_5)_4N$-GIC occurs in two steps, with a 5.0% mass loss at 85-110°C attributed to the volatilization of DMSO co-intercalate and the 15.3% mass loss at 110-550°C attributed to the degradation of $(C_2H_5)_4N^+$. For comparison, the salt $(C_2H_5)_4NBr$ is stable to 250°C, indicating the oft-observed catalytic effect of graphene sheets towards guest thermolysis.[33,34] Above 550°C, the steep mass loss is due to the combustion of graphitic carbon in the flowing O_2 gas stream. Based on these data, the composition of stage-1 $(C_2H_5)_4N$-GIC is found to be $[(C_2H_5)_4N]C_{57}\cdot 0.5DMSO$.

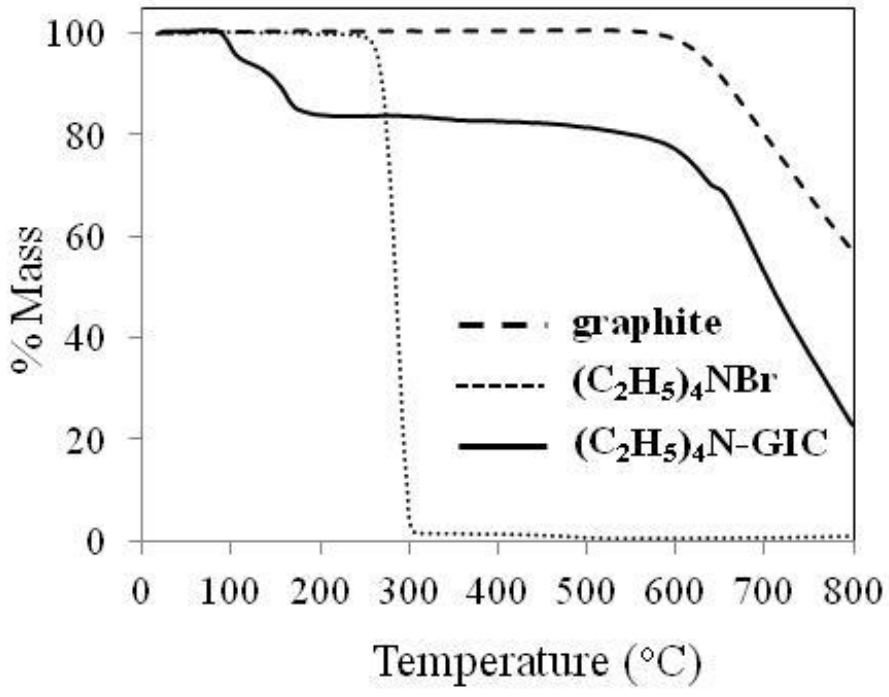

Figure 5.5 TGA plots for the $(C_2H_5)_4N$-GIC prepared after surface passivation by $(C_7H_{15})_4N^+$ in DMSO, and for SP-1 graphite and $(C_2H_5)_4NBr$.

From the observed gallery expansion and composition, the packing fraction of the GIC product, which is defined as a ratio of the intercalate (plus co-intercalate) guest volume to the volume opened by gallery expansion, is about 0.28. This can be compared to a packing fraction of 0.51 for $[Na(en)_{1.0}]C_{15}$ prior to ion exchange. The low value for $(C_2H_5)_4N$-GIC indicates that it contains open galleries with significant separation of cations, and suggests that packing considerations are not important in the final GIC composition and structure.

By quantifying the appearance of Na^+ and en, and the disappearance of the TAA cations $(C_7H_{15})_4N^+$ and $(C_2H_5)_4N^+$ in solutions, CZE provides a powerful way to evaluate the concentrations of all these species in solution and, by comparing with the amounts contained in reactants, yields the extent of ion exchange and the compositions of the GIC products. An electropherogram (Figure 5.6) shows peaks associated with en, Na^+, $(C_2H_5)_4N^+$ and $(C_7H_{15})_4N^+$ in solution following the surface passivation and ion exchange reactions. Recoveries of en and Na^+ from $[Na(en)_{1.0}]C_{15}$ are quantitative, indicating that the $Na(en)^+$ complex has been completely displaced from the GIC galleries. $(C_7H_{15})_4N^+$ and $(C_2H_5)_4N^+$ show 5% (0.0012 mmol) and 46% (0.092 mmol) depletion from starting concentrations. The former TAA cations is being consumed to form the passivation layer, while the latter undergoes the ion exchange with $Na(en)^+$ complex. These depletions indicate a GIC composition of $[(C_2H_5)_4N]C_{50}$·yDMSO (the DMSO co-intercalate is not measured by CZE), which is in reasonable agreement with the composition obtained from the TGA data. The TGA data provide more direct and reproducible results, and are therefore more accurate for reporting the GIC composition. The consumption of

$(C_7H_{15})_4N^+$ is on the order of 1% of that of $(C_2H_5)_4N^+$, consistent with its participation in only an edge surface reaction.

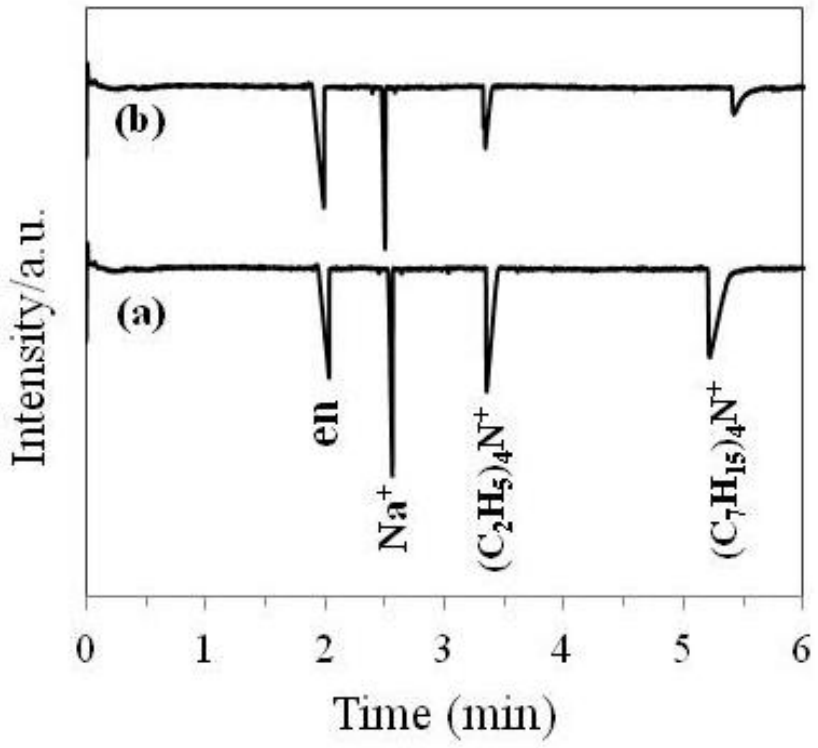

Figure 5.6 Electropherogram for separations of (a) 0.1 mM of standard solution and (b) a combined solution following surface passivation by $(C_7H_{15})_4N^+$ and ion exchange of $Na(en)^+$ by $(C_2H_5)_4N^+$.

The surface passivation model was further investigated by stability tests of a stage-1 $(C_7H_{15})_4N$-GIC under a range of oxidizing conditions. Figure 5.7a shows the PXRD pattern for $(C_7H_{15})_4N$-GIC, with strong narrow diffraction peaks indicating a well-ordered structure. After 24 h reaction with either distilled water or even in aqueous acid, the stage-1 GIC phase still predominates, with some decomposition indicated by a small

graphite reflection at 2θ ≈ 26° and a broadening of the strong *(003)* peaks (Figure 5.7b and c). Even following the addition of an oxidizing cation, Fe(III), to the aqueous acid solution, the stage-1 GIC phase dominates (Figure 5.7d) after 24 h reaction. In contrast, similar reaction with $I_2/CHCl_3$ results in formation of a high-stage GIC (Figure 5.7e). This less polar oxidant can more effectively attack $(C_7H_{15})_4N$-GIC. These results are consistent with GIC passivation by the formation of a hydrophobic surface on the reactive graphene sheet edge surfaces.

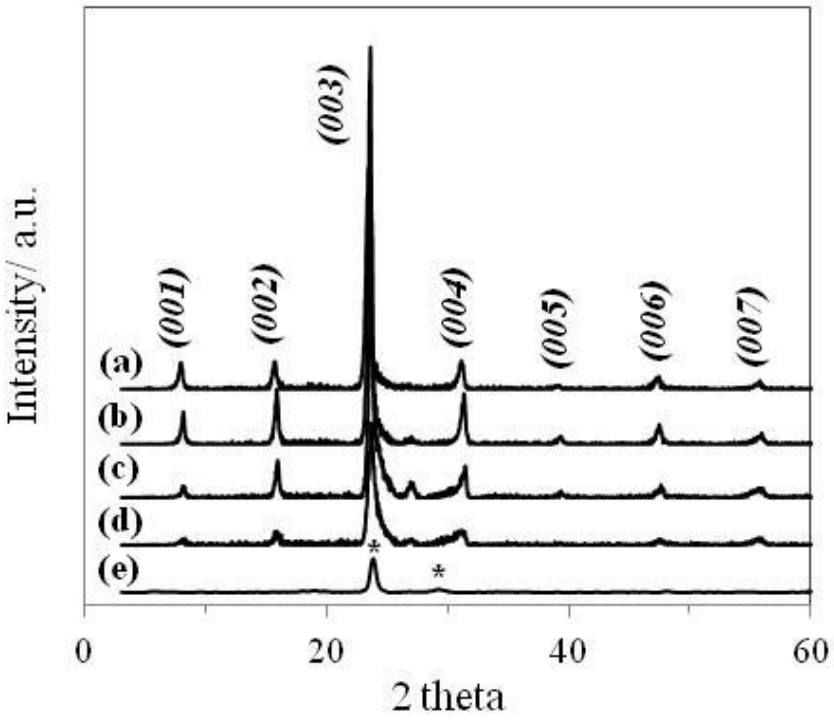

Figure 5.7 PXRD patterns of (a) $(C_7H_{15})_4N$-GIC, and $(C_7H_{15})_4N$-GIC samples exposed to (b) distilled water, (c) 1 M HCl (aq), (d) 0.1 M $FeCl_3$ / 1 M HCl (aq) and (e) 0.01 M I_2 / $CHCl_3$. Reactions proceeded at 20°C for 24 h. Asterisks indicate reflections from a high-stage GIC.

5.5 REFERENCES

(1) Hennig, G. R. *Prog. Inorg. Chem.* **1959**, 1, 125-205.

(2) Ebert, L. B. *Annu. Rev. Mater. Sci*. **1976**, 6, 181-211.

(3) Forsman, W. C.; Dziemianowicz, T.; Leong, K.; Carl, D. *Synth. Met.* **1983**, 5, 77-100.

(4) Dresselhaus, M. S.; Dresselhaus, G. *Adv. Phys.* **2002**, 51(1), 1-86.

(5) Enoki, T.; Suzuki, M.; Endo, M. *Graphite intercalation compounds and applications.* Oxford University Press: New York, 2003.

(6) Maluangnont, T.; Sirisaksoontorn, W.; Lerner, M. M. *Carbon* **2012**, 50, 597-602.

(7) Herold, C.; Herold, A.; Lagrange, P. *J. Phys. Chem. Solids* **1996**, 57, 655-662.

(8) Özmen-Monkul, B.; Lerner, M. M.; Pawelke, G.; Willner, H. *Carbon* **2009**, 47, 1592-1597.

(9) Noel, M.; Santhanam, R. *J. Power Sources* **1998**, 72, 53-65.

(10) Beguin, F.; Setton, R.; Facchini, L. *Synth. Met.* **1983**, 7, 263-269.

(11) Beguin, F.; Vast, P. *Synth. Met.* **1988**, 23, 427-433.

(12) Inagaki, M.; Tanaike, O. *Synth. Met.* **1995**, 73, 77-81.

(13) Kang, F.; Leng, Y.; Zhang, T. *Carbon* **1997**, 35(8), 1089-1096.

(14) Thomas, J. M.; Millward, G. R.; Schlögl, R. F.; Boehm, H. P. *Mater. Res. Bull.* **1980**, 15(5), 671-676.

(15) Sethuraman, V. A.; Hardwick, L. J.; Srinivasan, V.; Kostecki, R. *J. Power Sources* **2010**, 195, 3655-3660.

(16) Wang, F.; Yi, J.; Wang, Y.; Wang, C.; Wang, J.; Xia, Y. *Adv. Energy Mater.* **2013**, DOI:10.1002/aenm.201300600.

(17) Truong, Q.; Pokharel, P.; Song, G. S.; Lee, D. *J. Nanosci. Nanotechnol.* **2012**, 12, 4305-4308.

(18) Wei, T.; Fan, Z.; Luo, G.; Zheng, C.; Xie, D. *Carbon* **2009**, 47, 337-339.

(19) Sirisaksoontorn, W.; Adenuga, A. A.; Remcho, V. T.; Lerner, M. M. *J. Am. Chem. Soc.* **2011**, 133, 12436-12438.

(20) Sirisaksoontorn, W.; Lerner, M. M. *Inorg. Chem.* **2013**, 52, 7139-7144.

(21) Sirisaksoontorn, W.; Lerner, M. M. *ECS J. Solid State Sci. Technol.* **2013**, 2(9), M28-M32.

(22) Ue, M.; Ida, K.; Mori, S. *J. Electrochem. Soc.* **1994**, 141(11), 2989-2996.

(23) Ruch, P. W.; Hahn, M.; Rosciano, F.; Holzapfel, M.; Kaiser, H.; Scheifele, W.; Schmitt, B.; Novak, P.; Kotz, R.; Wokaun, A. *Electrochim. Acta* **2007**, 53, 1074-1082.

(24) Wang, H.; Yoshio, M. *J. Power Sources* **2012**, 200, 108-112.

(25) Simonet, J. *Electrochem. Commun.* **2013**, 30, 17-20.

(26) Besenhard, J. O.; Fritz, H. P. *J. Electroanal. Chem.* **1974**, 53, 329-333.

(27) Besenhard, J. O.; Möhwald, H.; Nickl, J. J. *Carbon* **1980**, 18, 399-405.

(28) Cooper, A. J.; Wilson, N. R.; Kinloch, I. A.; Dryfe, R. *Carbon* **2014**, 66, 340-350.

(29) Finkelstein, M.; Petersen, R. C.; Ross, A. D. *J. Am. Chem. Soc.* **1959**, 81, 2361-2364.

(30) Mayell, J. S.; Bard, A. J. *J. Am. Chem. Soc.* **1963**, 85, 421-425.

(31) Eggert, G.; Heitbaum, J. *Electrochimica. Acta* **1986**, 31, 1443-1448.

(32) Maluangnont, T.; Lerner, M. M.; Gotoh, K. *Inorg. Chem.* **2011**, 50, 11676-11682.

(33) Muradov, N.; Smith, F.; T-Raissi, A. *Catal. Today* **2005**, 102, 225-233.

(34) Sun, R.; Sun, L.; Chun, Y.; Xu, Q. *Carbon* **2008**, 46, 1757-1764.

CHAPTER 6

CONCLUSION

A series of TAA-GICs has been successfully prepared for the first time via both ion exchange and electrochemical methods. The TAA cations studied include symmetric $(C_nH_{2n+1})_4N^+$ (n = 1-8) and asymmetric $(CH_3)_3(C_{12}H_{25})N^+$, $(CH_3)_3(C_{18}H_{37})N^+$ and $(CH_3)_2(C_{18}H_{37})_2N^+$. Monolayer galleries with d_i ~ 0.80 nm are observed for $(C_3H_7)_4N^+$ and $(C_4H_9)_4N^+$ and the observed gallery dimensions require flattened intercalate conformations. GICs formed with larger TAA cations contain the bilayer galleries (d_i ~ 1.1 nm) of flattened TAA conformation with co-intercalation of DMSO. The existence of bilayers is confirmed by the generated 1D-electron density profiles. These large TAA intercalates decrease charge density on the graphene sheets. The observed gallery heights and compositions of TAA-GICs obtained are all summarized in Table 6.1. For small TAA cations such as $(CH_3)_4N^+$ and $(C_2H_5)_4N^+$, the formation of GICs does occur *in situ* but the products are not stable enough to be isolated. A passivation surface model by the alkylation of graphene edges is proposed to explain the enhanced stabilities of GICs containing larger TAA intercalates.

The use of passivated GIC surfaces by large TAA cations in $(C_2H_5)_4N$-GIC preparation is also studied. The resulting GIC provides a stage-1 compound with d_i = 0.81 nm and its composition is $[(C_2H_5)_4N]C_{57}\cdot 0.5DMSO$. Similar to other TAA-GICs, $(C_2H_5)_4N^+$ intercalates arranges with highly-flattened conformation in the encasing

graphene sheets. In addition, the hydrophobic passivated surface affords a dramatically-enhanced stability of TAA-GICs in aqueous media and under an oxidizing environment.

Table 6.1 Summary of TAA-GICs prepared in this thesis.

Method	TAA-GICs	Stage	d_i (nm)	Intercalate arrangement
Ion-exchange	$[(C_3H_7)_4N]C_x$	high stage[a]	0.760	monolayer
	$[(C_4H_9)_4N]C_{43}$	1	0.813	monolayer
	$[(C_5H_{11})_4N]C_x \cdot \delta DMSO$	2	1.123	bilayer
	$[(C_6H_{13})_4N]C_{59} \cdot 1.1DMSO$	1	1.122	bilayer
	$[(C_7H_{15})_4N]C_{63} \cdot 1.4DMSO$	1	1.144	bilayer
	$[(C_8H_{17})_4N]C_{76} \cdot 1.9DMSO$	1	1.148	bilayer
	$[(C_{12}H_{25})(CH_3)_3N]C_{44} \cdot 1.4DMSO$	1	1.109	bilayer
	$[(C_{18}H_{37})(CH_3)_3N]C_{60} \cdot 1.6DMSO$	1	1.126	bilayer
	$[(C_{18}H_{37})_2(CH_3)_2N]C_{85} \cdot 2.2DMSO$	1	1.118	bilayer
Electrochemical	$[(C_4H_9)_4N]C_{37} \cdot 0.1DMSO$	1[b]	0.811	monolayer
	$[(C_5H_{11})_4N]C_{47} \cdot 0.7DMSO$	1	1.134	bilayer
	$[(C_6H_{13})_4N]C_{56} \cdot 0.8DMSO$	1	1.138	bilayer
	$[(C_7H_{15})_4N]C_{54} \cdot 1.2DMSO$	1	1.154	bilayer
	$[(C_8H_{17})_4N]C_{56} \cdot 1.2DMSO$	1	1.139	bilayer
Surface passivation	$[(C_2H_5)_4N]C_{57} \cdot 0.5DMSO$	1	0.805	monolayer

[a,b] impurity ascribed to graphite and bilayer phases, respectively.

BIBLIOGRAPHY

(1) Abe, T.; Fukuda, H.; Iriyama Y.; Ogumi, Z. *J. Electrochem. Soc.* **2004**, 151, A1120-A1123.

(2) Akçay, M. *J. Colloid Interface Sci.* **2006**, 296, 16-21.

(3) Akuzawa, N.; Ikeda, M.; Amemiya, T.; Takahashi, Y. *Synth. Met.* **1983**, 7, 65-72.

(4) Asher, R. C. *J. Inorg. Nucl. Chem.* **1959**, 10, 238–249.

(5) Atkins, P.; Overton, T.; Rourke, J.; Weller, M.; Armstrong, F.; Hagerman, M. In *Shriver & Atkins' Inorganic Chemistry*; Oxford University Press: New York, 2010; pp. 3–33.

(6) Avdeev, V. V.; Nalimova, V. A.; Semenenko, K. N. *Synth. Met.* **1990**, 38, 363–369.

(7) Bach, B.; Ubbelohde, A. R. *Proc. R. Soc. Lond. A. Math. Phys. Sci.* **1971**, 325, 437–445.

(8) Barrer, R. M. *Zeolites and Clay Minerals*; Academic Press: New York, 1978.

(9) Beguin, F.; Gonzalez, B.; Conard, J.; Estrade-szwarckopf, H.; Guerard, D. *Synth. Met.* **1985**, 12, 187–193.

(10) Beguin, F.; Pilliere, H. *Carbon* **1998**, 36, 1759–1767.

(11) Beguin, F.; Setton, R. *Carbon* **1975**, 13, 293–295.

(12) Beguin, F.; Setton, R.; Facchini, L. *Synth. Met.* **1983**, 7, 263-269.

(13) Beguin, F.; Setton, R.; Facchini, L.; Legrand, A. P.; Merle, G.; Mai, C. *Synth. Met.* **1980**, 2, 161–170.

(14) Beguin, F.; Setton, R.; Hamwi, A.; Touzain, P. *Mater. Sci. Eng.* **1979**, 40, 167–173.

(15) Beguin, F.; Vast, P. *Synth. Met.* **1988**, 23, 427-433.

(16) Bensenhard, J. O.; Möhwald, H.; Nickl, J. J. *Carbon* **1980**, 18, 399-405.

(17) Bernard, G.; Simonet, J. *J. Electroanal. Chem.* **1979**, 96, 249–253.

(18) Bernard, G.; Simonet, J. *J. Electroanal. Chem.* **1980**, 112, 117–125.

(19) Berthelot, J.; Jubault, M.; Simonet, J. *J. Chem. Soc. Chem. Commun.* **1982**, 759–760.

(20) Besenhard, J. O. *Carbon* **1976**, 14, 111–115.

(21) Besenhard, J. O.; Fritz, H. P. *J. Electroanal. Chem.* **1974**, 53, 329-333.

(22) Besenhard, J. O.; Mohward, H.; Nickl, J. J. *Carbon* **1980**, 18, 399–405.

(23) Besenhard, J. O.; Theodoridou, E.; Möhwald H.; Nickl, J. J. *Synth. Met.* **1982**, 4, 211-223.

(24) Besenhard, J.O.; Möhwald, H.; Nickl, J. J. *Carbon* **1980**, 18, 399-405.

(25) Billaud, D.; Herold, A. *Bull. Soc. Chim. Fr.* **1978**, 3-4, 131–134.

(26) Boehm, H.; Setton, R.; Stumpp, E. *Pure Appl. Chem.* **1994**, 66, 1893–1901.

(27) Boersma, M. A. M. *Catal. Rev. Sci. Eng.* **1974**, 10, 243–280.

(28) Boolchand, P.; Bresser, W. J.; Mcdaniel, D.; Sisson, K.; Yeh, V.; Eklund, P. C. *Solid State Commun.* **1981**, 40, 1049–1053.

(29) Bottomley, M. J.; Parry, G. S.; Ubbelohde, A. R.; Young, D. A. *J. Chem. Soc.* **1963**, 5674–5680.

(30) Brock, S. L.; Sanabria, M.; Suib, S. L.; Urban, V.; Thiyagarajan, P.; Potter, D. *J. Phys. Chem. B* **1999**, 103, 7416–7428.

(31) Celzard, A.; Mareche, J. F.; Furdin, G. *Prog. Mater. Sci.* **2005**, 50, 93–179.

(32) Chun, Y.; Sheng, G.; Boyd, S. A. *Clays Clay Miner.* **2003**, 52, 415-420.

(33) Chung, D. D. L. *J. Mater. Sci.* **2002**, 37, 1475–1489.

(34) Clarke, R.; Elzinga, M.; Gray, J. N.; Homma, H.; Morelli, D. T.; Winokur, M. J.; Uher, C. *Phys. Rev. B* **1982**, 26, 5250–5253.

(35) Clearfield, A.; Smith, G. D. *Inorg. Chem.* **1969**, 8, 431–436.

(36) Cooper, A. J.; Wilson, N. R.; Kinloch, I. A.; Dryfe, R. *Carbon* **2014**, 66, 340-350.

(37) Craven, W. E.; Ostertag, W. *Carbon* **1966**, 4, 223–226.

(38) Dahm, C. E.; Peters, D. G. *J. Electroanal. Chem.* **1996**, 402, 91-96.

(39) Doll, G. L.; Eklund, P. C.; Fischer, J. E. *Phys. Rev. B* **1987**, 36, 4940-4945.

(40) Dresselhaus, M. S.; Dresselhaus, G. *Adv. Phys.* **2002**, 51(1), 1-86.

(41) Dresselhaus, M. S.; Dresselhaus, G. *Top. Appl. Phys.* **1982**, 51, 3-57.

(42) Duc, C. M.; Gole, J.; Mai, C.; Riviere, R. *J. Chim. Phys.* **1972**, 69, 991–&.

(43) Ebert, L. B. *Annu. Rev. Mater. Sci.* **1976**, 6, 181–211.

(44) Eggert, G.; Heitbaum, J. *Electrochim. Acta* **1986**, 31, 1443-1448.

(45) Emery, N.; Hérold, C.; Bellouard, C.; Delcroix, P.; Mareche, J. F.; Lagrange, P. *J. Solid State Chem.* **2008**, 181, 2924–2929.

(46) Emery, N.; Hérold, C.; Lagrange, P. *Carbon* **2008**, 46, 72–75.

(47) Emery, N.; Hérold, C.; Lagrange, P. *J. Solid State Chem.* **2005**, 178, 2947–2952.

(48) Enoki, T.; Miyajima, S.; Sano, M.; Inokuchi, H. *J. Mater. Res.* **1990**, 5, 435–466.

(49) Enoki, T.; Suzuki, M.; Endo, M. *Graphite Intercalation Compounds and Applications*; Oxford University Press: New York, 2003.

(50) Facchini, L.; Bouat, J.; Sfihi, H.; Legrand, A. P.; Furdin, G.; Melin, J.; Vangelisti, R. *Synth. Met.* **1982**, 5, 11–22.

(51) Facchini, L.; Quinton, M. F.; Legrand, A. P. *Physica* **1980**, 99B, 525–530.

(52) Falcao, E. H. L.; Blair, R. G.; Mack, J. J.; Viculis, L. M.; Kwon, C. W.; Bendikov, M.; Kaner, R. B.; Dunn, B. S.; Wuld, F. *Carbon* **2007**, 45, 1367–1369.

(53) Finkelstein, M.; Petersen, R. C.; Ross, A. D. *J. Am. Chem. Soc.* **1959**, 81, 2361-2364.

(54) Forsman, W. C.; Dziemianowicz, T.; Leong, K.; Carl, D. *Synth. Met.* **1983**, 5, 77-100.

(55) Fu, W.; Kiggans, J.; Overbury, S. H.; Schwartz, V.; Liang, C. *Chem. Commun.* **2011**, 47, 5265–5267.

(56) Fukada, S.; Shintani, Y.; Shimomura, M.; Tahara F.; Yagi, R. *Jpn. J. Appl. Phys.* **2012**, 51, 085101-085104.

(57) Fukuda, K.; Kato, H.; Sato, J.; Sugimoto, W.; Takasu, Y. *J. Solid State Chem.* **2009**, 182, 2997–3002.

(58) Gao, Q.; Giraldo, O.; Tong, W.; Suib, S. L. *Chem. Mater.* **2001**, 13, 778–786.

(59) Geng, Y.; Zheng, Q.; Kim, J. -K. *J. Nanosci. Nanotechnol.* **2011**, 11, 1084-1091.

(60) Gieseking, J. E. *Soil Sci.* **1938**, 47, 1–14.

(61) Golub, A. S.; Protsenko, G. A.; Gumileva, L. V.; Buyanovskaya, A. G.; Novikov, Y. N. *Russ. Chem. Bull.* **1993**, 42, 632–634.

(62) Golub, A. S.; Zubavichus, Y. V.; Slovokhotov, Y. L.; Novikov, Y. N.; Danot, M. *Solid State Ionics* **2000**, 128, 151–160.

(63) Goutfer-Wurmser, F.; Herold, C.; Lagrange, P. *Carbon* **1996**, 34, 821-823.

(64) Guerard, D.; Chaabouni, M.; Lagrange, P.; Makrini, M. E.; Herold, A. *Carbon* **1980**, 18, 257–264.

(65) Hagiwara, R.; Tozawa, K.; Ito, Y. *J. Fluor. Chem.* **1998**, 88, 201–206.

(66) He, H.; Frost, R. L.; Bostrom, T.; Yuan, P.; Duong, L.; Yang, D.; Xi, Y.; Kloprogge, J. T. *Appl. Clay Sci.* **2006**, 31, 262-271.

(67) Hennig, G. R. *Prog. Inorg. Chem.* **1959**, 1, 125-205.

(68) Hérold, A.; Mareche, J.-F.; Lelaurain, M. *Carbon* **2000**, 38, 1955–1963.

(69) Hérold, C.; Hérold, A.; Lagrange, P. *J. Phys. Chem. Solids* **1996**, 57, 655-662.

(70) Hérold, C.; Hérold, A.; Lagrange, P. *Solid State Sci.* **2004**, 6, 125–138.

(71) Horn, D.; Boehm, H. *Mater. Sci. Eng.* **1977**, 31, 87–89.

(72) Inagaki, M.; Ohira, M. *Carbon* **1993**, 31, 777-781.

(73) Inagaki, M.; Tanaike, O. *Synth. Met.* **1995**, 73, 77-81.

(74) Inagaki, M.; Tashiro, R.; Washino, Y.; Toyoda, M. *J. Phys. Chem. Solids* **2004**, 65, 133-137.

(75) Isaev, Y. V.; Lenenko, N. D.; Gumileva, L. V.; Buyanovskaya, A. G.; Novikov, Y. N.; Stumpp, E. *Carbon* **1997**, 35, 563-566.

(76) Isaev, Y. V.; Novikov, Y. N.; Vol'pin, M. E. *Synth. Met.* **1982**, 5, 23–30.

(77) Isaev, Y. V.; Novikov, Y. N.; Vol'pin, M. E.; Rashkov, I.; Panayotov, I. *Synth. Met.* **1983**, 6, 9–14.

(78) Jacobson, A. J. In *Solid State Chemistry Compounds*; Cheetham, A. K.; Day, P., Eds.; Clarendon Press: Oxford, 1992; pp. 182–233.

(79) Jacobson, A. J.; Nazar, L. F. Intercalation Chemistry. *Encycl. Inorg. Bioinorg. Chem.* **2011**, 1–37.

(80) Jaynes, W. F.; Boyd, S. A. *Soil Sci. Soc. Am. J.* **1991**, 55, 43-48.

(81) Jegoudez, J.; Mazieres, C.; Setton, R. *Carbon* **1986**, 24, 747–756.

(82) Jones, J. E.; Cheshire, M. C.; Casadonte, D. J.; Phifer, C. C. *Org. Lett.* **2004**, 6, 1915-1917.

(83) Kang, F.; Leng, Y.; Zhang, T. *Carbon* **1997**, 35(8), 1089-1096.

(84) Kanzaki, Y.; Konuma, M.; Matsumuto, O. *J. Phys. Chem. Solids* **1980**, 41, 525-529.

(85) Katayama, Y.; Yukumoto, M.; Miura, T. *Electrochem. Solid-State Lett.* **2003**, 6, A96-A97.

(86) Katinonkul, W.; Lener, M. M. *Carbon* **2007**, 45, 2672-2677.

(87) Kganyago, K. R.; Ngoepe, P. E.; Catlow, C. R. A. *Solid State Ionics* **2003**, 159, 21–23.

(88) Ko, Y.; Lee, C. T. *J. Ind. Eng. Chem.* **2012**, 18, 726-730.

(89) Kullberg, L.; Clearfield, A. *J. Phys. Chem.* **1981**, 85, 1585–1589.

(90) Kwon, O. -Y.; Choi, S. -W.; Park, K. -W.; Kwon, Y. -B. *J. Ind. Eng. Chem.* **2003**, 9, 743-747.

(91) Lagaly, G. *Clay Miner.* **1981**, 16, 1–21.

(92) Lagaly, G. *Solid State Ionics* **1986**, 22, 43–51.

(93) Leef, A.; Gilmour, A. *J. Appl. Electrochem.* **1979**, 9, 663-670.

(94) Lerner, M.; Hagiwara, R.; Bartlett, N. *J. Fluor. Chem.* **1992**, 57, 1–13.

(95) Letaief, S.; Detellier, C. *Clays Clay Miner.* **2009**, 57, 638-648.

(96) Leung, S. Y.; Underhill, C.; Dresselhaus, G.; Krapchev, T.; Ogilvie, R.; Dresselhaus, M. S. *Solid State Commun.* **1979**, 32, 635–639.

(97) Li, X.; Zhang, G.; Bai, X.; Sun, X.; Wang, X.; Wang, E.; Dai, H. *Nature Nanotech.* **2008**, 3, 538-542.

(98) Li, Z.; Jiang, W.T. *Thermochim. Acta* **2009**, 483, 58-65.

(99) Liu, J.; Durand, J. P.; Espinal, L.; Garces, L. J.; Gomez, S.; Son, Y. C.; Villegas, J.; Suib, S. L. In *Handbook of Layered Materials*; Auerbach, S. M.; Carrado, K. A.; Dutta, P. K., Eds.; Marcel Dekker, Inc.: New York, 2004; pp. 475–508.

(100) Liu, Z. -H.; Ooi, K.; Kanoh, H.; Tang, W. -P.; Tomida, T. *Langmuir* **2000**, 16, 4154-4164.

(101) Liu, Z. -H.; Wang, Z. -M.; Yang, X.; Ooi, K. *Langmuir* **2002**, 18, 4926-4932.

(102) Luzhkov, V.B.; Österberg, F.; Acharya, P.; Chattopadhyaya, J.; Åqvist, J. *Phys. Chem. Chem. Phys.* **2002**, 4, 4640-4647.

(103) Makotchenko, V. G.; Grayfer, E. D.; Nazarov, A. S.; Kim, S. -J.; Fedorov, V. E. *Carbon* **2011**, 49, 3233-3241.

(104) Makrini, M. E. L.; Gubrard, D.; Lagrange, P.; Hérold, A. *Carbon* **1980**, 18, 203–209.

(105) Makrini, M. E.; Guerard, D.; Lagrange, P.; Hérold, A. *Physica* **1980**, 99B, 481–485.

(106) Malik, S.; Vijayaraghavan, A.; Erni, R.; Ariga, K.; Khalakhan, I.; Hill, J. P. *Nanoscale* **2010**, 2, 2139-2143.

(107) Mallouk, T.; Bartlett, N. *J. Chem. Soc. Chem. Commun.* **1983**, 103–105.

(108) Maluangnont, T.; Bui, G. T.; Huntington, B. A.; Lerner, M. M. *Chem. Mater.* **2011**, 23, 1091–1095.

(109) Maluangnont, T.; Gotoh, K.; Fujiwara, K.; Lerner, M. M. *Carbon* **2011**, 49, 1040–1042.

(110) Maluangnont, T.; Lerner, M. M.; Gotoh, K. *Inorg. Chem.* **2011**, 50, 11676-11682.

(111) Maluangnont, T.; Sirisaksoontorn, W.; Lerner, M. M. *Carbon* **2012**, 50, 597–602.

(112) Matsumura, Y.; Wang S.; Mondori, J. *J. Electrochem. Soc.* **1995**, 142, 2914-2918.

(113) Mayell, J. S.; Bard, A. J. *J. Am. Chem. Soc.* **1963**, 85, 421-425.

(114) Mercier, L.; Detellier, C. *Clays Clay Miner.* **1994**, 42, 71–76.

(115) Metrot, A.; Fischer, J. E. *Synth. Met.* **1981**, 3, 201–207.

(116) Metrot, A.; Guerard, D.; Billaud, D.; Herold, A. *Synth. Met.* **1979**, 1, 363–369.

(117) Mizutani, Y.; Abe, T.; Ikeda, K.; Ihara, E.; Asano, M.; Harada, T.; Inaba, M.; Ogumi, Z. *Carbon* **1997**, 35, 61-65.

(118) Moissette, A.; Fuzellier, H.; Burneau, A.; Dubessy, J.; Lelaurain, M. *Carbon* **1995**, 33, 123-128.

(119) Mouras, S.; Hamwi, A.; Djurado, D.; Cousseins, J. C.; Fawal, Z.; Mohamad, A. H.; Dupuis, J. *J. Solid State Chem.* **1989**, 83, 115–120.

(120) Mukherjee, A.; Kang, J.; Kuznetsov, O.; Sun, Y.; Thaner, R.; Bratt, A. S.; Lomeda, J. R.; Kelly K. F.; Billups, W. E. *Chem. Mater.* **2011**, 23, 9-13.

(121) Muller-Warmuth, W.; Schollhorn, R. *Progress in Intercalation Research*; Kluwer Academic Publishers: The Netherlands, 1994.

(122) Muradov, N.; Smith, F.; T-Raissi, A. *Catal. Today* **2005**, 102, 225-233.

(123) Nakajima, T.; Matsui, T.; Motoyama, M.; Mizutani, Y. *Carbon* **1988**, 26, 831–836.

(124) Nakajima, T.; Watanabe, N.; Kameda, I.; Endo, M. *Carbon* **1986**, 24, 343–351.

(125) Nakayam, M.; Konishi, S.; Tagashira, H.; Oruga, K. *Langmuir* **2005**, 21, 354-359.

(126) Nakayama, M.; Fukuda, M.; Konishi, S.; Tonosaki, T. *J. Mater Res.* **2006**, 21, 3152-3160.

(127) Nakayama, M.; Konishi, S.; Tagashira, H.; Ogura, K. *Langmuir* **2005**, 21, 354–359.

(128) Nalimova, V. A.; Guerard, D.; Lelaurain, M.; Fateev, O. V. *Carbon* **1995**, 33, 177–181.

(129) Nicholls, J. T.; Speck, J. S.; Dresselhaus, G. *Phys. Rev. B* **1989**, 39, 10047–10055.

(130) Nobuhara, K.; Nakayama, H.; Nose, M.; Nakanishi, S.; Iba, H. *J. Power Sources* **2013**, 243, 585–587.

(131) Noel, M.; Santhanam, R. *J. Power Sources* **1995**, 56, 101-105.

(132) Noel, M.; Santhanam, R. *J. Power Sources* **1998**, 72, 53–65.

(133) Novoselov, K. S.; Geim, A. K.; Morozov, S. V.; Jiang, D.; Zhang, Y.; Dubonos, S. V.; Grigorieva, I. V.; Firsov, A. A. *Science* **2004**, 306, 666-669.

(134) O'Hare, D. In *Inorganic Materials*; Bruce, D. W.; O'Hare, D., Eds.; John Wiley & Sons, Ltd.: New York, 1992; pp. 165–235.

(135) Ogawa, M.; Handa, T.; Kuroda, K.; Kato, C. *Chem Lett.* **1990**, 71-74.

(136) Ogawa, M.; Kuroda, K. *Bull. Chem. Soc. Jpn.* **1997**, 70, 2593–2618.

(137) Ogumi, Z.; Inaba, M. *Bull. Chem. Soc. Jpn.* **1998**, 71, 521-534.

(138) Ogumi, Z.; Wang, H. In *Lithium-Ion Batteries*; Yoshio, M.; Kozawa, A.; Brodd, R. J., Eds.; Springer: New York, 2009; pp. 49–73.

(139) Ohzuku, T.; Iwakoshi, Y.; Sawai, K. *J. Electrochem. Soc.* **1993**, 140, 2490–2498.

(140) Okino, F.; Bartlett, N. *J. Chem. Soc. Dalt. Trans.* **1993**, 2081–2090.

(141) Okuyama, N.; Takahashi, T.; Kanayama, S.; Yasunaga, H. *Physica B&C* **1981**, 105, 298-301.

(142) Omomo, Y.; Sasaki, T.; Wang, L.; Watanabe, M. *J. Am. Chem. Soc.* **2003**, 125, 3568-3575.

(143) Oriakhi, C. O.; Lerner, M. M. In *Handbook of Layered Materials*; Auerbach, S. M.; Carrado, K. A.; Dutta, P. K., Eds.; Marcel Dekker, Inc.: New York, 2004; pp. 509–539.

(144) Ouvrard, G.; Guyomard, D. *Curr. Opin. Solid State Mater. Sci.* **1996**, 1, 260–267.

(145) Özmen-Monkul, B.; Lerner, M. M.; Hagiwara, R. *J. Fluorine Chem.* **2009**, 130, 581-585.

(146) Özmen-Monkul, B.; Lerner, M. M.; Pawelke, G.; Willner, H. *Carbon* **2009**, 47, 1592-1597.

(147) Parry, G. S.; Nixon, D. E. *Nature* **1967**, 216, 909-910.

(148) Parry, G. S.; Nixon, D. E.; Lester, K. M.; Levene, B. C. *J. Phys. C* **1969**, 2, 2156-2158.

(149) Peng, S.; Gao, Q.; Du, Z.; Shi, J. *Apply Clay Sci.* **2006**, 31, 229-237.

(150) Pilliere, H.; Goldmann, M.; Beguin, F. *J. Mater. Res.* **1993**, 8, 2288–2298.

(151) Platzer, N.; de la Martiniere, B. *Bull. Soc. Chim. Fr.* **1961**, 1961, 177–180.

(152) Purewal, J. J.; Keith, J. B.; Ahn, C. C.; Fultz, B.; Brown C. M.; Tyagi, M. *Phys. Rev. B.* **2009**, 79, 054305.

(153) Rao, B. L. M.; Halbert, T. R. *Mat. Res. Bull.* **1981**, 16, 919-922.

(154) Rao, C. N. R.; Sood, A. K.; Subrahmanyam, K. S.; Govindaraj, A. *Angew. Chem. Int. Ed.* **2009**, 48, 7752–7777.

(155) Rashkov, I. B.; Panayotov, I. M.; Shishkova, V. C. *Carbon* **1979**, 17, 103-108.

(156) Ravaine, D.; Boyce, J.; Hamwi, A.; Touzain, P. *Synth. Met.* **1980**, 2, 249–260.

(157) Resing, H. A.; Vogel, F. L.; Wu, T. C. *Mater. Sci. Eng.* **1979**, 41, 113–119.

(158) Rida, H.; Cahen, S.; Hérold, C.; Lagrange, P. *Carbon* **2010**, 48, 3190–3195.

(159) Ruch, P. W.; Hahn, M.; Rosciano, F.; Holzapfel, M.; Kaiser, H.; Scheifele, W.; Schmitt, B.; Novak, P.; Kotz, R.; Wokaun, A. *Electrochim. Acta* **2007**, 53, 1074–1082.

(160) Rudorff, W.; Schulze, E.; Rubisch, O. *Z. Anorg. Allg. Chem.* **1955**, 282, 232–240.

(161) Rüdorff, W.; Siecke, W.-F. *Chem. Ber.* **1958**, 91, 1348–1354.

(162) Santhanam, R.; Noel, M. *J. Power Sources* **1995**, 56, 101-105.

(163) Santhanam, R.; Noel, M. *J. Power Sources* **1998**, 72, 53-65.

(164) Sasa, T.; Takahashi, Y.; Mukaibo, T. *Carbon* **1971**, 9, 407–416.

(165) Sasaki, T.; Watanabe, M. *J. Am. Chem. Soc.* **1998**, 120, 4682-4689.

(166) Sasaki, T.; Watanabe, M. *Mol. Cryst. Liq. Cryst.* **1998**, 311, 417–422.

(167) Savoskin, M. V.; Yaroshenko, A. P.; Whyman, G. E.; Mysyk, R. D. *J. Phys. Chem. Solids* **2006**, 67, 1127–1131.

(168) Schaak, R. E.; Mallouk, T. E. *Chem. Mater.* **2000**, 12, 3427–3434.

(169) Schöllhorn, R. *Chem. Mater.* **1996**, 8, 1747–1757.

(170) Schollhorn, R. *Physica* **1980**, 99B, 89–99.

(171) Selig, H.; Vaknin, D.; Davidov, D.; Yeshurun, Y. *J. Chem. Soc. Chem. Commun.* **1985**, 1689–1690.

(172) Sethuraman, V. A.; Hardwick, L. J.; Srinivasan, V.; Kostecki, R. *J. Power Sources* **2010**, 195, 3655-3660.

(173) Shiguihara, A. L.; Bizeto, M. A.; Constantino, V. R. L. *Colloids Surfaces A* **2007**, 295, 123–129.

(174) Shornikova, O. N.; Sorokina, N. E.; Maksimova, N. V.; Avdeev, V. V. *Inorg. Mater.* **2005**, 41, 120-126.

(175) Sideris, P. J.; Nielsen, U. G.; Gan, Z.; Grey, C. P. *Science* **2008**, 321, 113–117.

(176) Simonet, J. *Electrochem. commun.* **2013**, 30, 17–20.

(177) Simonet, J. *J. Electrochem. Commun.* **2013**, 30, 17-20.

(178) Simonet, J.; Lund, H. *J. Electroanal. Chem.* **1977**, 75, 719–730.

(179) Sirisaksoontorn, W.; Adenuga, A. A.; Remcho, V. T.; Lerner, M. M. *J. Am. Chem. Soc.* **2011**, 133, 12436-12438.

(180) Sirisaksoontorn, W.; Lerner, M. M. *ECS J. Solid State Sci. Technol.* **2013**, 2(9), M28-M32.

(181) Sirisaksoontorn, W.; Lerner, M. M. *Inorg. Chem.* **2013**, 52, 7139-7144.

(182) Skowronski, J. M.; Krawczyk, P. *Solid State Ion.* **2010**, 181, 653-658.

(183) Smart, M. C.; Ratnakumar, B. V.; Surampudi, S.; Wang, Y.; Zhang, X.; Greenbaum, S. G.; Hightower, A.; Ahn, C. C.; Fultz, B. *J. Electrochem. Soc.* **1999**, 146, 3963-3969.

(184) Solin, S. A. *Annu. Rev. Mater. Sci.* **1997**, 27, 89-115.

(185) Stumpp, E.; Alheid, H.; Schwarz, M.; Janssen, J.; Muller-Warmuth, W. *J. Phys. Chem. Solids* **1996**, 57, 925–930.

(186) Stumpp, E.; Wloka, K. *Synth. Met.* **1981**, 3, 209.

(187) Sun, R. Q.; Sun, L. B.; Chun, Y.; Xu, Q. H. *Carbon* **2008**, 46, 1757-1764.

(188) Sun, R.; Sun, L.; Chun, Y.; Xu, Q. *Carbon* **2008**, 46, 1757-1764.

(189) Takahashi, Y.; Akuzawa, N.; Béguin, F. *Synth. Met.* **1995**, 73, 45-48.

(190) Takahashi, Y.; Oi, K.; Terai, T.; Akuzawa, N. *Carbon* **1991**, 29, 283–284.

(191) Takenaka, A.; Tsumura, T.; Toyoda, M. *Synth. Met.* **2010**, 160, 1247-1251.

(192) Tamura, K.; Nakazawa, H. *Clays Clay Miner.* **1996**, 44, 501-505.

(193) Thomas, J. M.; Millward, G. R.; Schlögl, R. F.; Boehm, H. P. *Mater. Res. Bull.* **1980**, 15(5), 671-676.

(194) Touzain, P. *Synth. Met.* **1979**, 1, 3–11.

(195) Toyoda, M.; Inagaki, M. *Carbon* **2000**, 38, 199-210.

(196) Truong, Q. T.; Pokharel, P.; Song G. S.; Lee, D. S. *J. Nanosci. Nanotechnol.* **2012**, 12, 4305-4308.

(197) Tsukamoto, J.; Matsumura, K.; Takahashi, T.; Sakoda, K. *Synth. Met.* **1986**, 131, 255-264.

(198) Udod, I. A.; Orman, H. B.; Genchel, V. K. *Carbon* **1994**, 32, 101–106.

(199) Ue, M. In *Lithium-Ion Batteries*; Yoshio, M.; Kozawa, A.; Brodd, R. J., Eds.; Springer: New York, 2009; pp. 75–115.

(200) Ue, M.; Ida, K.; Mori, S. *J. Electrochem. Soc.* **1994**, 141(11), 2989-2996.

(201) Underhill, C.; Krapchev, T.; Dresselhaus, M. S. *Synth. Met.* **1980**, 2, 47–55.

(202) Vallés, C.; Drummond, C.; Saadaoui, H.; Furtado, C. A.; He, M.; Roubeau, O.; Ortolani, L.; Monthioux, M.; Pénicaud, A. *J. Am. Chem. Soc.* **2008**, 130, 15802-15804.

(203) Verma, P.; Sasaki, T.; Novak, P. *Electrochim. Acta* **2012**, 82, 233–242.

(204) Viculis, L. M.; Mack, J. J.; Kaner, R. B. *Science* **2003**, 299, 1361.

(205) Vora, P.; York, B. R.; Solin, S. A. *Synth. Met.* **1983**, 7, 355-360.

(206) Wang, F.; Yi, J.; Wang, Y.; Wang, C.; Wang, J.; Xia, Y. *Adv. Energy Mater.* **2013**, DOI:10.1002/aenm.201300600.

(207) Wang, H.; Yoshio, M. *J. Power Sources* **2012**, 200, 108–112.

(208) Wang, J.; Manga, K. K.; Bao, Q.; Loh, K. P. *J. Am. Chem. Soc.* **2011**, 133, 8888–8891.

(209) Watanabe, N. *J. Fluorine Chem.* **1983**, 22, 205-230.

(210) Wei, T.; Fan, Z.; Luo, G.; Zheng C.; Xie, D. *Carbon* **2009**, 47, 337-339.

(211) Weiss, A. *Angew. Chem. Int. Ed.* **1963**, 2, 134–144.

(212) Whittingham, M. S.; Jacobson, A. J. *Intercalation Chemistry*; Academic Press: New York, 1982.

(213) Xi, Y.; Frost, R. L.; He, H.; Kloprogge, T.; Bostrom, T. *Langmuir* **2005**, 21, 8675-8680.

(214) Xu, K.; Cresce, A. *J. Mater. Res.* **2012**, 27, 2327-2341.

(215) Yuqin, C.; Hong, L.; Lie, W.; Tianhong, L. *J. Power Sources* **1997**, 68, 187-190.

(216) Zhang, X.; Lerner, M. M. *Chem. Mater.* **1999**, 11, 1100-1109.

(217) Zhao, Y. H.; Abraham, M. H.; Zissimos, A. M. *J. Org. Chem.* **2003**, 68, 7368-7373.

(218) Zheng, H.; Jiang, K.; Abe, T.; Ogumi, Z. *Carbon* **2006**, 44, 203–210.

(219) Zheng, H.; Li, B.; Fu, Y.; Abe, T.; Ogumi, Z. *Electrochim. Acta* **2006**, 52, 1556-1562.